STATE OF THE CALIFORNIA CURRENT 2017–18: STILL NOT QUITE NORMAL IN THE NORTH AND GETTING INTERESTING IN THE SOUTH

ANDREW R. THOMPSON*
National Marine Fisheries Service
Southwest Fisheries Science Center
8901 La Jolla Shores Drive
La Jolla, CA 92037-1509
andrew.thompson@noaa.gov

ISAAC D. SCHROEDER[1,2], STEVEN J. BOGRAD[1], ELLIOTT L. HAZEN[1], MICHAEL G. JACOX[1,3], ANDREW LEISING[1], AND BRIAN K. WELLS[4]
[1]Southwest Fisheries Science Center
National Marine Fisheries Service
99 Pacific Street, Suite 255A
Monterey, CA 93940-7200
[2]Institute of Marine Sciences
University of California, Santa Cruz, CA
and Southwest Fisheries Science Center
NOAA
Monterey, CA
[3]Earth System Research Laboratory
NOAA
Boulder, CO 80305
[4]Southwest Fisheries Science Center
National Marine Fisheries Service
NOAA
Santa Cruz, CA 95064

JOHN L. LARGIER
Bodega Marine Laboratory
University of California Davis,
Bodega Bay, CA 94923

JENNIFER L. FISHER[1], KYM JACOBSON[2], SAMANTHA ZEMAN[1]
[1]Cooperative Institute for
Marine Resources Studies
Oregon State University
Hatfield Marine Science Center
Newport, OR 97365
[2]Northwest Fisheries Science Center
Hatfield Marine Science Center
Newport, OR 97365

ERIC P. BJORKSTEDT[1] AND ROXANNE R. ROBERTSON[2]
[1]Southwest Fisheries Science Center
National Marine Fisheries Service
NOAA
Santa Cruz, CA 95064
[2]CIMEC, Humboldt State University

FRANCISCO P. CHAVEZ
Monterey Bay Aquarium Research Institute
Moss Landing, CA 95039

MATI KAHRU AND RALF GOERICKE
Scripps Institution of Oceanography
University of California, San Diego
La Jolla, CA 92093

SAM MCCLATCHIE
38 Upland Rd, Huia
Auckland 0604, New Zealand

CLARE E. PEABODY
National Marine Fisheries Service
Southwest Fisheries Science Center
8901 La Jolla Shores Drive
La Jolla, CA 92037-1509

TIMOTHY R. BAUMGARTNER, BERTHA E. LAVANIEGOS, AND JOSE GOMEZ-VALDES
Oceanology Division
Centro de Investigación Científica y
Educación Superior de Ensenada
Carretera Ensenada-Tijuana No. 3918
Zona Playitas C.P. 22860
Ensenada, Baja California, Mexico

RICHARD D. BRODEUR[1], ELIZABETH A. DALY[2], CHERYL A. MORGAN[2], TOBY D. AUTH[2] AND BRIAN J. BURKE[3]
[1]NOAA-Fisheries
Northwest Fisheries Science Center
Hatfield Marine Science Center
Newport, OR 97365
[2]Cooperative Institute for
Marine Resources Studies
Oregon State University
Hatfield Marine Science Center
Newport, OR 97365
[3]Fish Ecology Division
Northwest Fisheries Science Center
National Marine Fisheries Service
National Oceanic and
Atmospheric Administration
2725 Montlake Boulevard E
Seattle, WA 98112

JOHN FIELD AND KEITH SAKUMA
Southwest Fisheries Science Center
National Marine Fisheries Service
NOAA
Santa Cruz, CA 95064

EDWARD D. WEBER AND WILLIAM WATSON
National Marine Fisheries Service
Southwest Fisheries Science Center
8901 La Jolla Shores Drive
La Jolla, CA 92037-1509

JULIA COATES[1], RYAN SCHOENBAUM[1], AND LAURA ROGERS-BENNETT[2]
[1]California Department of Fish and Wildlife
1933 Cliff Drive, Suite 9
Santa Barbara, CA 93109
[2]California Department of Fish and Wildlife
Bodega Marine Laboratory
University of California, Davis
2099 Westshore Road
Bodega Bay, CA 94923

ROBERT M. SURYAN[1], JANE DOLLIVER[2], AND STEPHANIE LOREDO[2]
[1]NOAA Alaska Fisheries Science Center
Auke Bay Laboratories/
Ted Stevens Marine Research Institute
17109 Pt. Lena Loop Road
Juneau, AK 99801
[2]Department of Fisheries and Wildlife
Oregon State University
Hatfield Marine Science Center
Newport, OR 97365

JEANNETTE E. ZAMON
Northwest Fisheries Science Center
Point Adams Research Station
520 Heceta Place
Hammond OR 97121

STEPHANIE R. SCHNEIDER[1] AND RICHARD T. GOLIGHTLY[2]
[1]Moss Landing Marine Labs
8272 Moss Landing Road
Moss Landing, CA 95039
[2]Department of Wildlife
Humboldt State University
1 Harpst Street
Arcata, CA 95521

PETE WARZYBOK AND JAIME JAHNCKE
Point Blue Conservation Science
3820 Cypress Drive, Suite 11
Petaluma, CA 94954

JARROD A. SANTORA[1], SARAH ANN THOMPSON[2], AND WILLIAM SYDEMAN[2]
[1]Department of Applied Mathematics
and Statistics
Center for Stock Assessment Research
University of California, Santa Cruz
Santa Cruz, CA 95060
[2]Farallon Institute for
Advanced Ecosystem Research
Petaluma, CA 94952

SHARON R. MELIN
National Marine Fisheries Service
Alaska Fisheries Science Center
Marine Mammal Laboratory
NOAA
7600 Sand Point Way N. E.
Seattle, WA 98115

ABSTRACT

Following the marine heat wave of 2014–16, the California Current System (CCS) trended towards more typical conditions north of Point Conception, California, from mid-2017 to mid-2018, but became highly abnormal in the south by mid-2018. Two basin-scale indices (Pacific Decadal Oscillation and Oceanic Niño Index) were close to neutral, but the North Pacific Gyre Oscillation was extremely low at the end of 2017 and beginning of 2018. Regional analyses demonstrated that upwelling was close to normal throughout most of the CCS with the exception of high upwelling from northern California to Washington in summer and fall of 2017. Sea surface temperature was close to normal throughout most of the CCS but warmed to record levels in summer 2018 in southern California and northern Baja California. In spring 2018, surface chlorophyll *a* was negatively anomalous throughout most of the US West Coast with localized hot spots around the Columbia River, in the Gulf of Farallones, and Monterey Bay. Lipid-rich copepod densities and sizes returned to normal levels in the northern CCS, and euphausiid abundances were above average in central California but below average in southern California in spring 2018. Abundances of 7 zooplankton taxa were slightly to well above average off of northern Baja California in late 2017. Pyrosomes, which are associated with warm water, were found throughout the CCS.

The fish assemblage off Oregon and Washington was comprised of both northern and southern/offshore species. In the central region (near Monterey Bay) most fishes were close to long-term mean abundances; however, adult northern anchovy (*Engraulis mordax*) abundance was the highest on record. The ichthyoplankton assemblage off southern California had a tropical signal similar to 2014–15 as warm-water associated mesopelagic abundances were close to record highs and cold water mesopelagics abundances were very low. Anchovy larvae abundances in southern California were the highest since the 1960s.

Indicators that can affect salmon survival were mixed in 2018. On the one hand, several indices forecast high salmon return (moderate-high salmon yearling abundance, high larval fish (salmon prey) abundance, normal lipid-rich copepod abundances). On the other hand, low survival was predicted by high fall PDO, high abundances of offshore larval fishes, and above average abundance of lipid-poor copepods. This unusual mix of indicators makes it difficult to forecast salmon returns in upcoming years.

Common murre (*Uria aalge*) reproduction was historically low in the northern CCS in 2017 as colonies experienced complete reproductive failure both at Yaquina Head, Oregon, and Castle Rock, California. In both cases, forage was scarce, birds conducted long foraging excursions which left eggs unattended for extended periods, and many eggs were consumed by avian predators. Brandt's (*Phalacrocorax peniscillatus*) and pelagic (*P. pelagicus*) cormorants had above average reproductive success in 2017 at Yaquina Head, but Brandt's cormorant also had total reproductive failure in 2017 at Castle Rock. At Southeast Farallon Island murre, Brandt's cormorant, and pelagic cormorant productivity was close to average in 2017, and Brandt's cormorant and murre were slightly above average in 2018. Preliminary 2018 results from Yaquina Head also indicated that murre successfully produced chicks for the first time since 2014. At-sea bird surveys in the north demonstrated that sooty shearwater and common murre abundances were historically low in 2017, but increased to some of the highest values on record in 2018. By contrast, the at-sea surveys off central California found that murre densities were anomalously high in 2017 but fell to an average level in 2018.

Improving California sea lion (*Zalophus californianus*) pup condition continued from 2016 into 2017 as live pup counts, pup weight, and rate of growth were above average. Augmented pup conditions in 2016–17 was likely driven by increased availability of anchovy, as anchovy remains were found in nearly 100% of sea lion scat. There were record high encounters with Humpback whales (*Megaptera novaeangliae*) off central California in 2018.

Overall, much of the CCS was in more of a normal state through mid-2018 relative to the past 5 years. However, remnants of the 2014–16 marine heat wave were still resonating in the north, and another highly anomalously warm water event affected the southern part of the CCS in summer 2018. Thus, while the CCS was returning to typical conditions in the north, it was anything but normal in the south in 2018.

INTRODUCTION

The California Current System (CCS; fig. 1) is nothing if not dynamic with physical and biological conditions often changing greatly between years. Analyses of data from the earliest days of the California Cooperative Oceanic Fisheries Investigations (CalCOFI) program in the 1950s demonstrated that oceanographic conditions can be highly variable from year to year, leading to substantial changes in the distributions and abundances of marine organisms (Moser et al. 1987; Hsieh et al. 2005). Changes can either be confined to particular regions within the larger system (Brodeur et al. 2006; Goericke et al. 2007) or permeate the entire area, affecting biological assemblages from Baja California, Mexico to Washington, USA (Black et al. 2018).

TABLE 1

Overview of conditions throughout the California Current. For basin indices and physical conditions, blue font suggests that conditions are cool, pink font that conditions are moderately warmer than average and red that conditions are much warmer than normal. For biological indices, green indicates that conditions are conducive for high production, pink moderately below average production, and red well below average.

Indicator	Basin	Oregon/ Washington	Central/Northern California	Southern California	Northern Baja California
ONI	Slightly below average				
PDO	average				
NPGO	very, very low				
NPH	Below average				
Upwelling (spring 2018)		average	slightly above average	slightly above average	
Cumulative upwelling		average	average	slightly above average	
SST (spring 2018)		average	average	average (but far above average in summer 2018)	average (but far above average in summer 2018)
Chlorophyll *a*		Slightly below average	Slightly below average	Slightly below average	Slightly below average
Copepods/krill		southern species above average; northern species average	*Euphausia pacifica* larger than average at Trinidad Head Line. Euphausid abundances above average in central CA.		Highest abundance of copepods since records began in 1998. Euphausids average.
Forage fish and squid		post-larval biomass very low in spring 2018; larval fish abundance high in winter 2018 but dominated by southern taxa	anchovy, squid, and sanddabs high; hake and sardine low	anchovy very high; subtropical mesopelagics very high	
Salmon survival		yearling Chinook abundance high and yearling coho average. Salmon forage assemblage suggests poor salmon survival and adult return			
Seabird productivity (summer 2017)		complete reproductive failure for murre, average reproduction for Brandt's cormorant and high reproduction for Pelagic cormorant	complete reproductive failure for murre in no. CA. Average murre reproduction in central CA.		
Seabird at-sea abundance (summer 2018)		common murre average, sooty shearwater high	black-footed albatross, Cassian's auklet, murre, pink-footed shearwater low, rhinocerous auklet average, sooty shearwater high	black-footed albatross, Cook's petrel low; pink-footed shearwater, sooty shearwater average; elegant turn, Sabine's gull high	
Sea lions				pup number, weight and growth high	
Whales			record high encounters of humpback		

The entire CCS was affected by anomalously warm conditions from 2014–16. The heating began in late 2013 in the Gulf of Alaska and by mid-2014 elevated sea surface temperature (SST) was observed all the way to southern Baja California (Bond et al. 2015; Leising et al. 2015). The 2014 warming event was primarily confined to near-surface waters (Leising et al. 2015), but it was widespread and persistent, and was augmented in 2015–16 by one of the strongest El Niños on record (Di Lorenzo and Mantua 2016; McClatchie et al. 2016b; Rudnick et al. 2017). Warming ultimately penetrated deeper waters, to at least several hundred meters, and persisted for several years. This long temporal stretch of warm water, termed a marine heat wave, was unprecedented as 2014–16 was the warmest 3-year stretch on record (Jacox et al. 2018a).

From 2016 to 2017 oceanographic conditions backed off from the extremes of the previous 3 years (Wells et al. 2017). In the central and southern regions of the CCS, SST, chlorophyll *a*, and many biological conditions (e.g., forage fish assemblages) approached long-term averages. In the northern part of the CCS, however, above-normal SST and low chlorophyll *a* persisted into 2016–17,

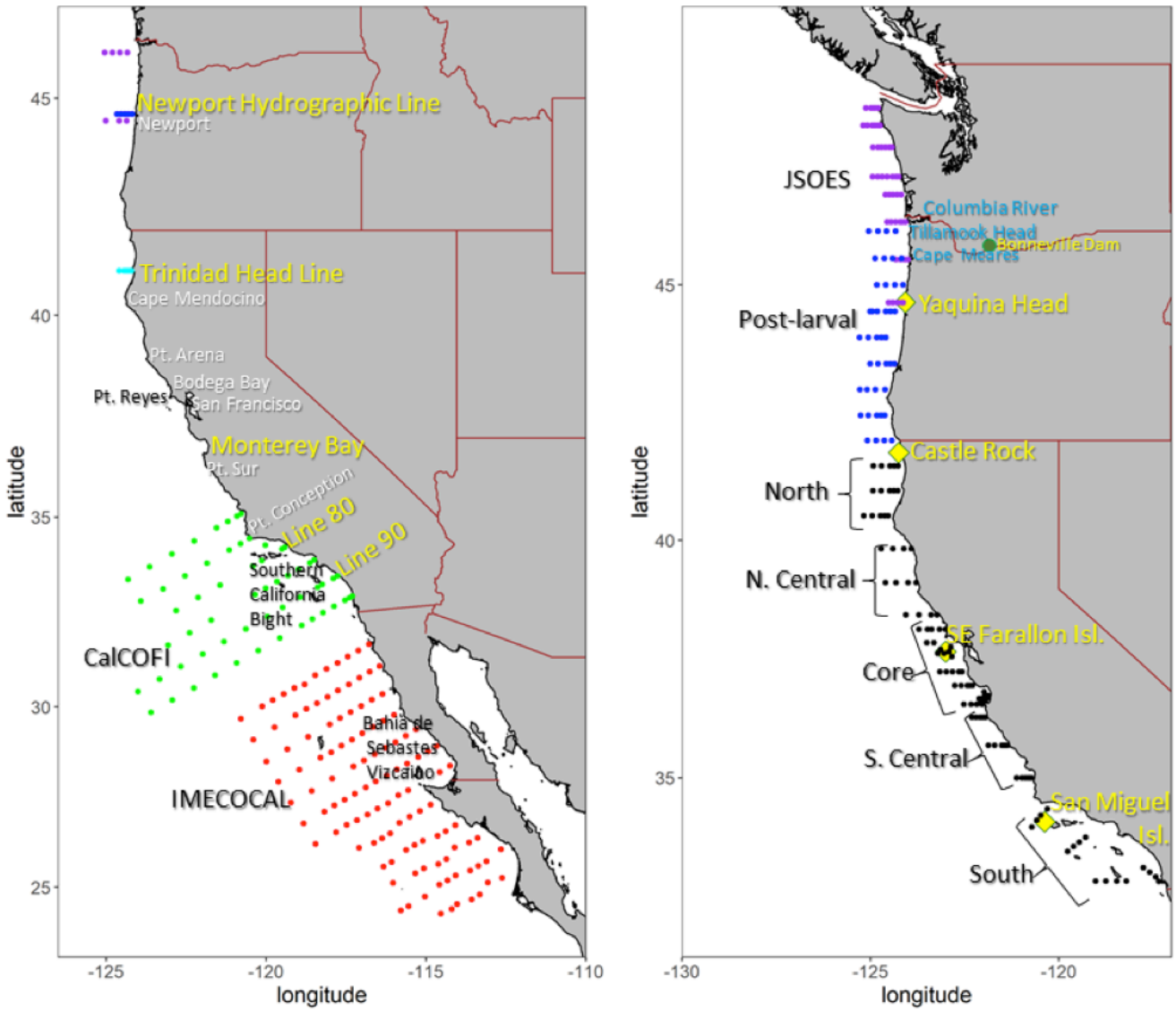

Figure 1. Left: Map where bongo tows were conducted. From north: purple = pre-larval surveys taken in summer; blue = pre-larval survey from winter; cyan = Trinidad Head taken year-round; green = core CalCOFI stations sampled quarterly; red = IMECOCAL stations sampled roughly quarterly. Right: Map where rope trawls and fixed observations for birds or marine mammals were taken. From north: purple = juvenile salmon and Ocean Ecosystem Survey (JSOES) in the upper 20 m; blue = post-larval midwater trawl; black = Rockfish Recruitment and Ecosystem Assessment Survey (RREAS), brackets define the five regions of the RREAS. Yellow diamonds define locations of bird (Yaquina Head, Castle Rock, Southeast Farallon Islands) and sea lion (San Miguel Island) surveys. The Bonneville Dam, (where salmon returns to the Columbia River are tracked) is depicted by the green circle.

and in some places anomalous warming had yet to dissipate through spring 2018 (Jackson et al. 2018). The goal of the current report is to track conditions through 2018 to determine if the return to average conditions persisted past mid-2017 or if recent conditions continued to deviate from average.

BASIN-SCALE CONDITIONS

North Pacific Climate Indices

Temperatures tended to cool throughout the CCS from mid-2016 to mid-2017 (Wells et al. 2017), following the large marine heat wave that brought record-high temperatures to the CCS from 2014 to 2016 (Bond et al. 2015; Jacox et al. 2018a). Temperatures in 2017 were near the long-term mean; however, there were regional differences with higher temperature anomalies in the northern CCS (Wells et al. 2017). From mid-2017 to mid-2018 temperatures throughout much of the CCS were similar to those observed the previous year. However, in the Southern California Bight and northern Baja California, temperatures rapidly increased though July and August 2018, and record high SSTs were recorded near the coast in La Jolla, California.[1]

[1]https://scripps.ucsd.edu/news/highest-ever-seawater-temperature-recorded-scripps-pier

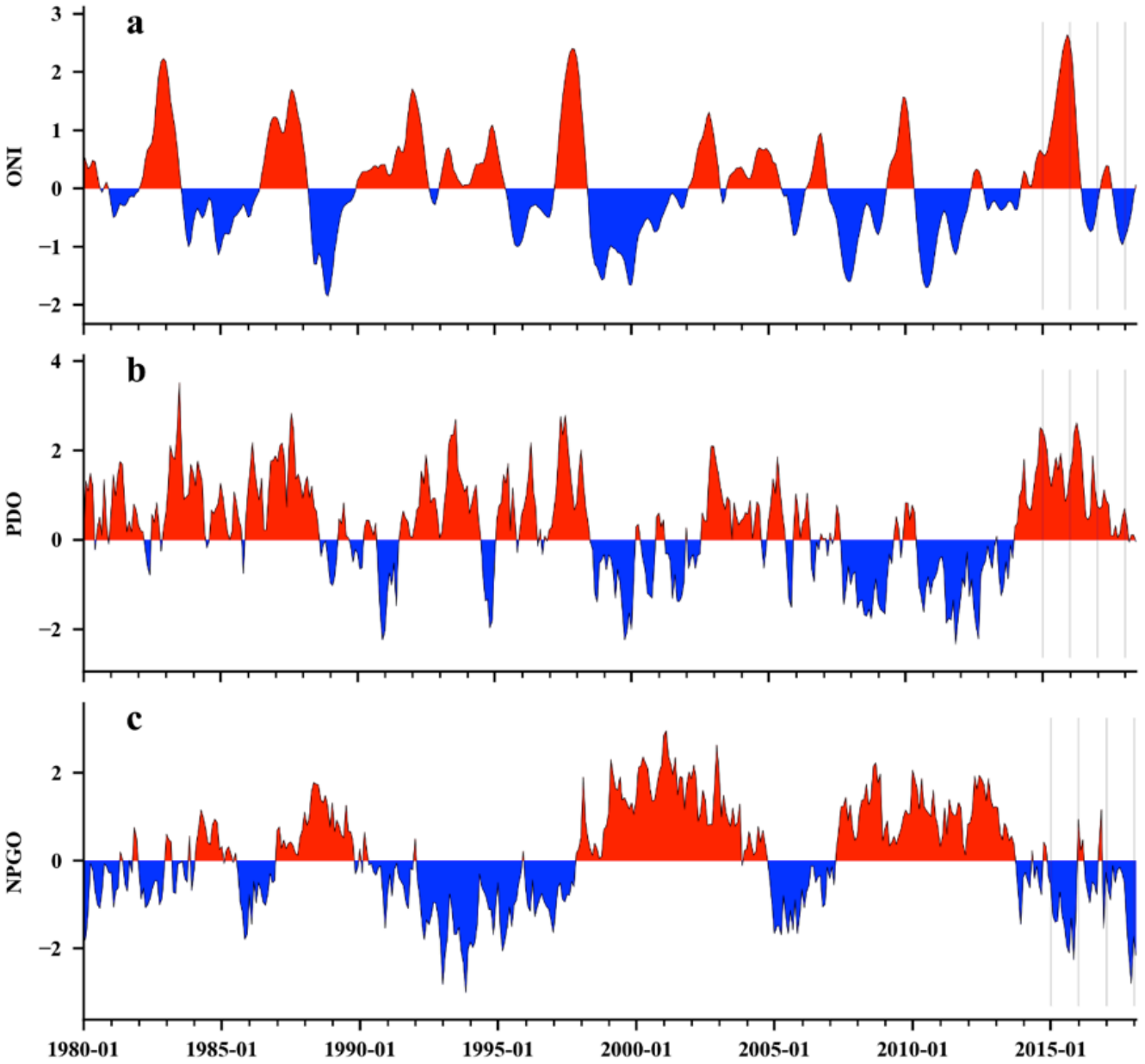

Figure 2. Time series of monthly values for three ocean climate indices especially relevant to the California Current: a) Oceanic Niño Index (ONI; January 1980 to June 2018), b) Pacific Decadal Oscillation (PDO; January 1980 to June 2018), and c) North Pacific Gyre Oscillation (NPGO; January 1980 to February 2018). Vertical lines mark January 2015, 2016, 2017, and 2018. Monthly data obtained from http://upwell.pfeg.noaa.gov/erddap/.

The Oceanic Niño Index[2] (ONI), a three-month running mean of SST anomalies averaged over 5°S–5 °N and 120°W–170°W (NINO3.4 region), transitioned from peak El Niño conditions at the start of 2016 to weak La Niña conditions by the end of 2016 (fig. 2A). While the 2015–16 ONI values rivaled those of the record 1997–98 El Niño event, its impact along the US West Coast was less pronounced (Jacox et al. 2016). In 2017 ONI values briefly switched to positive during the spring and summer, but were lower than the 0.5°C threshold that signifies an El Niño event. Negative ONI values lower than –0.5°C (the threshold for a La Niña event) occurred during October 2017 and lasted until March 2018 (fig. 2A). The ONI then increased in the subsequent 3 months and was at 0.1 in July 2018. As of 24 September 2018 NOAA's Climate Prediction Center[3] forecast a 55% chance for a tropical El Niño to develop in fall 2018 and a 70% chance by winter 2018–19.

The Pacific Decadal Oscillation[4] (PDO) index describes the temporal evolution of dominant spatial patterns of SST anomalies over the North Pacific

[2]http://www.cpc.ncep.noaa.gov/data/indices/

[3]http://www.cpc.ncep.noaa.gov/products/analysis_monitoring/lanina/

[4]http://research.jisao.washington.edu/pdo/PDO.latest.txt

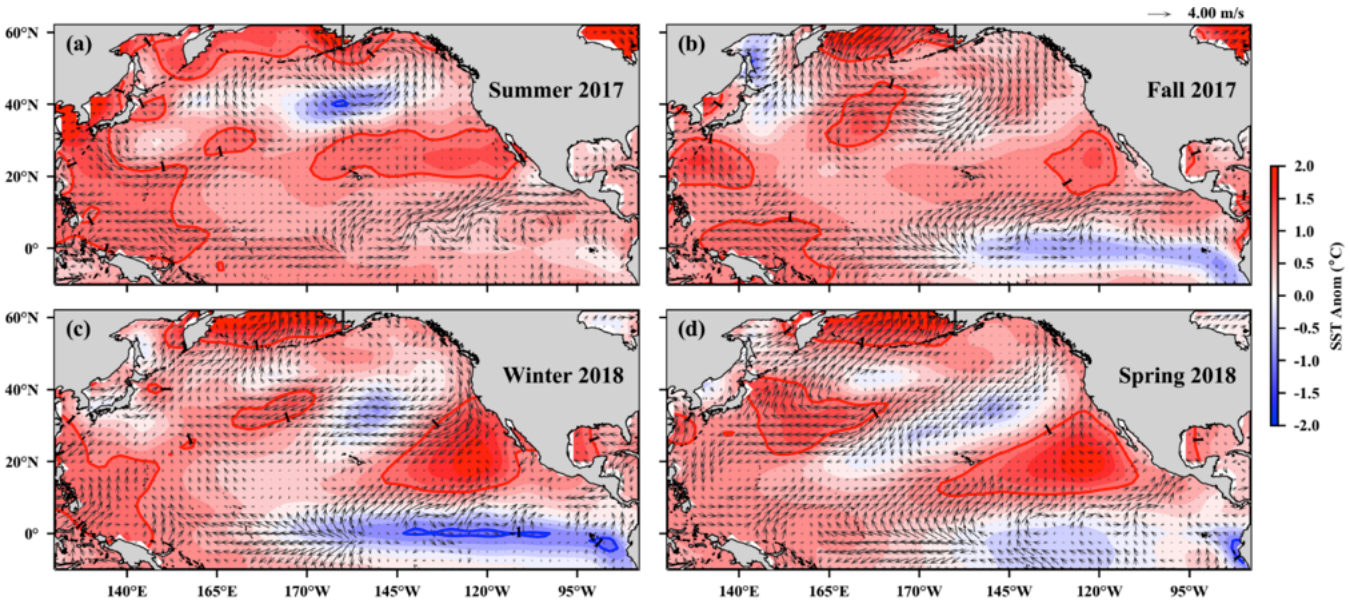

Figure 3. Anomalies of surface wind velocity and sea surface temperature (SST) in the North Pacific Ocean for summer (a: June–August) 2017, fall (b: September–November) 2017, winter (c: December–February) 2018, and spring (d: March–May) 2018. Arrows denote magnitude and direction of wind anomaly (scale arrow at top right). Contours denote SST anomaly. Shading interval is 0.25°C and contour intervals at ±1°C are shown. Wind climatology period is 1968–96. SST climatology period is 1950–79. Wind NCEP/NCAR Reanalysis data and NOAA Extended Reconstructed SST V5 data were obtained from http://www.esrl.noaa.gov.

(Mantua et al. 1997). Positive PDO values are associated with a shallower upwelling cell in the northern CCS (Di Lorenzo et al. 2008). The PDO was positive for all of 2016 with peak values in the spring and lowest values in the summer (fig. 2B). The April 2016 value of 2.62 was the largest value during the large marine heat wave and El Niño event of 2014–16. Positive PDO values persisted for all of 2017 but were relatively low, particularly during the summer. As of March 2018 the PDO recorded the first negative value since December 2013 (–0.05) and remained close to zero (–.04) through June 2018.

The North Pacific Gyre Oscillation[5] (NPGO) is a low-frequency signal of sea surface height variations across the North Pacific, indicating variations in the circulation of the North Pacific Subtropical Gyre and Alaskan Gyre (Di Lorenzo et al. 2008). Positive values of the NPGO are linked with increased equatorward flow in the California Current, along with increased surface salinities, nutrients, and chlorophyll *a* values in the southern-central CCS (Di Lorenzo et al. 2009). Negative NPGO values are associated with decreases in these variables, inferring less subarctic source waters, fewer nutrients, reduced upwelling, and generally lower production in the CCS. The NPGO had short-duration positive values in the winter of 2016–17 and fall of 2016, which were some of the few positive values observed since 2013 (fig. 2C). The 2017 NPGO values were negative throughout the year, with the largest negative values in the fall. In fact, the negative values from October 2017 to February 2018 were some of the lowest NPGO values documented in records dating back to 1950.

North Pacific Climate Patterns

A basin-scale examination of seasonal SST and surface wind anomalies allows for the interpretation of the spatial evolution of climate patterns and wind forcing over the North Pacific (figs. 2, 4). During summer 2017, positive SST anomalies extended across the central and eastern Equatorial Pacific (fig. 3), which was reflected in the positive ONI values (fig. 2). Tropical La Niña conditions emerged during fall 2017 and were fully actualized by winter 2018, with temperature anomalies between –0.5 to –1°C in the NINO3.4 region[6] (fig. 3). However, the spring 2018 temperature anomalies increased and only a small region along the South American coast had temperature anomalies less than –1°C. Warm temperature anomalies persisted from fall 2017 through spring 2018 in the Bering Sea and the Gulf of Alaska, with the Bering Sea having temperature anomalies higher than 1°C. In the eastern Pacific a general pattern of negative anomalies centered along 40°N and positive anomalies centered along 20°N appeared in all seasons, though the negative anomalies were very small in spatial extent during fall 2017. The negative anomalies were mostly less than –1°C and were a continuation of spatial patterns observed since the summer of 2016 (Wells et al.

[5]http://www.o3d.org/npgo/roms.html

[6]The NINO3.4 region is bound by 90°W-150°W and 5°S–5°N

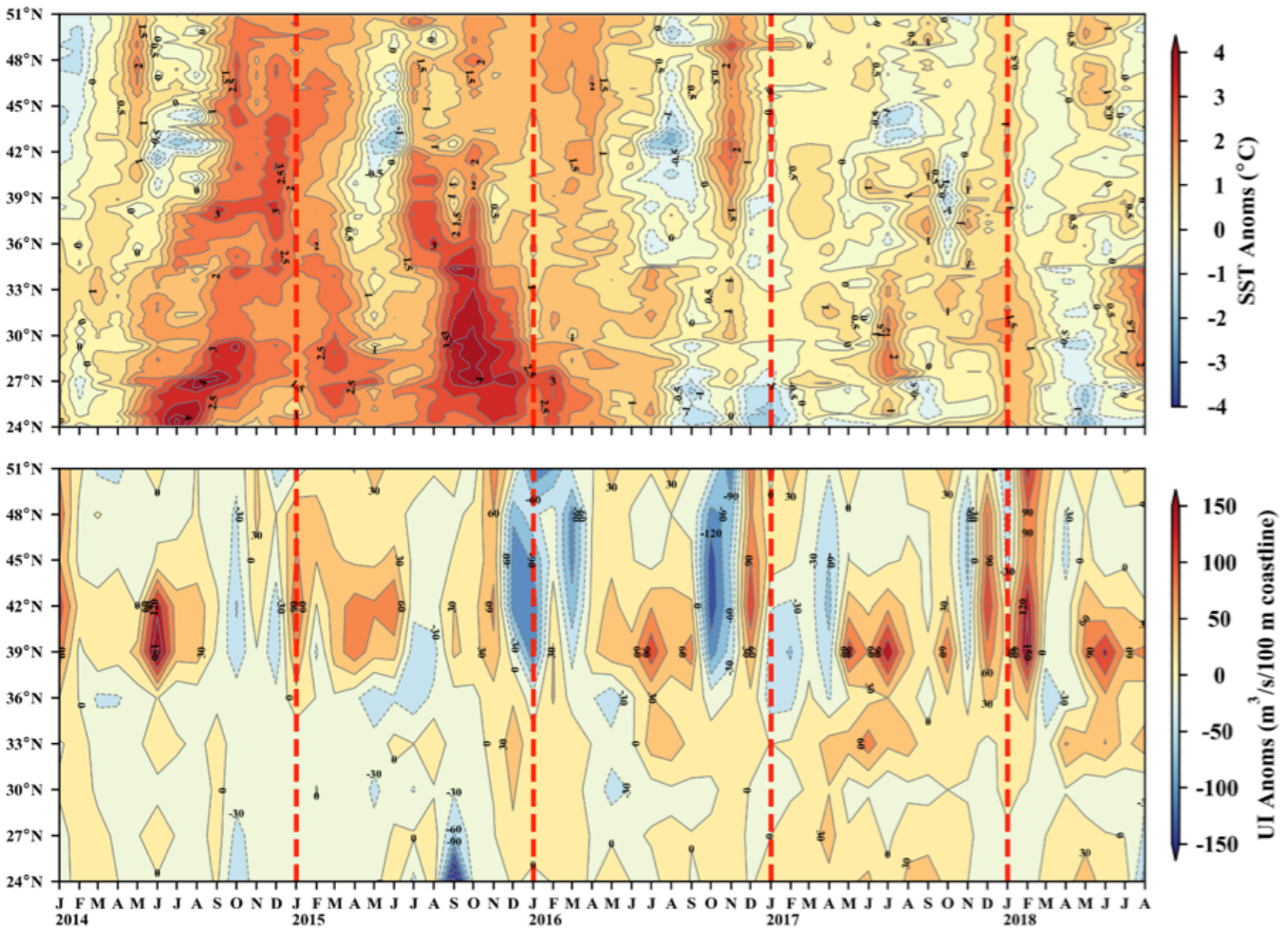

Figure 4. (A) Monthly sea surface temperature (SST) anomalies (top) and upwelling index (UI) anomalies (bottom) for January 2014–August 2018. The SST anomalies are averaged from the coast to 75 km offshore. Positive and negative upwelling anomalies denote greater than average upwelling or downwelling (usually during the winter), respectively. Anomalies are relative to 1982–2018 monthly means. Daily optimum interpolation AVHRR SST data obtained from http://coastwatch.pfeg.noaa.gov/erddap/griddap/ncdcOisst2Agg. Six-hourly upwelling index data obtained from http://oceanview.pfeg.noaa.gov/erddap/tabledap/.

2017). The positive anomalies were above 1°C, with the largest onshore values extending from San Francisco Bay, California, to southern Baja California, Mexico, during winter 2017–18 and spring 2018.

The trade winds over the western Equatorial Pacific were stronger than normal in all four seasons from summer 2017 to spring 2018 as indicated by the anomalous easterly winds between 165°E–180° (fig. 3). Lower than average sea-level pressure during summer 2017 produced cyclonic wind anomalies in the Gulf of Alaska. By fall 2017 and winter 2018 the low pressure was replaced by anomalously high pressure and anticyclonic wind patterns in the Bering Sea and Gulf of Alaska. Within the CCS winds along the coast were near the long-term average during summer and fall 2018. Large northerly wind anomalies occurred during winter 2017–18 indicating stronger upwelling-favorable winds in the central CCS region and a relaxation of downwelling winds along the coast of Washington and Oregon. The upwelling-producing winds that usually start during the spring were considerably weaker than the long-term average as indicated by the southerly wind anomalies.

COAST-WIDE CONDITIONS

Upwelling in the California Current

Monthly anomalies of SST (averaged from the coast to 100 km offshore) and upwelling are used to examine anomalous coastal upwelling conditions within the CCS from January 2016 to May 2018 (fig. 4). Upwelling estimates come from two sources: the Bakun upwelling index (UI; fig. 4A) (Bakun 1973; Schwing et al. 1996), and the Coastal Upwelling Transport Index (CUTI), which is derived from a data-assimilative regional ocean model (fig. 4B) (Jacox et al. 2014; Jacox et al. 2018b). We present both upwelling indices because the UI has long been used in many past studies of the California Current, but in some places, particularly south of 39°N,

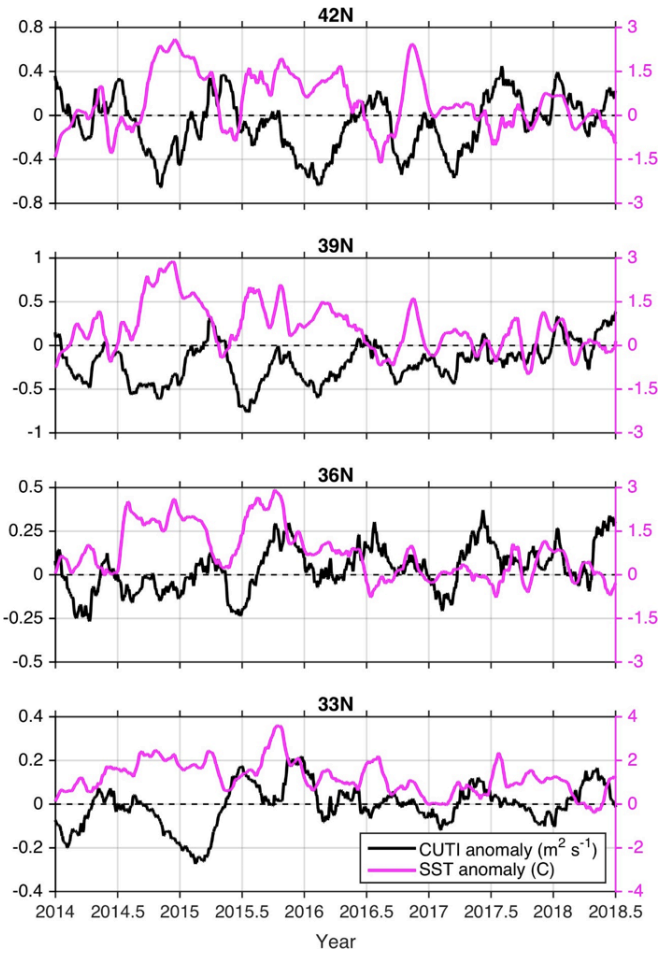

Figure 4. (B) The Coastal Upwelling Transport Index (CUTI; black) and SST anomalies (magenta) relative to the 1980-2010 climatology, derived from a data assimilative ocean reanalysis of the California Current System (Jacox et al. 2018), are shown at four latitudes off the US West Coast. Values are averaged from the coast to 75 km offshore. SST is smoothed with a 30-day running mean; CUTI is smoothed with a 90-day running mean. Model output is obtained from oceanmodeling.ucsc.edu and CUTI is obtained from https://oceanview.pfeg.noaa.gov/products/upwelling/.

it is a less reliable indicator of upwelling due to relatively poor estimation of the wind stress and modulation of upwelling by the cross-shore geostrophic flow (Bakun 1973; Jacox et al. 2014; Jacox et al. 2018b).

High SST anomalies due to the 2014–16 marine heat wave were evident until spring 2016 (fig. 4). Positive SST anomalies (>1°C) persisted through much of the region during winter 2015–16 and spring 2016, especially for locations north of 42°N and south of 30°N. From January to May 2017, SST anomalies north of 42°N were near the long-term average, with the exception of a few localized periods of ~ +0.5°C anomalies. Positive SST anomalies were higher for latitudes south of 42°N and a few locations experienced anomalies greater than 1°C during summer/fall 2017. January 2018 SST anomalies were 0.5 to 1°C warmer than average for all latitudes. A slight drop in temperature anomalies, to near climatological values, occurred in February to March. Starting in June 2018, large positive anomalies appeared in the southern California Bight between latitudes 27–33°N, culminating with anomalies exceeding 2°C by August.

In the winter of 2015–16, upwelling anomalies were negative north of 33°N (fig. 4), which reflects conditions during the previous El Niño winters. However, these upwelling anomalies were positive at 33°N and farther south, an atypical pattern that contributed to a relatively muted impact of the 2015–16 El Niño off California (Jacox et al. 2016; Frischknecht et al. 2017). The most upwelling-favorable anomalies during 2016 occurred from July to September for latitudes between 36°–42°N, followed by strong downwelling anomalies in October and November 2016 north of 36°N. The largest negative upwelling anomalies during early 2017 were for latitudes 36°–45°N. Upwelling during May to October 2017 was generally average to above average for the whole coast, with the largest positive anomalies in late spring/early summer. Strong positive upwelling anomalies occurred between 39°–42°N at the end of 2017 and beginning of 2018. Upwelling anomalies were positive again in late spring 2018 after a period of average to slightly below average upwelling in the preceding months. SST and upwelling anomalies along the coast are highly negatively correlated throughout the CCS, with the strongest correlations at more northern latitudes due to a strong coupling between local winds and SST (fig. 4B) (Frischknecht et al. 2015).

The cumulative upwelling index (CUI) is the cumulative sum of the daily UI values starting January 1 and ending on December 31, and it provides an estimate of the net influence of upwelling on ecosystem structure and productivity over the course of the year (Bograd et al. 2009). In general, upwelling was slightly stronger in 2018 than the previous two years (fig. 5). During winter 2015–16, upwelling north of 39°N was low due to the El Niño and strong upwelling only began in the summer. South of 39°N, upwelling anomalies were neutral to positive in early 2016, counter to what would be expected from a strong El Niño (Jacox et al. 2015). Upwelling during 2017 was near the long-term average for the whole coast except between 36°–42°N. For these latitudes, the CUI curves during winter 2017–18 were below the climatological curve, and upwelling began in early May. Strong upwelling during February 2018 pushed the CUI curves to above the long-term average; however, downwelling starting in April dropped the CUI curves towards the long-term average for latitudes 36°N and 45°–48°N. Summer 2018 upwelling was strong at 39°N, with the CUI curve at one of its highest yearly values at the end of August.

Periods of upwelling, or farther north reduced downwelling, during the winter can limit stratification

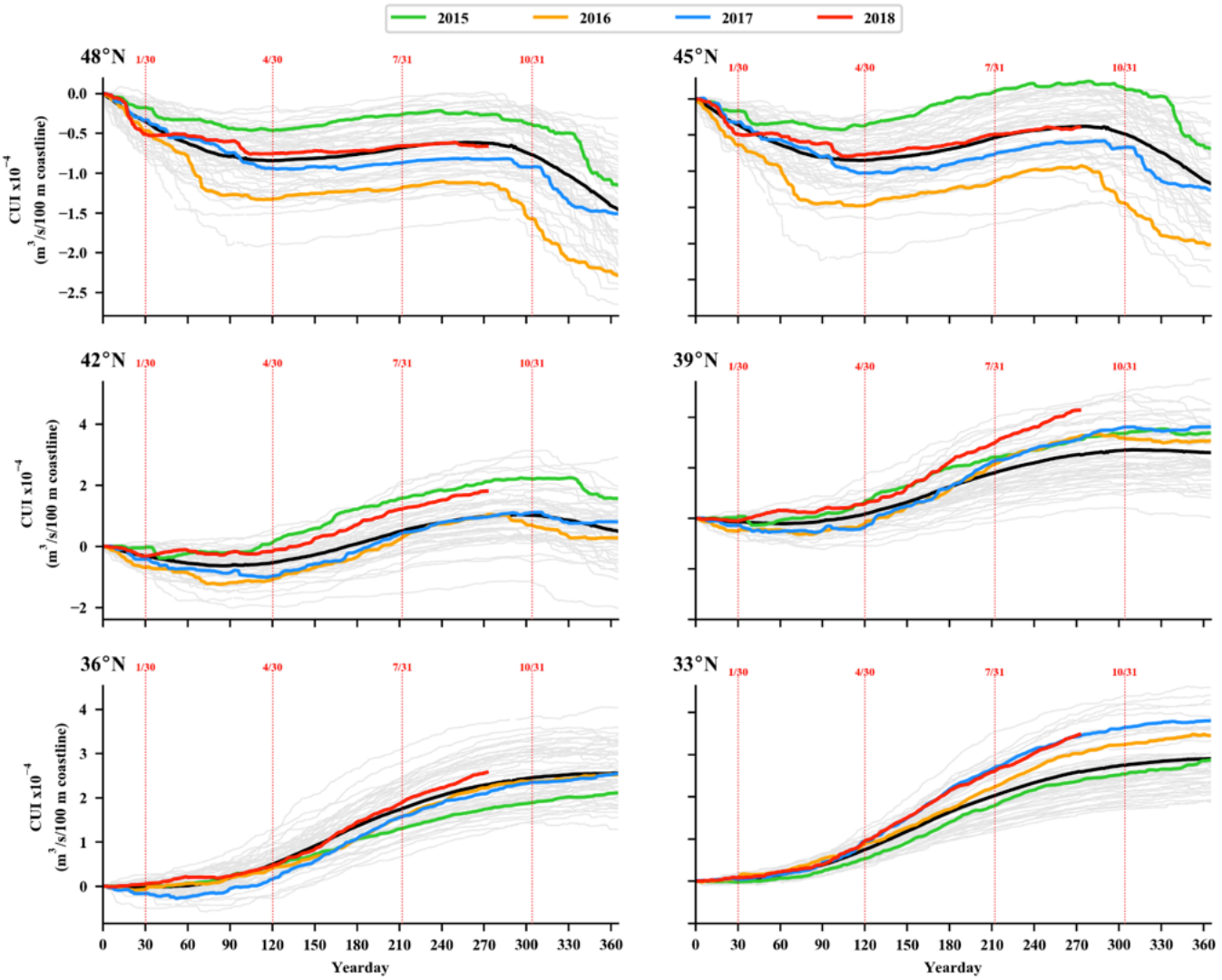

Figure 5. Cumulative upwelling index (CUI) starting on January 1 calculated from the daily upwelling index at three locations along the West Coast of North America. Grey lines are all yearly CUI for 1967–2014, colored CUI curves are for the years 2015–18. The climatological mean CUI is the black line. The red dashed vertical lines mark the end of January, April, July, and October. Daily upwelling index data obtained from http://upwell.pfeg.noaa.gov/erddap/.

and facilitate introduction of nutrients to the surface, acting to precondition the ecosystem for increased production in the spring (Schroeder et al. 2009; Black et al. 2010). The area of the surface atmospheric pressures associated with the North Pacific High (NPH) can be used as an index of this winter preconditioning (Schroeder et al. 2013). Since 2014 there has been a continual weak NPH during the winter (January–February; fig. 6). The NPH area increased in 2018 relative to the past four years but was still much smaller than the exceptionally large area in 2013.

Coastal Sea Surface and Subsurface Temperatures

SSTs measured by National Data Buoy Center buoys along the West Coast were generally above the long-term mean for all buoys from 2015–18 (fig. 7). There were periods of reduced temperatures that were below the long-term mean, such as during August 2016 for buoys north of Bodega Bay and during October 2017 for buoys 46022 (northern California) and 46013 (Bodega Bay). During 2018 a shift towards cooler temperatures occurred in February for buoys north of Santa Monica. These shifts to cooler temperatures were associated with increased northerly, upwelling-favorable winds. In February 2018 winds were strongly upwelling-favorable but switched directions or diminished during March. Buoys along the southern California coast (46011 and 46025) experienced periods of very high temperatures during summer 2018, with buoy 46025 (Santa Monica) experiencing the longest duration of sustained positive anomalies.

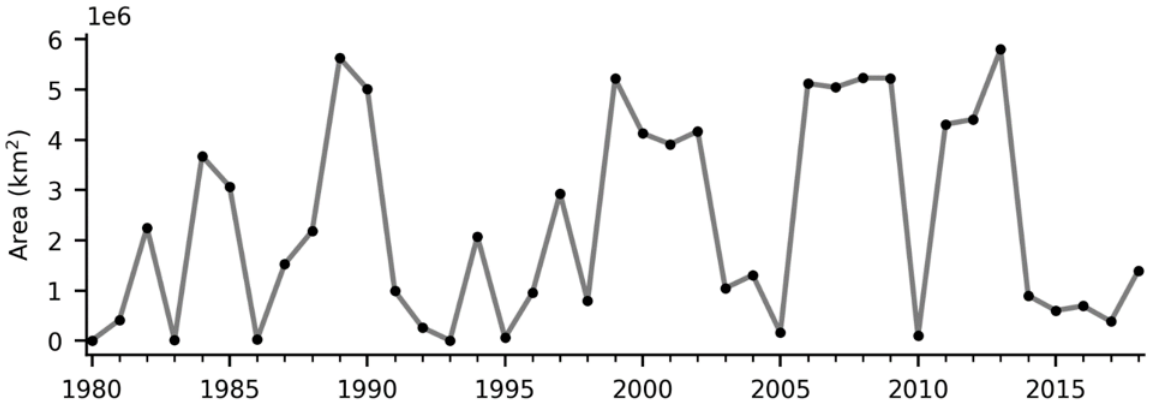

Figure 6. The area of high atmospheric pressure of the North Pacific High averaged over January and February each year, 1980-2018. The area is the areal extent of the 1020 hPa isobar located in the eastern North Pacific.

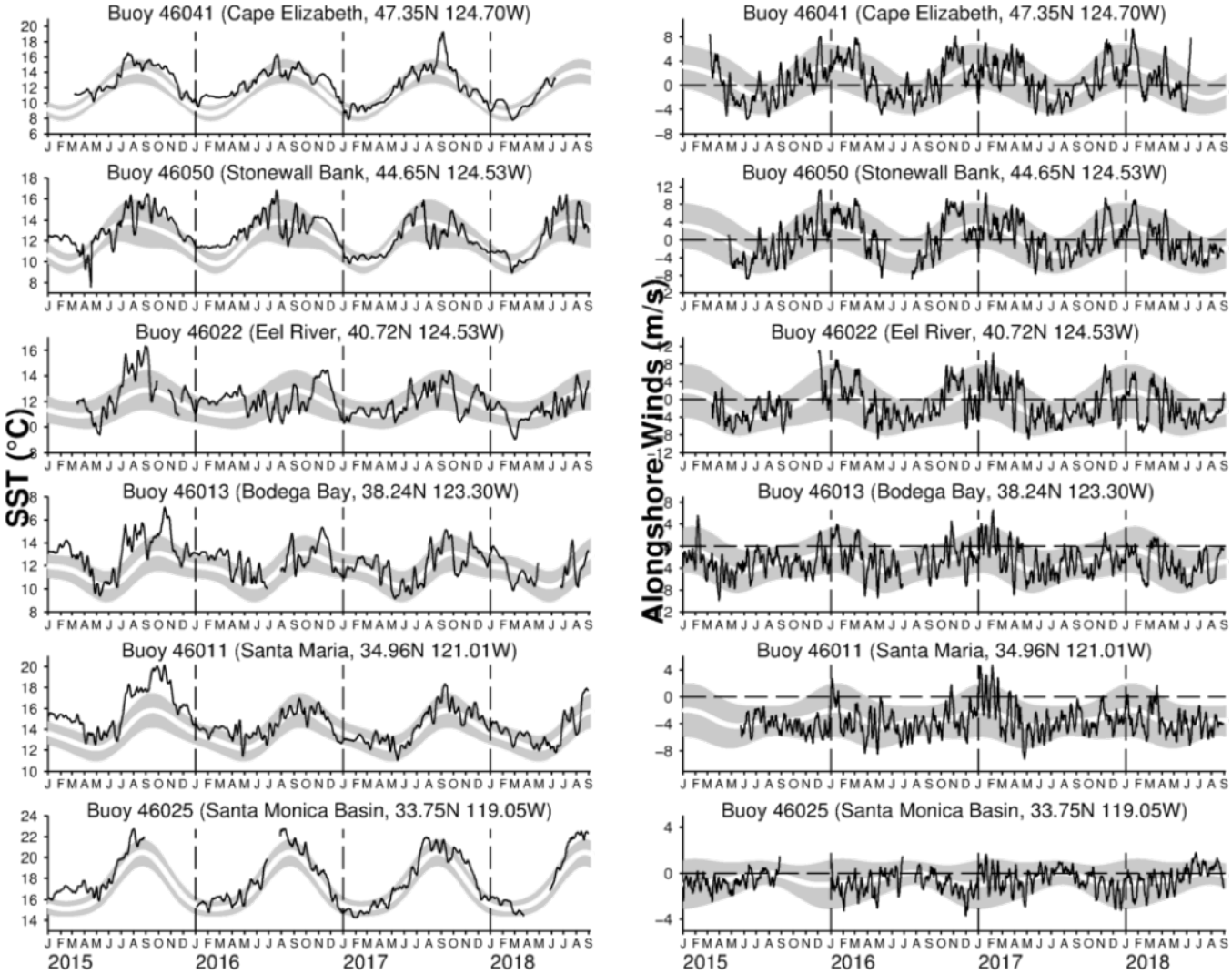

Figure 7. Time series of daily sea surface temperatures (left) and alongshore winds (right) from various National Data Buoy Center (NDBC) coastal buoys along the CCS for January 2016 to August 2018. The wide white line is the biharmonic annual climatological cycle at each buoy. Shaded areas are the standard errors for each Julian day. Series have been smoothed with a 7-day running mean. Data provided by NOAA NDBC. Additional buoy information can be found at http://wwwndbc.noaa.gov/.

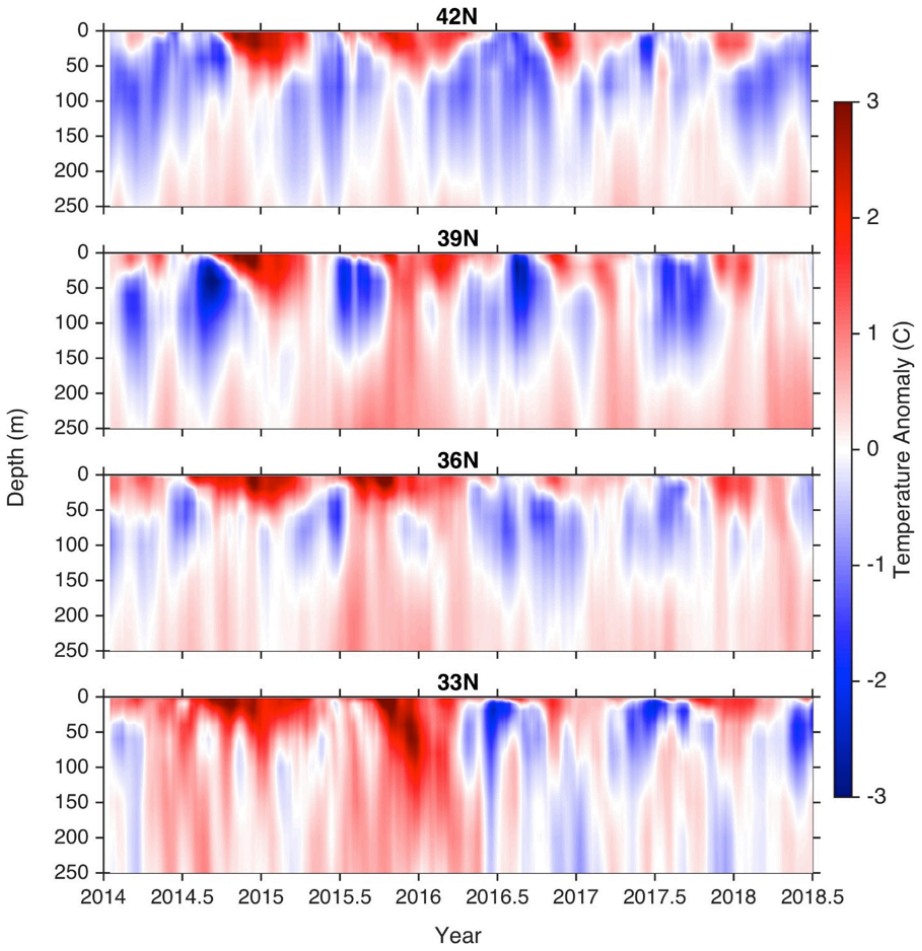

Figure 8. Temperature anomalies relative to the 1999–2011 climatology, derived from a data assimilative ocean reanalysis of the California Current System (http://oceanmodeling.ucsc.edu/ccsnrt/), are shown at four latitudes off the US West Coast. Temperatures are averaged from the coast to 100 km offshore and smoothed with a 30-day running mean.

The signature of the northeast Pacific marine heat wave was evident at all latitudes beginning in late 2014 and extending through mid-2016, with penetration deeper in the water column at more southern latitudes (fig. 8), based on upper ocean temperature anomalies from ROMS averaged from the coast to 100 km offshore at latitudes of 33°, 36°, 39° and 42°N. Since mid-2016, subsurface temperatures cooled throughout much of the CCS (fig. 8), though surface temperatures remain elevated particularly in winter, which may indicate reemergence of preexisting temperature anomalies when the mixed layer deepens (Alexander et al. 1999).

Primary Production in the California Current System

Spring 2018 chlorophyll *a* anomalies had similar spatial patterns to those in 2017, with negative anomalies along the majority of the coast (fig. 9, top panels).[7] Positive anomalies in 2018 were localized around the Columbia River, San Francisco Bay, and along the coast south of Monterey Bay. Predicted domoic acid concentrations were higher and more widespread between Monterey Bay and the southern US border in 2018 than in the previous two years (fig. 9, bottom panels). Furthermore, predicted domoic acid concentrations did not appear to be concentrated in areas of positive chlorophyll anomalies, unlike in previous years (Wells et al. 2017).

Despite widespread predictions of high domoic acid concentrations in 2017–18, harmful algal blooms along the California coast returned to "normal" conditions, with toxin events localized to many previously identified hot spots, including southern California, Santa Barbara Channel, Monterey Bay, and off the coast of Humboldt County, California. While there were no region-wide blooms or closures, domoic acid levels in southern California and the Santa Barbara Channel equaled or exceeded the 2015

[7]https://www.nwfsc.noaa.gov/research/divisions/efs/microbes/hab/habs_toxins/hab_species/pn/index.cfm

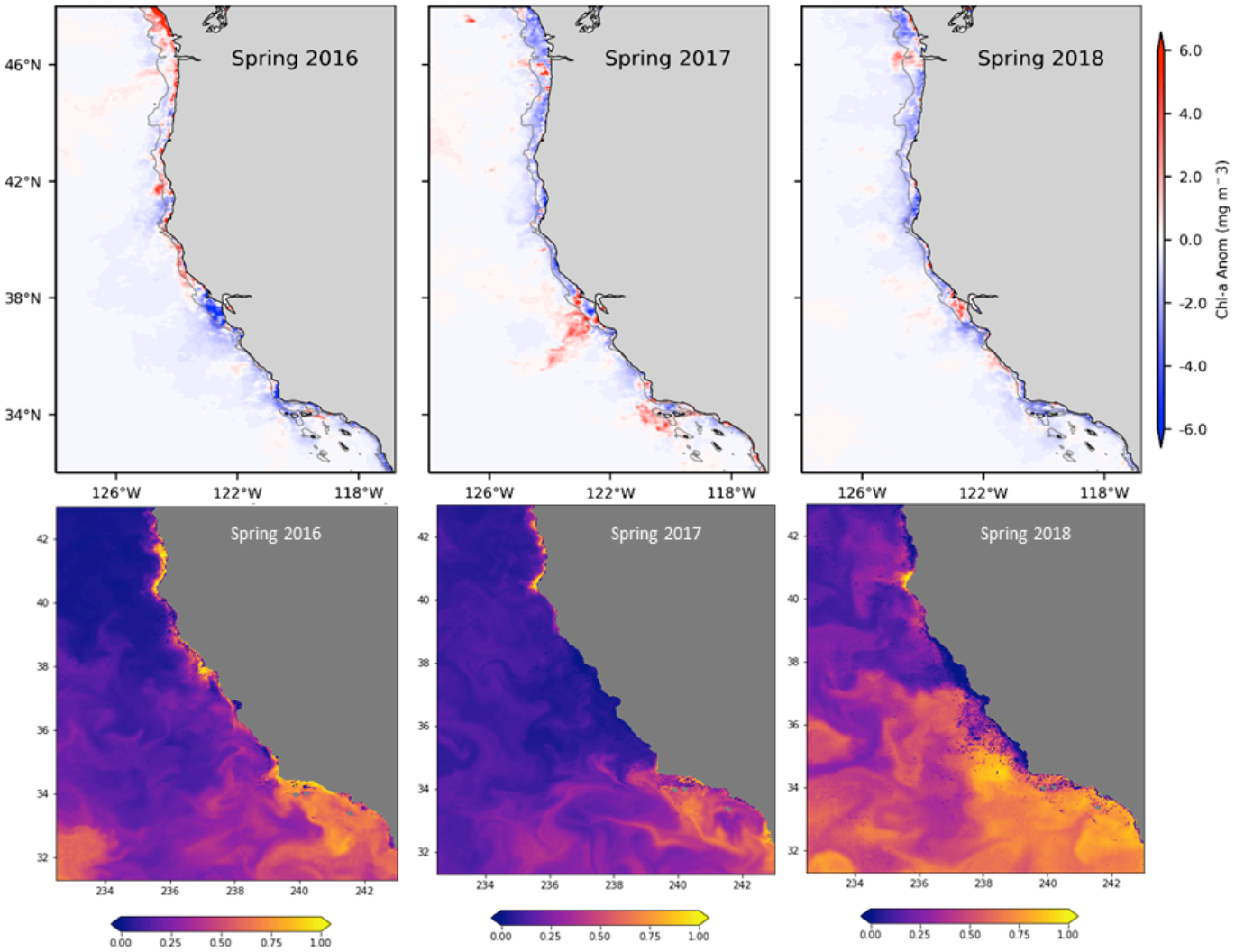

Figure 9. Top) Chlorophyll *a* anomalies from Aqua MODIS for: spring (March–May) of 2016–18. Monthly anomalies were averaged onto a 0.1˚ x 0.1˚ grid and the climatology was based on the time period from 2003–17. The data were obtained from http://coastwatch.pfel.noaa.gov/. Bottom) Predicted probability of domoic acid > 500 nanograms/L from spring 2016-18 from http://www.cencoos.org/data/models/habs/previous.

bloom event and resulted in a suspected bird die-off and elevated marine mammal strandings in that region during spring 2017.

Currents

During spring 2017 surface currents[8] were predominantly southward from the Columbia River (46˚N) south to Point Conception (34˚N) and continued to be southward south of Point Conception in the far-western portion of the Southern California Bight (fig. 10). Although the southward tendency continued through summer, surface currents were marked by a noted offshore orientation throughout the region. In the fall, alongshore flow switched northward for the region north of Cape Mendocino (40˚N), while it remained southward and offshore-directed south of Cape Mendocino. Offshore anticyclonic mesoscale eddies, centered around 39˚N and 36˚N, interacted with shelf jets off Point Arena, Point Reyes, and Point Sur. Coherent westward flow out of the Santa Barbara Channel continued from summer through fall and into winter. Over the shelf in winter, northward transport was observed from Point Conception (34˚N) north to the Columbia River (46˚N) and broad coherent northward flows were observed north of Cape Mendocino, whereas farther south, offshore-directed flow persisted and the influence of offshore mescoscale features were observed around 35˚N.

[8]These data on surface currents were obtained from High-Frequency (HF) Radar, with vectors calculated hourly at 6-km resolution using optimal interpolation. Real-time displays can be viewed at www.sccoos.org/data/hfrnet/ and www.cencoos.org/sections/conditions/Google_currents/ as well as at websites maintained by the institutions that contributed the data reported here.

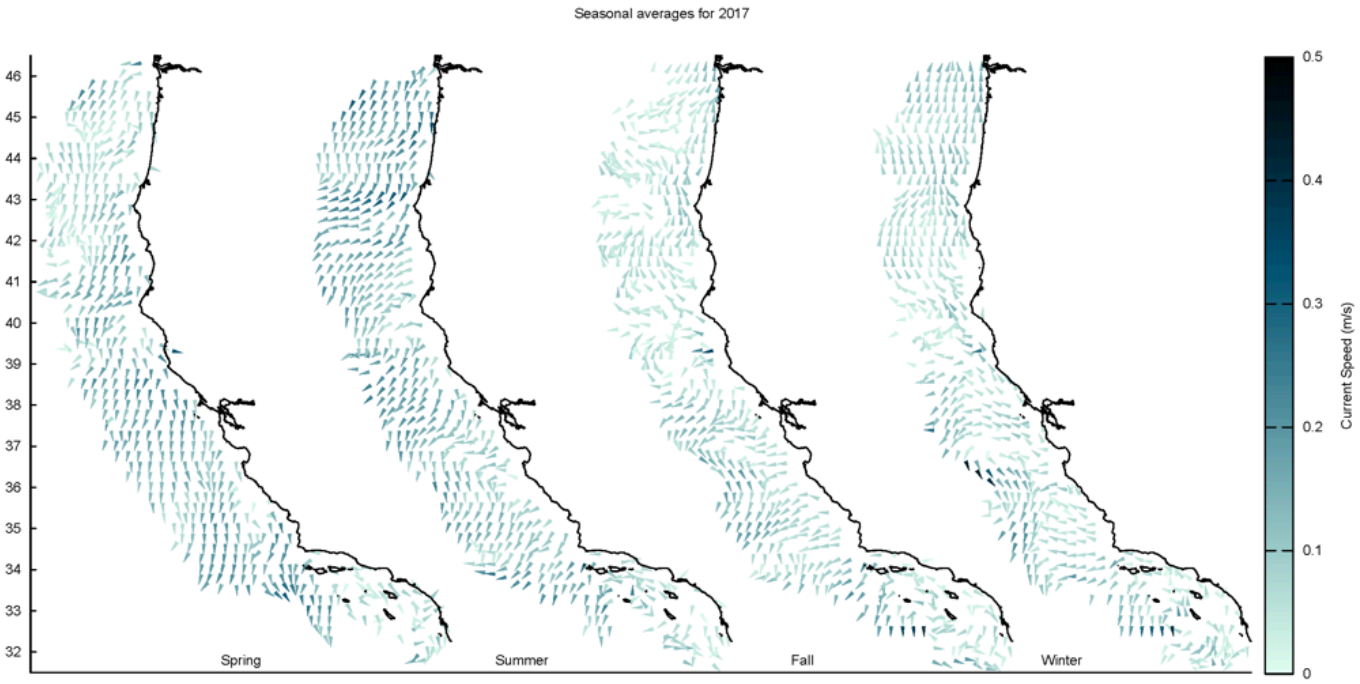

Figure 10. Maps of seasonal mean surface currents observed in the CCS with HF radar. From left to right, the panels present data for spring (March–May 2017), summer (June–August 2017), fall (September–November 2017), and winter (December–February 2018). Current speed is indicated by depth of shading and direction given by orientation of arrow extending from observation location. Currents are displayed with a spatial resolution of 0.25° which means that nearshore flows are not well represented here.

REGIONAL OBSERVATIONS OF ENVIRONMENT AND LOWER TROPHIC LEVELS

Northern California Current: Oregon (Newport Hydrographic Line)

The temperature anomaly at 50 m from station NH-5 off Newport, Oregon, was positive for almost the entire duration between 2014 and 2018, although the magnitude of the anomaly decreased in 2017 and 2018 (fig. 11). At 150 m at station NH-25 off Newport, the temperature anomaly was also strongly positive from the spring of 2014 until summer 2017. In late 2017 the temperature anomaly at 150 m was quite high, but it fell to a negative anomaly in early 2018, then rose again and became positively anomalous in mid-2018. Warm ocean conditions in this region are associated with a lipid-poor copepod community and a gelatinous-dominated zooplankton community that has persisted from September of 2014 (Peterson et al. 2017) into 2018. However, the strength of the anomalies has lessened since fall 2017, signaling that the pelagic ecosystem may be in a state of flux.

In 2017, the upwelling season (physical spring transition) began on April 26, eleven days later than the 40-year climatological average, and ended on 15 October (figs. 4, 5). The resulting upwelling season was average in length, with overall cumulative upwelling being slightly higher than the long-term mean (figs. 4, 5). Upwelling was weak in May and June 2017 with some strong periods of downwelling which resulted in positive SST anomalies and strongly positive 150 m temperature anomalies on the shelf (fig. 7, buoy 46050). Upwelling was persistent from mid-June until mid-September. During this period SST anomalies were negative and temperature at 150 m on the shelf was neutral. Hypoxic oxygen concentrations below 1.4 ml/L were observed[9] on the shelf, with an oxygen value of 0.29 ml/L recorded in September of 2017 that was the lowest measurement observed in the 12-year time series (data not shown). Following the upwelling season in 2017, strong winter storms mixed the deep water on the slope off Oregon and negative temperature anomalies persisted for two months during the winter of 2017–18; however, the shelf waters remained warmer than average throughout the winter and into the summer of 2018 (fig. 11). With the exception of two months during the 2015 and 2017 upwelling season, nitrogen concentrations on the shelf remained below average since the fall of 2015 and continue to be low into 2018 (fig. 11).

The zooplankton community[10] was largely comprised of lipid-poor southern species from September 2014 until the summer of 2017 when the copepod

[9]https://www.nwfsc.noaa.gov/news/blogs/display_blogentry.cfm?blogid=1&month=9&year=2017

[10]Copepod data were based on samples collected with a 0.5 m diameter ring net of 202-µm mesh, hauled from near the bottom to the sea surface. A TSK flowmeter was used to estimate volume of water sampled.

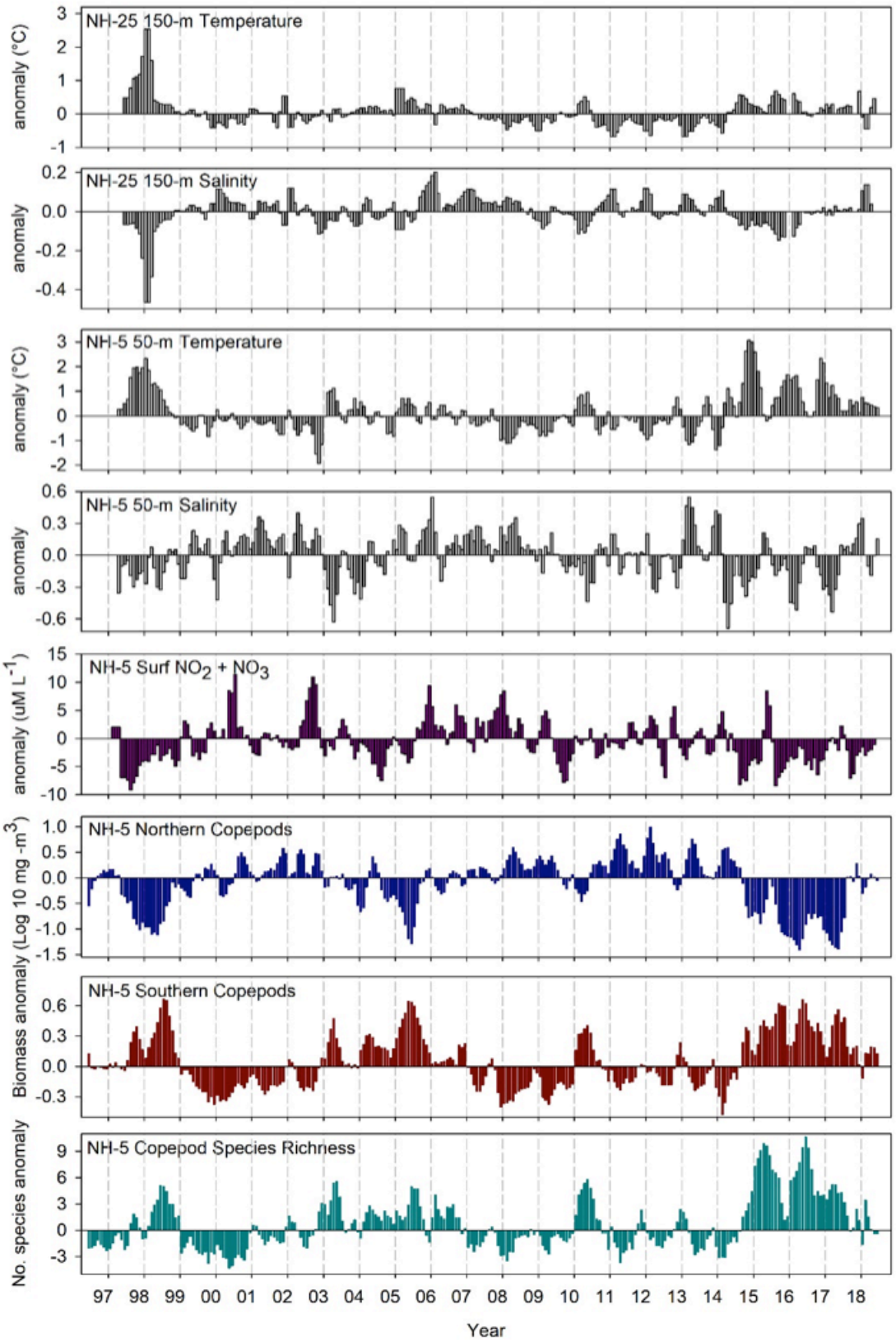

Figure 11. Time series plots of local physical and biological anomalies (monthly climatology removed) from 1996–present at NH-25 (Latitude: 44.6517 N Longitude: 124.65 W; top two panels) NH-5 (Latitude: 44.6517 N Longitude: 124.1770 W; lower six panels) along the Newport Hydrographic Line. Temperature and salinity are from 150 m and 50 m at NH-25 and NH-5, respectively, NO2 + NO3 from the surface, and copepod biomass and species richness anomalies are integrated over the upper 60 m. All data were smoothed with a 3-month running mean to remove high frequency variability.

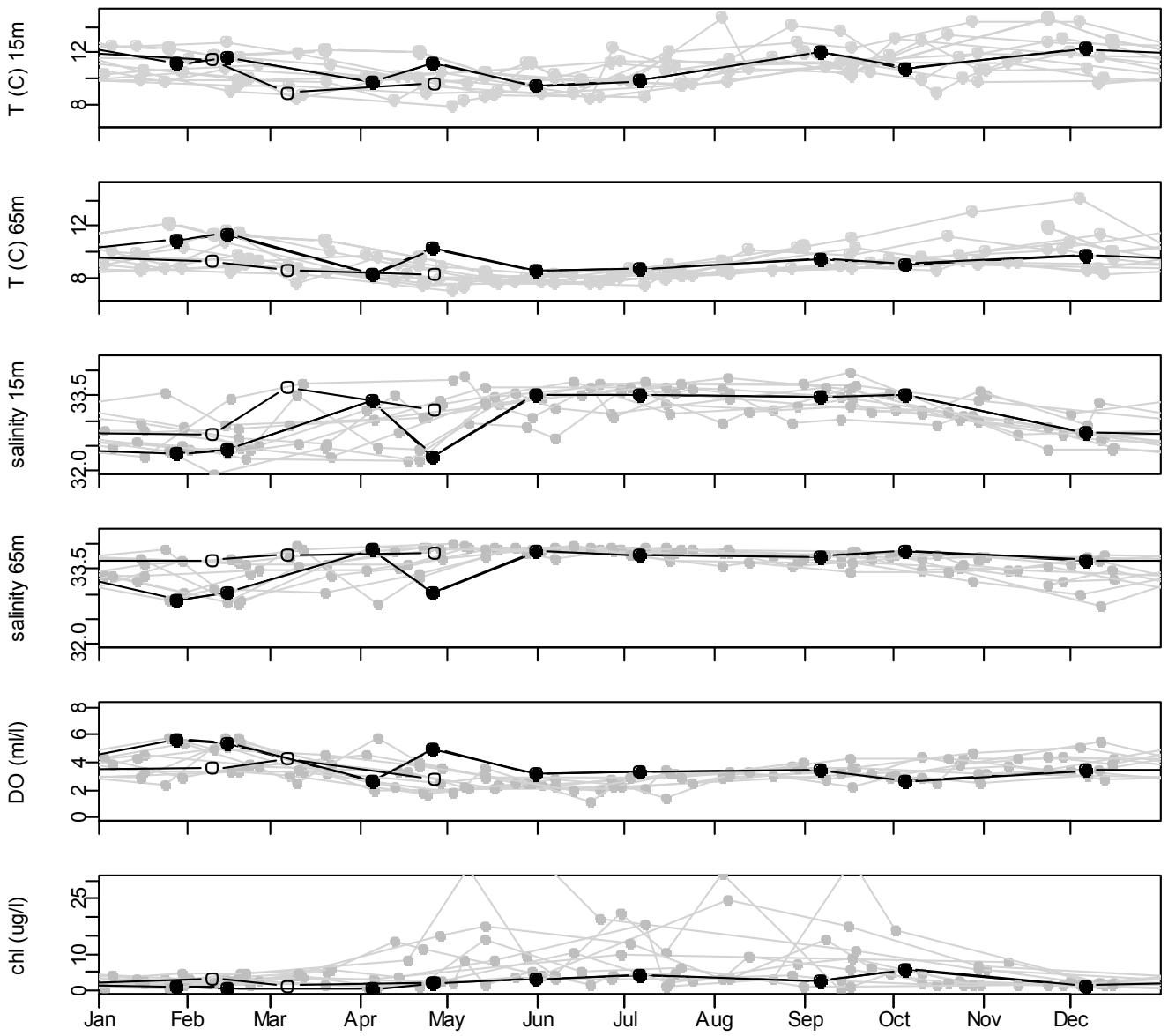

Figure 12. Hydrographic observations along the Trinidad Head Line (THL) at station TH02. Panels from top to bottom show temperature (T) at 15 m, temperature at 65 m (near the sea floor), salinity at 15 m, salinity at 65 m, dissolved oxygen (DO) at 65 m, and mean (uncalibrated) chlorophyll *a* (chl) concentration from 2–30 m. Closed black circles are 2017, open circles are 2018, and grey are previous years of the time series.

community transitioned to a more neutral state (fig. 11). When strongly positive temperature anomalies occurred from fall 2014 until summer 2017, strongly positive anomalies of copepod species richness and southern copepod biomass were observed on the Oregon shelf, coupled with strongly negative anomalies of northern copepod biomass. During the persistent upwelling season in 2017 (June–September), the positive temperature anomalies on the shelf and slope weakened as did the strongly positive southern copepod biomass and species richness anomalies, while the northern copepod biomass became neutral. In winter of 2017–18, species richness anomalies and the biomass anomalies of the northern copepods oscillated from weakly positive to weakly negative, while positive anomalies of the southern copepods persisted.

In 2015 and 2016, the copepod community did not transition from a warm-water winter copepod community to a cold-water summer community (data not shown). This ecologically important biological transition to a lipid-rich, cold-water community also did not occur in 1998, when warm ocean conditions occurred in the NCC. However, this transition did occur in late June 2017, 52 days later than the 21-year average climatology. In 2018 this biological transition occurred in late May, 22 days later than the climatology (data not shown). During the spring and summer of 2018, the shelf and slope water were still warmer than average off

Oregon and abundances of southern copepods on the shelf were higher than normal. However, the biomass of the northern copepods was more neutral, signaling that the pelagic ecosystem was in a state of flux between a warm and a cold upwelling copepod community.

Another indication that the pelagic ecosystem did not fully return to a cold water, lipid-rich state in 2018 is the presence in high densities of the subtropical colonial tunicate (*Pyrosoma atlanticum*; pyrosomes). These organisms are common in subtropical open ocean environments, and they bloomed in large numbers throughout the coastal waters from Oregon to the Gulf of Alaska during the winter of 2016 (Brodeur et al. 2018). These organisms were collected in large numbers throughout 2017 when they increased in density and individual size compared to 2016 (data not shown). After the onset of upwelling in 2017, these organisms were rarely collected on the shelf off Newport Oregon, but following the fall transition, they again started washing up on Oregon beaches in high densities. Pyrosomes were collected again during our surveys in the winter and spring of 2018 when they were observed in the highest densities compared to our previous surveys, indicating that the pelagic ecosystem has still not returned to a neutral state.

Northern California Current: Northern California (Trinidad Head Line: THL)

Coastal waters off northern California (THL, station TH02), were relatively warm and fresh during early 2017, but cooled in response to moderate upwelling during summer, and remained near typical (seasonal) temperatures throughout the rest of the year (fig. 12).[11] Limited relaxation from upwelling and minimal storm activity during winter 2018 maintained relatively cool, salty waters over the shelf, and near-bottom waters continued to cool as spring upwelling commenced. Surface waters warmed in late spring, but were still cool relative to 2017. Chlorophyll *a* concentrations remained low throughout 2017 and spring 2018. No hypoxic events were observed.

Zooplankton community and population data in 2017 and 2018 indicated a shift toward assemblages and size structure more typical of conditions prior to the marine heat wave. Warm water krill *Euphausia recurva* and *Nyctiphanes simplex* were observed during the first half of 2017 but have since been absent along the THL. In contrast, observations of *Thysanoessa spinifera* adults, a cool-water species which had been largely absent during the marine heat wave, increased in frequency in 2017. By early 2018 *T. spinifera* was observed in relatively high abundance compared to the previous three years (data not shown). Mean length of *Euphausia pacifica* increased throughout the 2017 upwelling season and for most of the year average size was near or slightly above the time series mean, but did not achieve sizes typical of the seasonal summer maxima observed prior to the marine heat wave (fig. 13). The decline in mean length observed during 2017–18 winter was typical of pre-heat wave conditions, with wintertime mean lengths remaining greater than those observed during much of the previous three years. Early 2018 data indicated a relatively strong response to seasonal upwelling: by late April average length was comparable to lengths measured prior to the arrival of the marine heat wave in late 2014. Large pyrosomes were frequently encountered in early 2017 but had mostly disappeared by summer. Small pyrosomes persisted through fall. Large pyrosomes were again observed in early 2018, but less frequently and at lower densities relative to 2016 and 2017. Small ctenophores were abundant for a brief time during spring 2018.

[11]Hydrographic data and plankton samples have been collected along the Trinidad Head Line since late 2007 as a source of information on ecosystem state and response to climate forcing. Hydrographic data are collected with a Sea Bird Electronics (SBE) model 19 plus V2 CTD (19 plus until September 2014) cast to a maximum depth of 500 m (150 m until August 2014) or to within a few meters of the seafloor. Zooplankton are sampled with a 0.7 m diameter Bongo net fitted with dark mesh (505 µm) and General Oceanics flowmeters deployed rapidly to a maximum depth of 100 m (or within a few meters of the sea floor) and retrieved along an oblique profile by maintaining a steady wire retrieval rate (20 m min-1) and adjusting ship speed through the water to maintain a wire angle (45° ± 5°) throughout the tow.

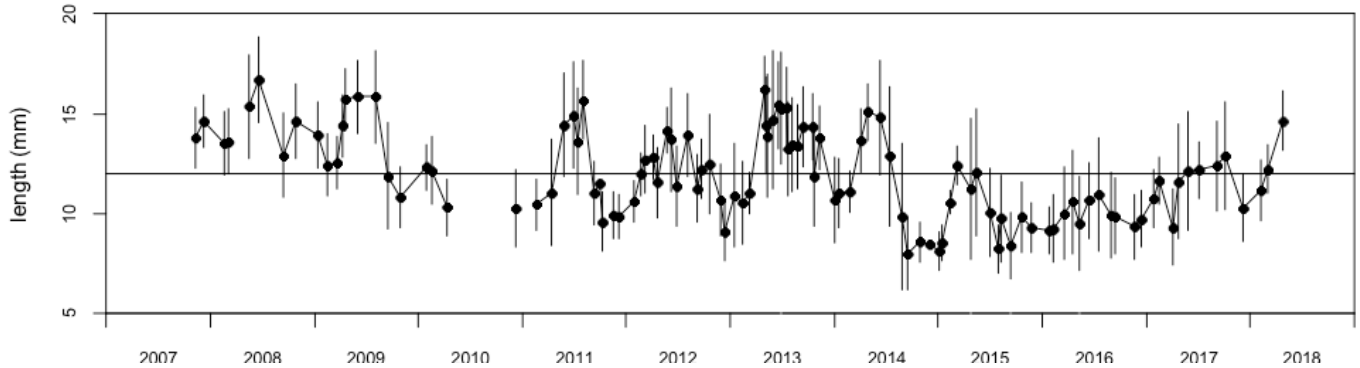

Figure 13. Density-weighted mean (points) and standard deviation (whiskers) of rostral-dorsal length of adult *Euphausia pacifica* collected along the Trinidad Head Line (aggregated over stations TH01 to TH05). Horizontal line indicates mean length taken over entire time series. Samples are collected by fishing bongo nets (505 um mesh) obliquely from a maximum depth of 100 m (or within a few meters of the sea floor in shallower areas) to the surface.

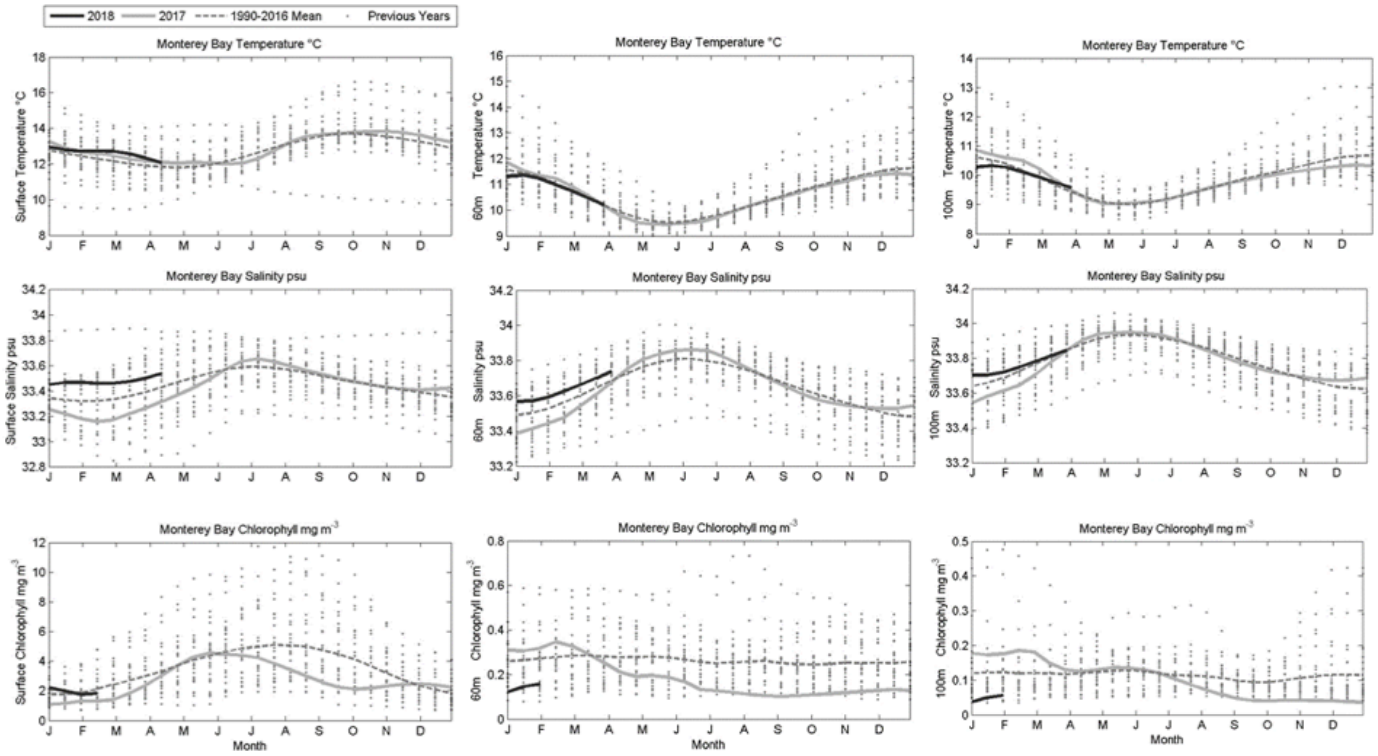

Figure 14. Temperature (top panels), salinity (middle panels), and chlorophyll *a* concentration (bottom panels) at the surface (left panels), 60 m (center panels), and 100 m (right panels) observed at the M1 mooring in Monterey Bay, CA.

Central California Current: Monterey Bay

Temperatures at the surface, 60 m and 100 m, were very close to average through 2017 and the first four months in 2018 (fig. 14). Salinity was also close to average at all depths throughout all months in 2017, was slightly elevated near the surface from January–April in 2018, but was closer to average in 2018 at 60 m and 100 m. In contrast with temperature and salinity, chlorophyll *a* patterns changed greatly with depth. At the surface, chlorophyll *a* was average from January–June, fell well below average from August–October, then returned to average in November 2017 and remained at average values through mid-February 2018. At 60 m chlorophyll *a* was slightly above average in the beginning of 2017, fell below average in April, and was well below average from June 2017–February 2018. At 100 m chlorophyll *a* was above average at the onset of 2017, became average from April–July 2017, then fell to well below average from August 2017 to February 2018.

Central and Southern California: Remotely Sensed SST and Chlorophyll *a*

Remotely-sensed[12] SST and chlorophyll *a* data were averaged throughout inshore (fig. 15A, area 3) and transitional (fig. 15A, area 2) regions in central California and inshore (fig. 15A, area 6) and transitional areas (fig. 15A, area 5) in southern California. Analyses showed that conditions in 2017 and the first half of 2018 were close to typical in all four regions; this was a marked change from extreme anomalies of 2014–16 that in many areas resulted in all-time highest measurements of SST and all-time lowest chlorophyll *a* (Kahru et al. 2018) and minima in the frequency of surface fronts. During 2017 SST remained slightly above the long-term average (by nearly 1°C), but by mid-2018 the SST values were close to the long-term means (fig. 15B). In July–August 2018, however, SST in southern California waters rose rapidly and had a positive anomaly >2°C in July 2018. Elevated SST was restricted to the inshore southern California region in July 2018 (fig. 15B, area 6) as offshore SST values were close to average (fig. 15B, area 5). Chlorophyll *a* values were close to normal in 2017 and in the first half of 2018 (fig. 15C, area 6). In 2017–18 chlorophyll *a* was slightly below the long-term means in the transitional areas (fig. 15C, areas 2 and 5) and very close to normal in the coastal areas (fig. 15C, areas 3 and 6). Despite high SST in southern California, chlorophyll *a* was at an average level in July 2018.

[12]SST data were derived from the version 2.0 daily datasets of optimally interpolated global blended AVHRR temperatures (https://podaac.jpl.nasa.gov/dataset/AVHRR_OI-NCEI-L4-GLOB-v2.0?ids=Platform&values=NOAA-18). Chla data were derived from the merged multisensor regionally optimized Anomalies were calculated relative to the long-term (1981-2018 for SST, 1996–2018 for Chla) mean monthly values. For SST these were difference anomalies; for Chla the anomalies are reported as ratio anomalies expressed as %.

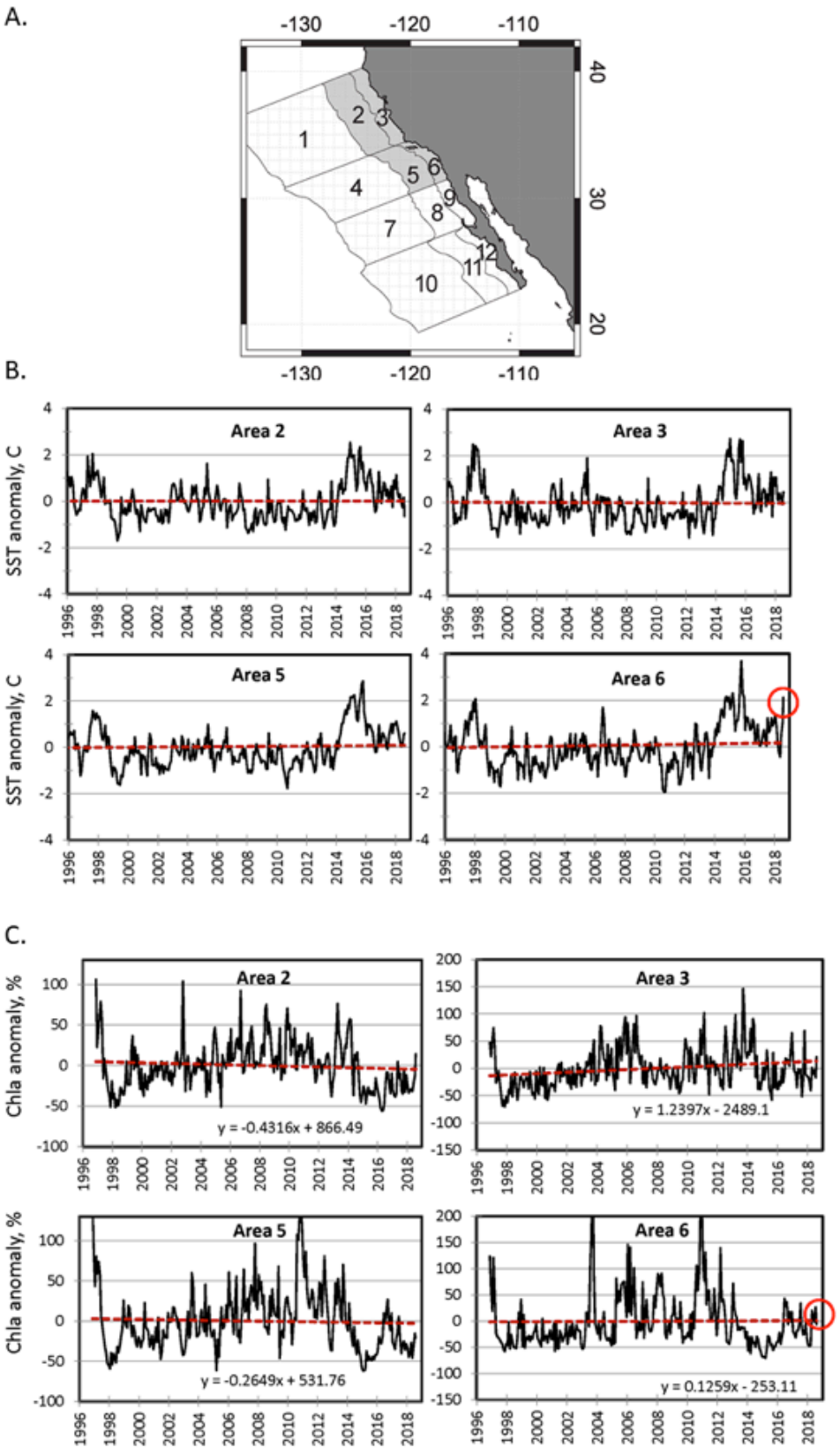

Figure 15. A) Map of the selected coastal (0–100 km from coast, areas 3, 6) and transition (100–300 km from coast, areas 2, 5) areas off central and southern California; B) SST anomalies relative to monthly means of Sept. 1981–June 2018; and C) chlorophyll *a* anomalies relative to monthly means of Nov. 1996–June 2018 in each area. The red dashed lines show the mean linear trends. Red circles in Area 6 highlight June 2018 when SST rose dramatically but chlorophyll *a* remained close to the long-term mean.

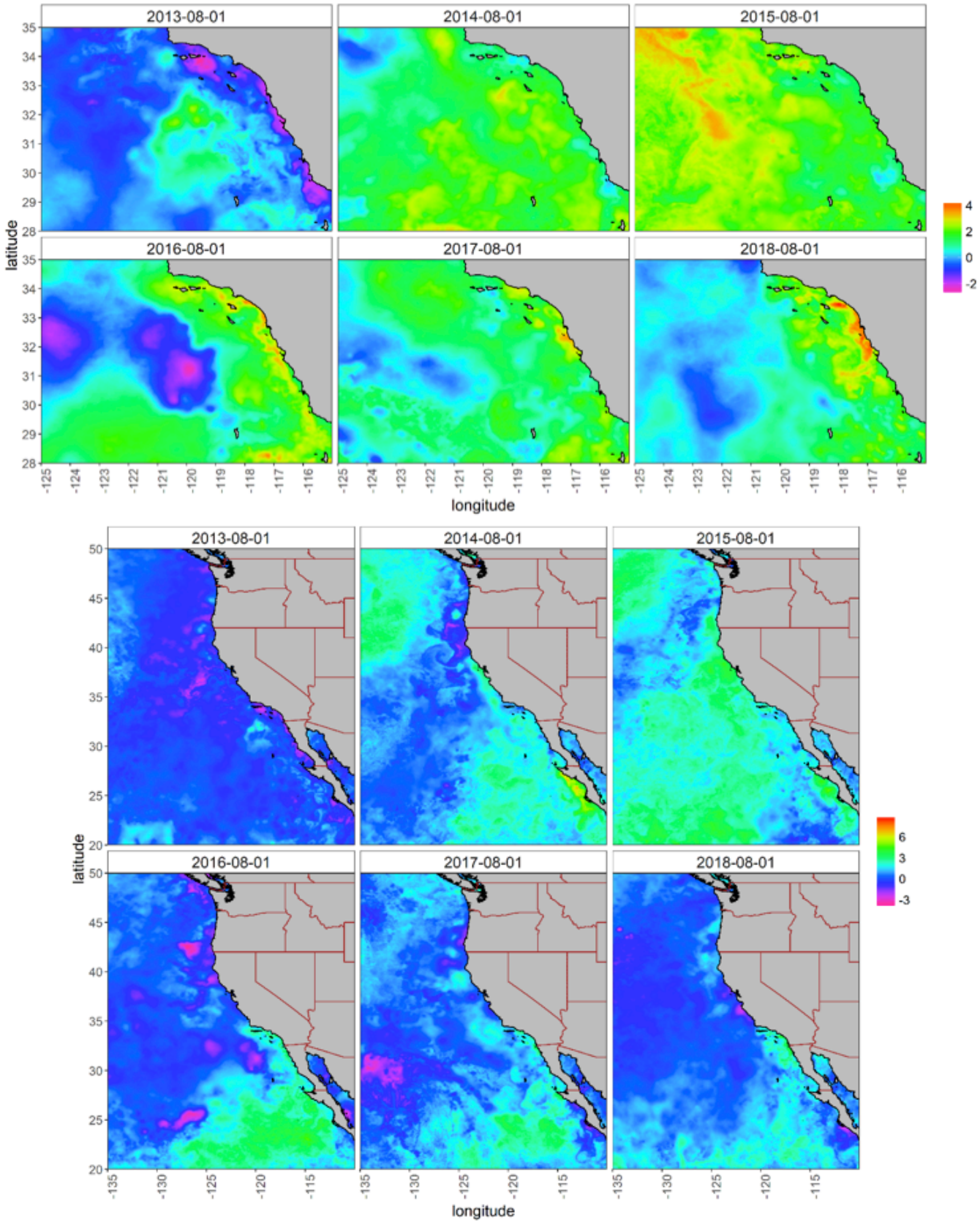

Figure 16. Remotely sensed SST anomalies on August 1, 2013–18. Top panels are centered on the southern California Bight. Bottom panels expand the focus to also envision the central and northern CCS.

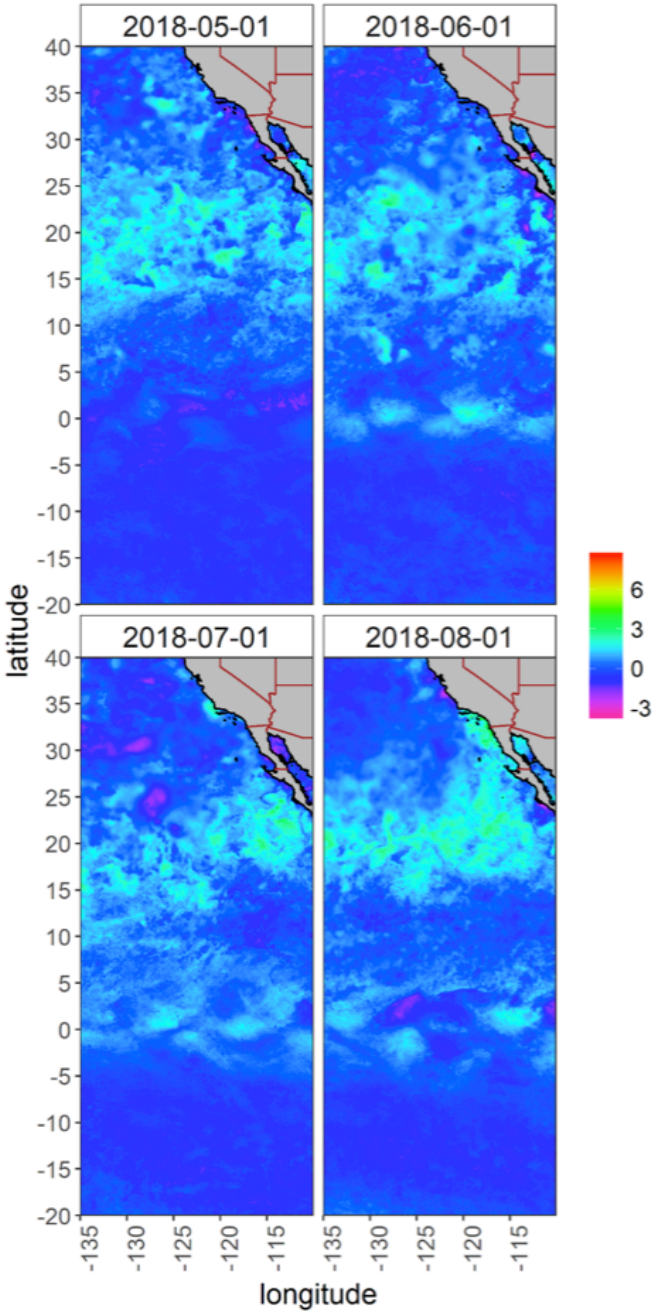

Figure 17. Remotely sensed SST anomalies on the first day of May–August 2018 in the central and equatorial Pacific with the SCB in the upper right corner of each panel.

Satellite SST[13] imagery in August from 2013–18 demonstrated that subsequent to 2013 temperatures were consistently anomalously high in southern California (fig. 16 top panels). While elevated summer SST extended north of Point Conception and permeated most of the CCS in 2014–15, warm SST in the CCS was primarily between Point Conception and Bahia de Sebastes Vizcaino, Baja California, in August 2016–18 (fig. 16 bottom panels). Evaluation of SST anomalies at a broader scale shows the evolution of the warm water off southern California and northern Baja California in summer 2018 (fig. 17). While SST was consistently above normal in the central Pacific between May and August 2018, SST was actually below normal on May 1 between southern California and Bahia de Sebastes Vizcaino. By June 1 and through July 1 SST from southern California to Bahia de Sebastes Vizcaino was slightly above normal. By August 1, however, SST was close to 4°C above normal in many areas in this region. In fact, the daily maximal temperature of 25.9°C recorded August 1 off the Scripps Pier in La Jolla, California, was the highest in the 102-year record (fig. 18). Further, SST increased in the central and eastern Pacific between approximately 20° and 30°N such that a swath of warm water linked the central Pacific with southern California and northern Baja California (fig. 17).

Southern California Current: CalCOFI Survey in Southern California[14]

From mid-2017 to spring 2018, mixed layer (ML) temperature anomalies were slightly, but significantly, above the long-term average (fig. 19A) in spite of mild La Niña conditions at the equator (according to the ONI index; fig. 2B). Higher than normal ML temperatures were observed in all regions of the CalCOFI study area except the upwelling region[15] through spring. During June 2018, however, very high temperature anomalies were observed in the northern part of the Southern California Bight (fig. 20A). ML salinity increased significantly from the summer of 2017 through early 2018 (fig. 19B, C). This increase was particularly strong in the far offshore and the California Current region, less so in the coastal upwelling regions, and undetectable in the Southern California Bight (data not shown). In the California Current region, the anomalies reached depths of 125 m, but only 75 m in the offshore region. The association of the anomalies with the offshore and the California Current is evident during the early summer of 2018 (fig. 20B) when positive salinity anomalies were particularly strong in the California Current region. These patterns make it likely that these anomalies are linked

[13]SST measured by Multi-scale Ultra-high Resolution (MUR) SST Analysis Anomaly fv04.1, Global, 0.01°, Daily. https://podaac.jpl.nasa.gov/dataset/MUR-JPL-L4-GLOB-v4.1

[14]Methods used to collect and analyze samples from CalCOFI cruises are described in detail at CalCOFI.org/methods. Results are presented as time series of properties averaged over all 66 standard CalCOFI stations covered during a cruise or as anomalies of such values with respect to the 1984–2012 period.

[15]When appropriate, averages from selected regions are used based on a subset of the 66 standard CalCOFI stations. These regions (and corresponding CalCOFI stations) are the offshore (Line77Station100, L80St100, L83St100, L87St100-110, L90St90-120, L93St80-120), the southern California Current (L77St70-90, L80St70-90, L83St70-90, L87St70-90, L90St60-80), upwelling areas (L77St49-60; L80St51-60; St82.46, L83St51-60, L87St45-55) and the Southern California Bight (L83St41-42, L87St33-40, L90St28-45, L93St27-45).

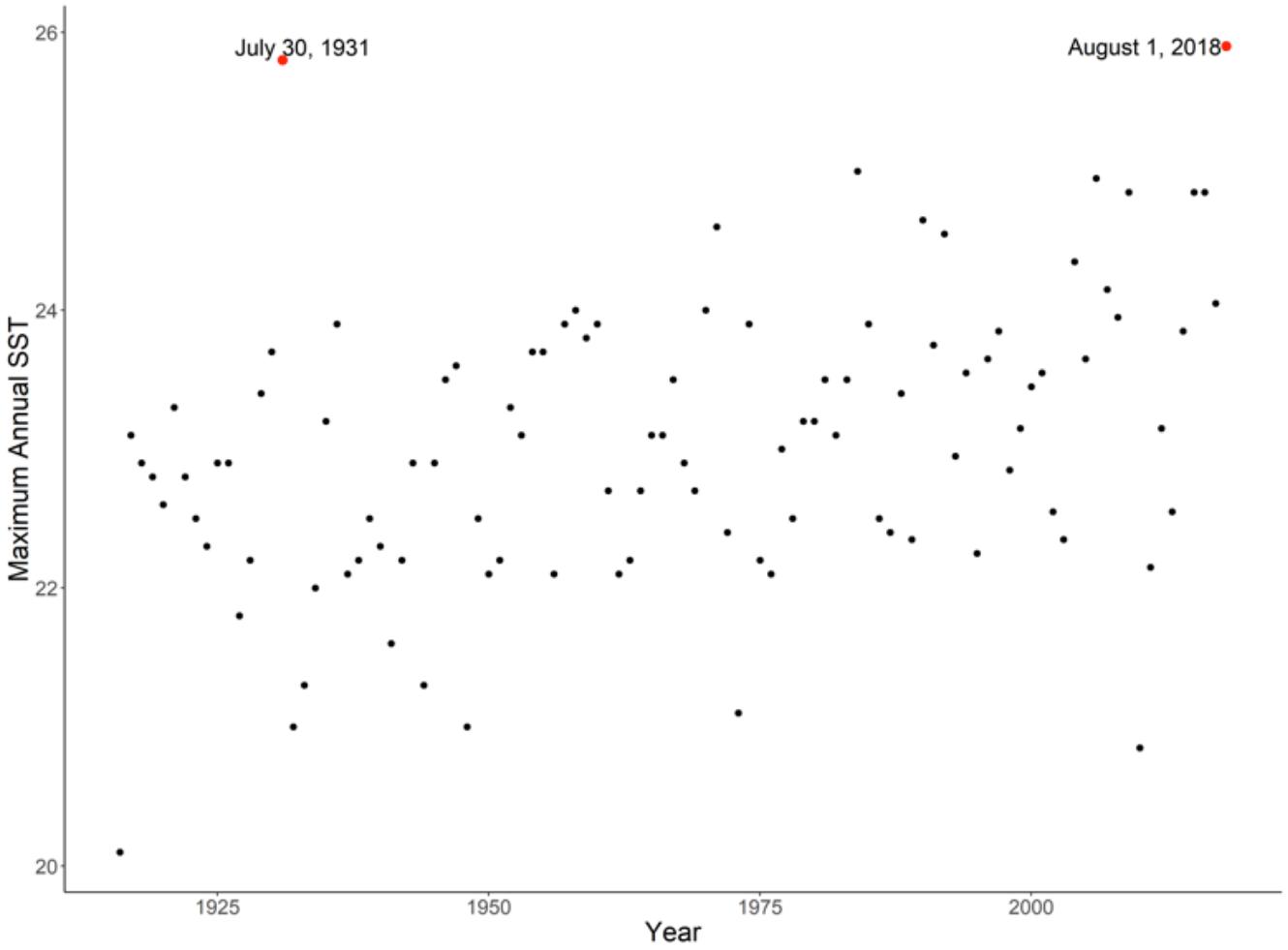

Figure 18. Maximum daily SST in a year from the Scripps Pier in La Jolla, California. The two highest days, July 30, 1931 and August 1, 2018 are highlighted in red.

to changes in the surface waters of the eastern North Pacific. Indeed, the remote-sensing based salinity time series of Xie et al. (2014)[16] shows a large salinity anomaly in the eastern North Pacific during 2016, moving towards the North American continent during 2016–17 and impinging on the CalCOFI sample frame in spring and summer 2018.

Strong variations of ML salinity (fig. 19C) in the past have been linked to changes in the NPGO index, which is also thought to control concentrations of nutrients and phytoplankton biomass in the California Current System (Di Lorenzo et al. 2008). However, recent trends in salinity in southern California and NPGO do not align. To further investigate this pattern, CalCOFI domain salinities (fig. 19B, n=137) were regressed against values of the NPGO at coupled sampling times. The regression was highly significant, but the r^2 was very low (0.12). Further, the residuals were significantly temporally autocorrelated (Durbin-Watson test $p < 0.0001$). A partial autocorrelation analysis suggested that the salinity time series needed to be modeled as an autroregressive (AR1) process. Thus, an ARX(1,0) model was fit to the salinity time series with the NPGO time series as a predictor. The autoregressive part of the regression was large ($a = 0.59$) and highly significant ($p < 0.001$), but the effect of the NPGO on salinity was no longer significant ($p > 0.4$). These results suggest that CalCOFI domain salinity variability over the last few decades is no longer "explained" by the NPGO. This result adds to the growing body of evidence that cautions against using ocean climate indices such as the PDO, and by inference the NPGO, to predict ocean state (Newman et al. 2016).

To investigate the salinity maximum further, properties on the σ_t 25.8 isopycnal averaged over the California Current were studied. Since the beginning of 2017, the depth of the isopycnal, on average 117 m (range of 95–149 m), was close to its long-term average (fig. 21A). Spiciness on the isopycnal over the last year increased (fig. 21B), mirroring the increase in ML

[16]updated at ftp://ftp.cpc.ncep.noaa.gov/precip/BASS/)

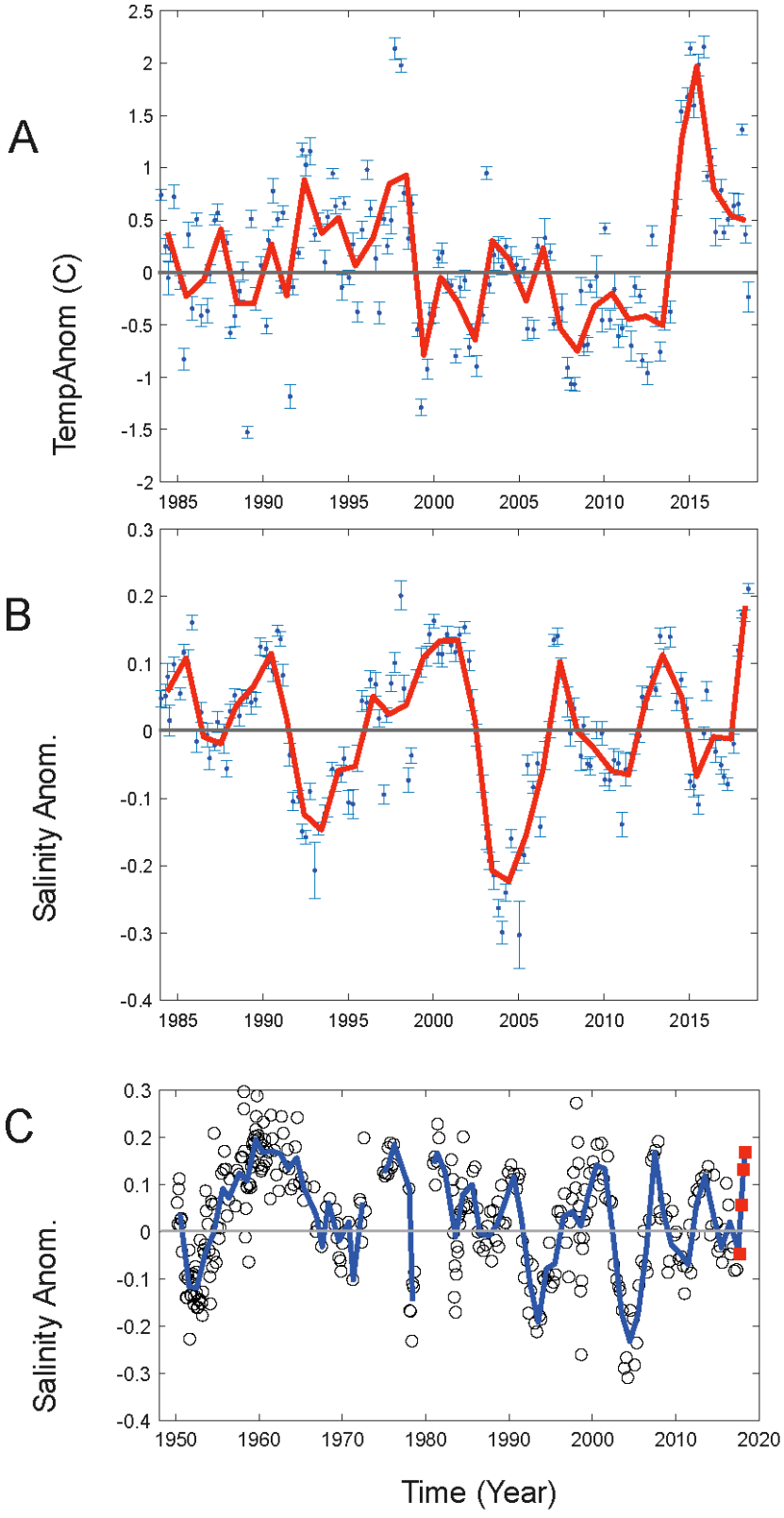

Figure 19. Cruise averages of mixed layer (ML) temperature anomalies (A) and ML salinity anomalies (B) for the 66 standard CalCOFI stations (fig. 1) for 1984 to the summer (June) of 2018, and C) ML salinity anomalies along CalCOFI Line 90 (St 30–90) are shown for 1950 to the present. Whiskers indicate the 95% confidence intervals for the means. Red solid lines represent annual averages, grey horizontal lines the climatological mean, which is zero in the case of anomalies. Anomalies are based on the 1984 to 2012 period.

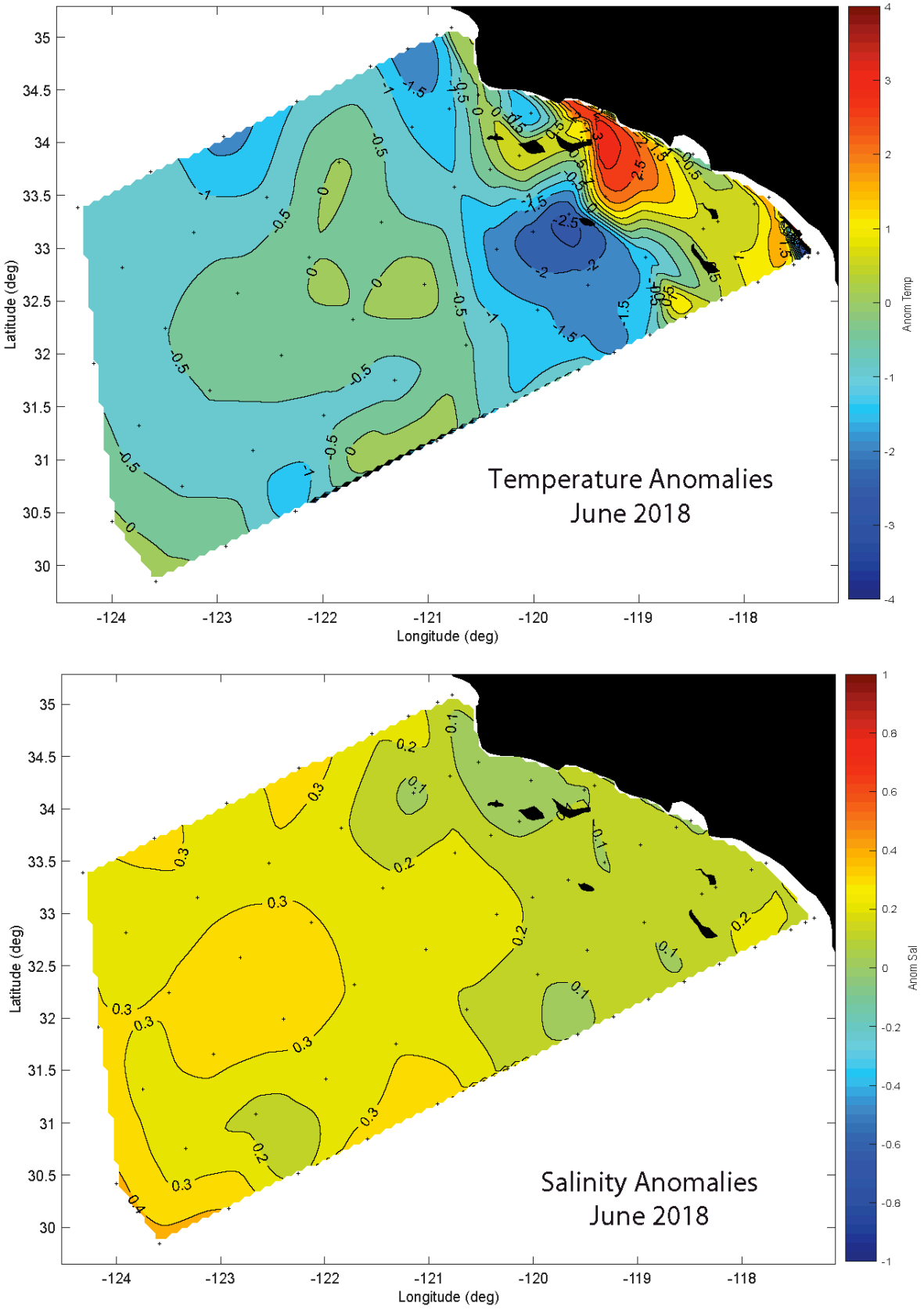

Figure 20. A) Temperature and B) salinity anomalies at 10 m for the summer 2018 CalCOFI cruise.

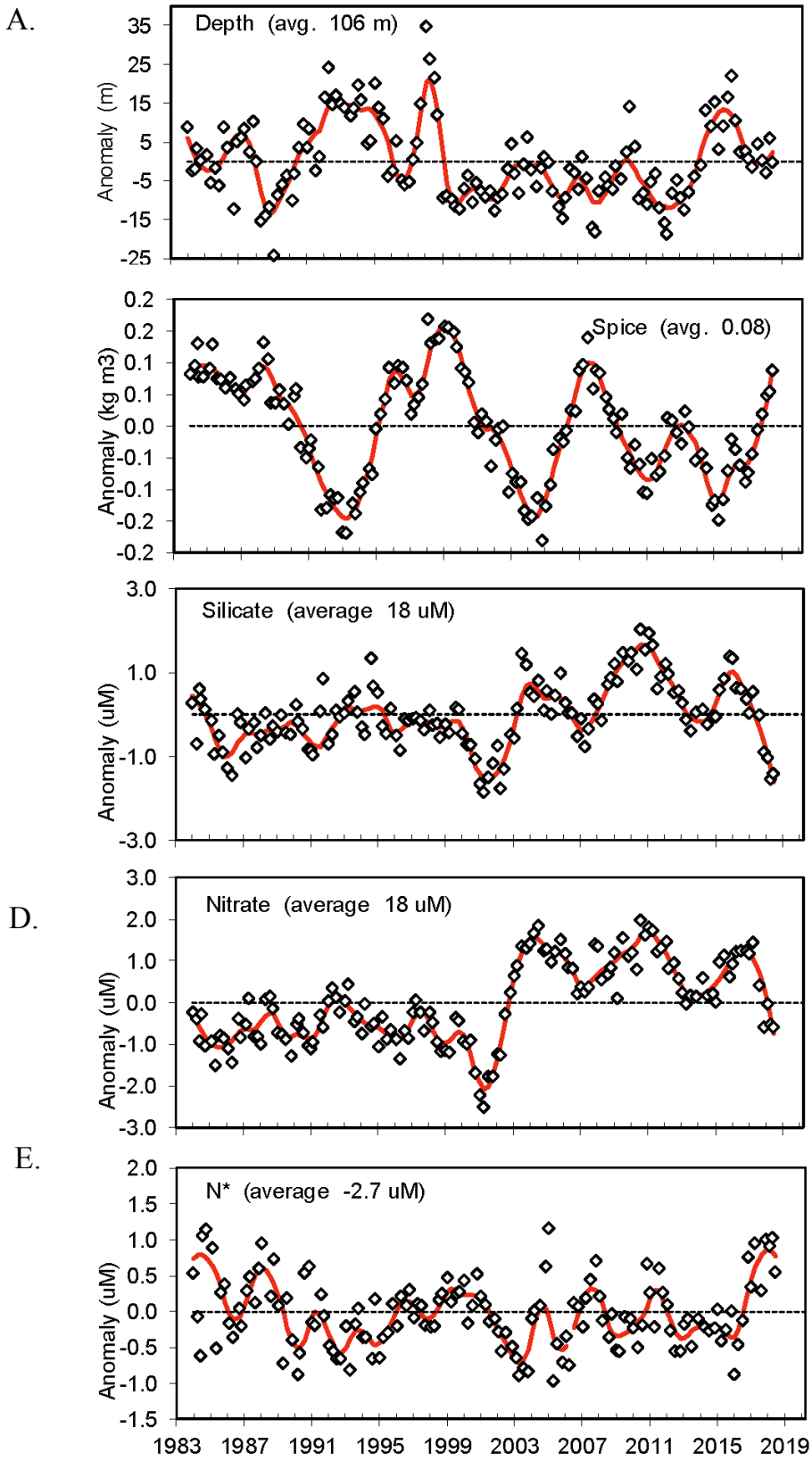

Figure 21. Anomalies of hydrographic properties at the σ_t 25.8 isopycnal (open diamonds) averaged over the 66 standard CalCOFI stations. Shown are anomalies of A) isopycnal depth, B) spiciness, and concentrations of C) silicate D) nitrate, and E) phosphate (N*). The solid red line represents a loess fit to the data; average values for the properties are listed.

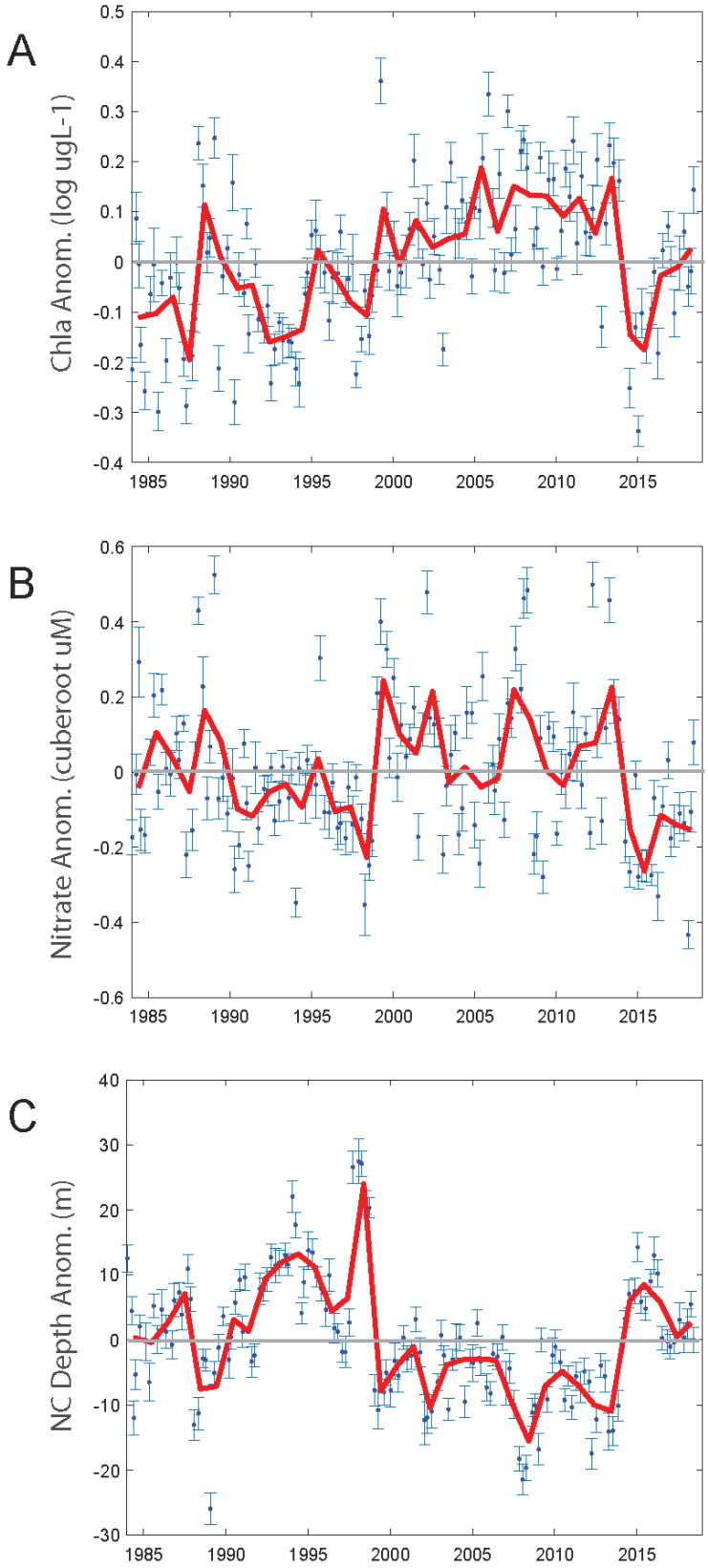

Figure 22. Cruise averages of properties at 10 m depth for the CalCOFI standard 66-station grid. A) The log10 of chlorophyll *a*. B) the cube root of nitrate. C) nitracline depth. Data are derived and plotted as described for Figure 19.

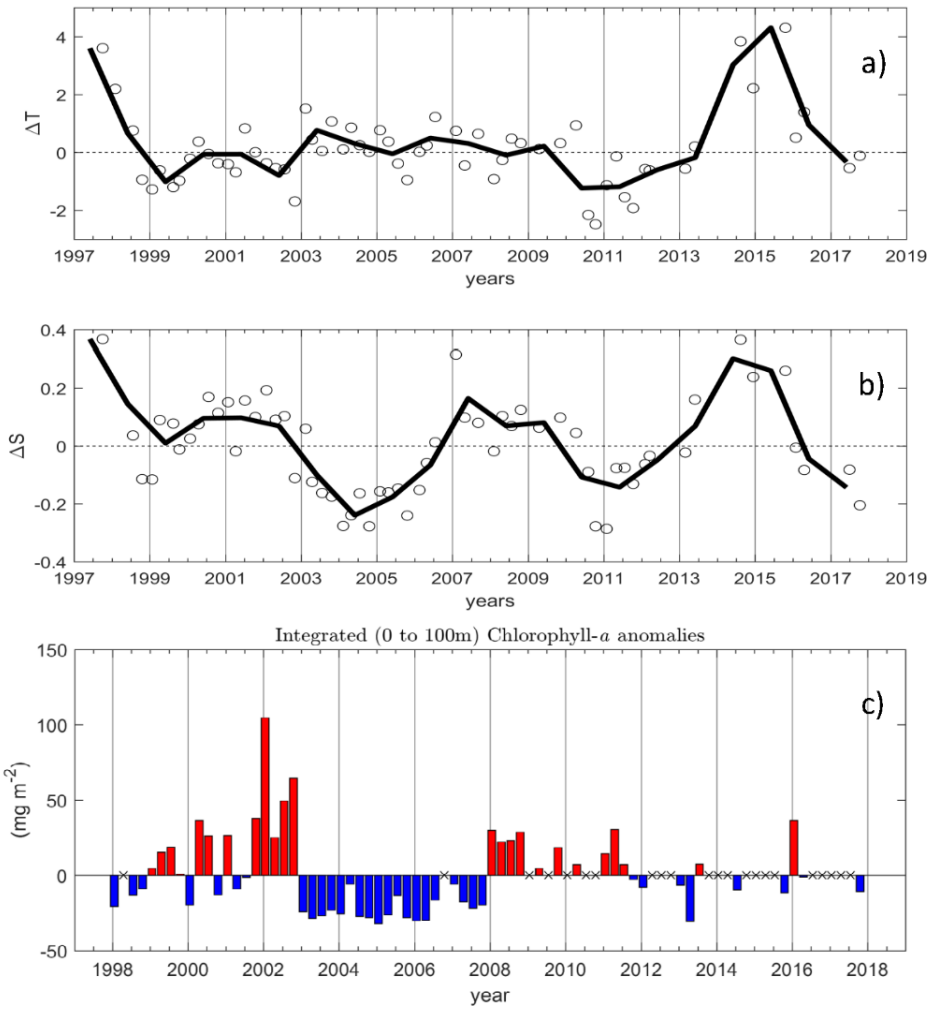

Figure 23. Interannual variability of a) mixed layer temperature (°C); b) mixed layer salinity (UPS) anomalies in the IMECOCAL survey area from October, 1997 through October, 2017 (white circles) and the mean of each year (heavy line); c) depth integrated (0–100 m) chlorophyll *a* anomalies (mg m²) over the IMECOCAL survey area indicated by red and blue bars. The anomalies were obtained by removing the seasonal means from the chlorophyll *a* data (1998-2017). Missing data points from the series of chlorophyll *a* anomalies are indicated by "x."

salinity. Concurrent with the increase of spiciness, concentrations of nutrients on the isopycnal decreased dramatically (fig. 21C–E). These results are similar to those of McClatchie et al. (2018) and are consistent with an increasing impact of warm saline and low nutrient subtropical waters in the CalCOFI region, suggesting a change in the balance of its source waters.

During the 2014 marine heat wave and the 2015–16 El Niño ML chlorophyll *a* was extremely low, but over the last two years it increased to values similar to the long-term average (fig. 22A). Depth distributions of chlorophyll *a* in different regions paint a similar picture; in the offshore and the Southern California Bight it was similar to long-term averages with the exception of the California Current region where chlorophyll *a* was below average (data not shown). It is possible that this difference is driven by a decrease of nutrients in the California Current (fig. 21). ML nitrate concentrations (fig. 22B) have covaried with ML chlorophyll *a* since 2014 suggesting that the latter was controlled by the former. Variations of nitracline depth[17] suggest that the supply of nitrate from depth limits ML nitrate concentrations (fig. 22C).

Southern California Current: Baja California (IMECOCAL)[18]

Temperature anomalies within the ML from October, 1997 through October 2017 over the northern IMECOCAL region (fig. 23A) demonstrated that the anomalous warming in 2014–15 began to diminish

[17]The nitracline depth is defined as the depth where concentrations of nitrate reach values of 1 μM, calculated from measurements at discrete depths using linear interpolation

[18]The IMECOCAL program has conducted quarterly cruises of the Baja California peninsula beginning in October 1997. However after 2012 has been more sporadic and during 2016 and 2017 coverage was limited to the northern region off Baja California (28–32°N).

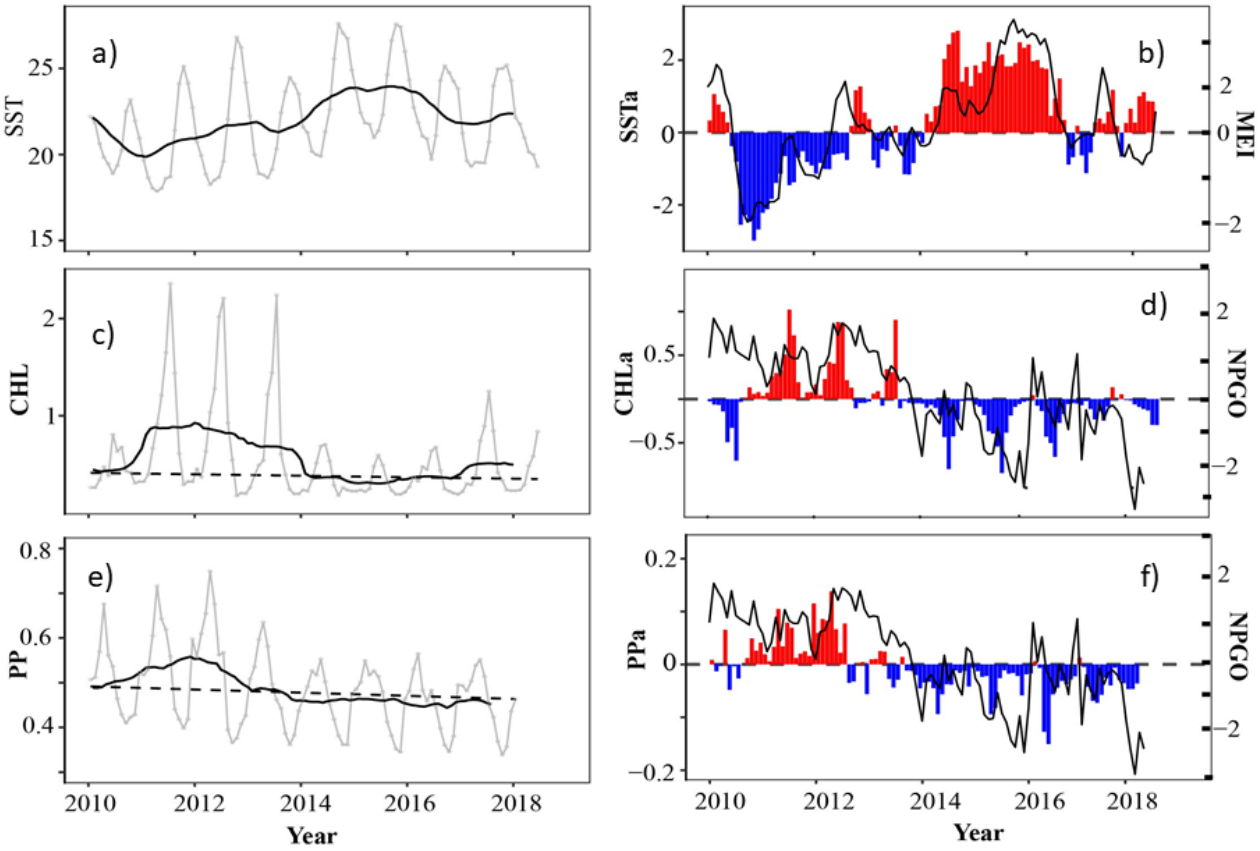

Figure 24. Satellite-derived time series (left panels) and anomalies (right panels) from 2010 through 2018 in the northern region of the IMECOCAL survey domain (28°–32°N) for a) sea surface temperature (SST: C°) and b) anomalies (SSTa: C°); c) chlorophyll *a* (CHL: mg m^{-3}) and d) anomalies (CHLa: mg m^{-3}); and e) primary production (PP: gCm–2 d–1) and f) anomalies (PPa: gCm–2 d–1). The SST anomalies (SSTa) are shown together with the Multivariate ENSO Index (MEI); the chlorophyll anomalies (CHLa) and the primary production anomalies (PPa) are shown along with the NPGO index. The light grey lines are the annual cycles composed of monthly averages in the SST, CHL, and PP plots; the heavy black lines are 12 month running means. The long-term means of CHL and PP are shown by heavy dashed lines.

in early 2016, and ML temperature anomalies in 2017 were slightly negative. Similarly, ML salinity anomalies decreased to negative levels in 2016 and 2017 (fig. 23B).[19] Chlorophyll *a* anomalies averaged from the surface to 100 m were slightly negative in October 2017 (fig. 23C).

Evaluation of interannual variability of depth-integrated chlorophyll *a* anomalies[20] from 1998 through October 2017 in the IMECOCAL region indicates that there is significant decadal-scale as well as interannual variability (fig. 23C). It should be noted that there are important differences in this chlorophyll *a* anomaly series from the IMECOCAL region compared to that presented in Figure 18 in Wells et al. (2017) due to a necessary correction in the calibration of the chlorophyll *a* data. The series now appears to better agree with the chlorophyll *a* anomalies in areas 5 and 6 of the CalCOFI region (fig. 4 in McClatchie et al. 2016b).

Monthly satellite-derived measurement of SST[21] over the IMECOCAL region showed that it was cooler than normal in early 2017 but became warmer than normal in late 2017 and was approximately 1°C above normal by mid-2018 (figs. 24A, B). Satellite measurements of chlorophyll *a* and primary production were mostly negatively anomalous from mid-2017 to early 2018 (figs. 24C–F). In fact, these variables have been below average nearly all the time within the IMECOCAL region from late 2013 to early 2018 (figs. 24C–F). Notably, trends in SST, chlorophyll *a*, and primary production seemed to correspond with basin scale indices as SST correlated positively with the Multivariate

[19]The hydrographic data were Seabird sensors factory calibrated prior to each cruise. CTD data were processed with Seasoft based on EOS-80; thermodynamic variables were then computed using MATlab functions from SEA-MAT. The mixed layer depth was estimated following methodology in Jeronimo and Gomes-Valdes (2010) for the IMECOCAL grid. Harmonics were computed for mixed layer properties for all stations for wich sufficient data exists. The long-term variability follows the approach used by (Bograd and Lynn 2003).

[20]Phytoplankton chlorophyll *a* data were taken from water collected at discrete depths in the upper 100 m, filtering through Whatman GF/F filters following the fluorometric method (https://www.nodc.noaa.gov/archive/arc0001/9900162/2.2/data/0-data/jgofscd/Files/protocols/chap14.html). Depth integrated chlorophyll *a* (0–100m) anomalies were estimated by removing seasonal means.

[21]Monthly composites of satellite sea surface temperature and chlorophyll at 4 x 4 km resolution derived from the MODIS-Aqua sensor were downloaded from http://coastwatch.pfeg.noaa.gov.

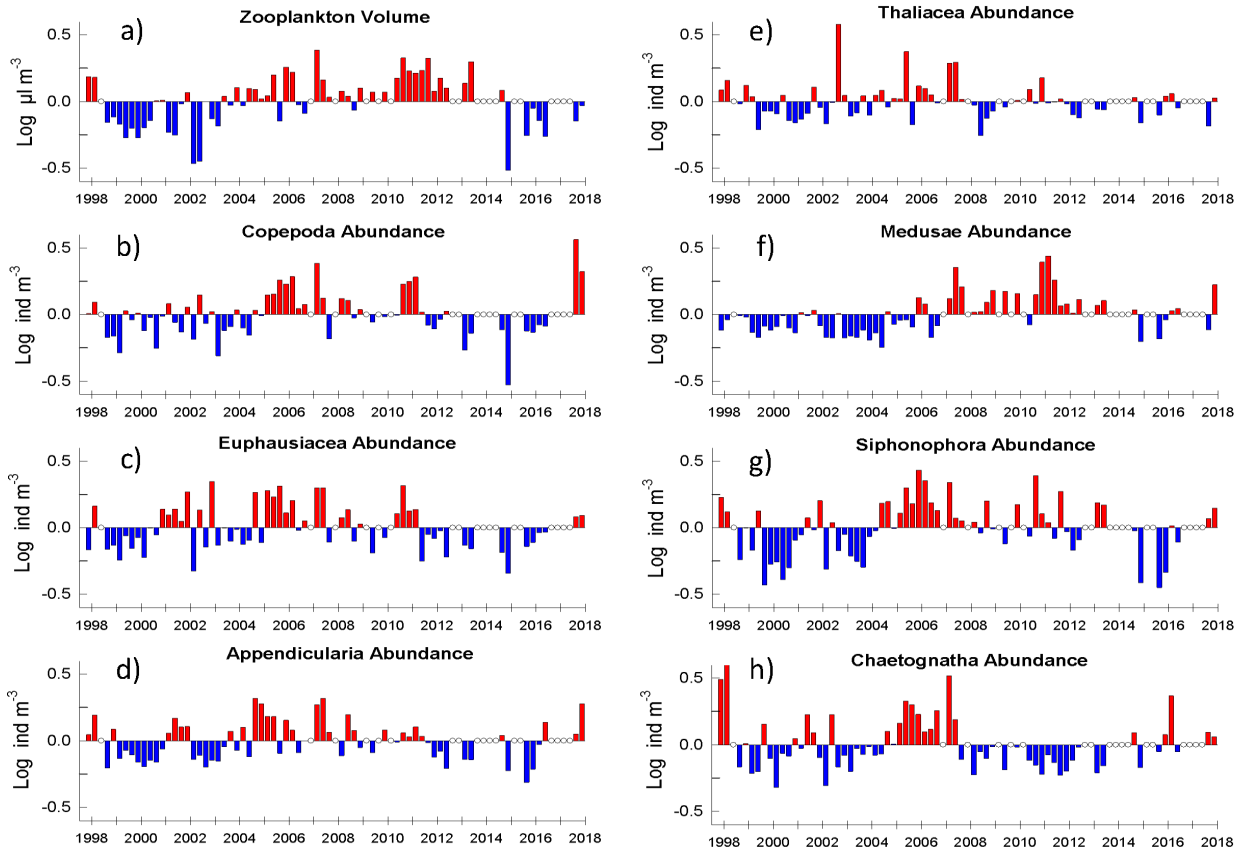

Figure 25. Zooplankton anomalies from bongo tows between Bahia Sebastian Vizcaino and Ensenada. The upper left panel shows zooplankton volume anomalies (a) and the rest show zooplankton abundance anomalies for the main functional groups: Copepoda (b), Euphausiacea (c), Appendicularia (d), Thaliacea (e), Medusae (f), Siphonophora (g), and Chaetognatha (h). Each bar represents a single cruise and open circles represent cruises that did not take place or were omitted due to limited sampling. Data were converted to logarithms prior to estimation of anomalies. The anomalies were season-specific.

ENSO Index[22] (fig. 24B), and both chlorophyll *a* and primary production correlated positively with the NPGO (fig. 2, figs. 24D, F).

In June 2017 the zooplankton[23] volume anomaly was slightly negative and much closer to average than the extremely low values from 2014–16 (fig. 25A). The rise in zooplankton volume in 2017 was largely driven by a large increase in copepod abundance (fig. 25B). Euphausiid abundance also rose in 2017 relative to 2014–16 but not as much as copepod abundance (fig. 25C). Among gelatinous herbivores, Appendicularia increased greatly (fig. 24D) and Thaliacea slightly (fig. 25E) in October 2017. In June 2017, however, the Thaliacea abundance anomaly was negative (fig. 25D) mainly due to low numbers of salps and doliolids. Because salps can constitute a large proportion of the overall zooplankton volume (Lavaniegos and Ohman 2007), the negative zooplankton volume anomaly in late 2017 was likely driven by low salp abundances (fig. 25A). Gelatinous carnivores, Medusae (fig. 25F) and Siphonophora (fig. 25G) displayed moderately positive anomalies in October 2017. Chaetognath abundance anomaly was very close to zero in October 2017 (fig. 25H).

REGIONAL EPIPELAGIC MICRONEKTON AND SALMON OBSERVATIONS

Northern California Current: Washington and Oregon

Newport Hydrographic Line and Pre-Recruit Survey[24]

The ichthyoplankton assemblage along the central-

[22]https://www.esrl.noaa.gov/psd/enso/mei/

[23]Zooplankton were sampled with oblique tows of a bongo net (500-µm mesh) from 210 m to the surface. Displacement volume was measured for all samples; zooplankton taxa were only counted for nighttime samples.

[24]Ichthyoplankton samples were collected from 3–4 stations representing coastal (<100 m in depth), shelf (100–1000 m), and offshore (>1000 m) regions along both the Newport Hydrographic (NH; 44.65°N, 124.35–125.12°W) and Columbia River (CR; 46.16°N, 124.22–125.18°W) lines off the coast of Oregon during May–July in 2007–18 (For complete sampling methods, see Auth [2011]). Post-larval (i.e., juvenile and adult) fish were collected using a modified-Cobb midwater trawl (MWT) with a 26-m headrope and a 9.5-mm codend liner fished for 15 min at a headrope depth of 30 m and ship speed of ~2 kt. MWT collections were made at 3-6 evenly-spaced, cross-shelf stations representing coastal, shelf, and offshore regions along nine half-degree latitudinal transects between 42.0 and 46.0°N latitude in the northern California Current region during May–July in 2011–18 (although no sampling was conducted in 2012). Sampled volume was assumed to be uniform for all hauls. All fish collected were counted and identified to the lowest taxonomic level possible onboard, although pre-recruit rockfish were frozen and taken back to the lab for identification using precise meristic and pigmentation metrics.

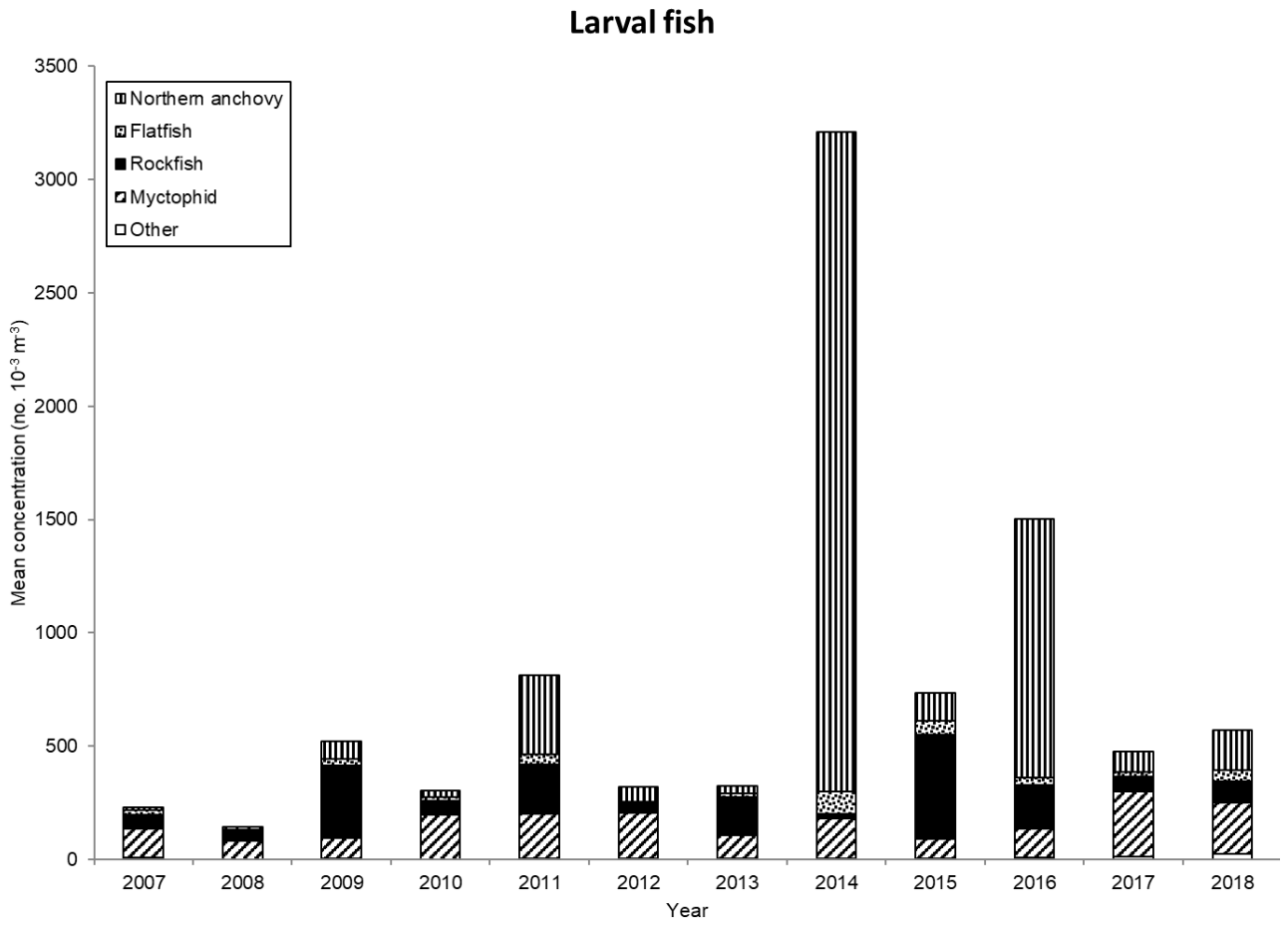

Figure 26. Mean concentrations (no. 10^{-3} m^{-3}) of the dominant larval fish taxa collected during May–July in 2007–18 along the Newport Hydrographic (NH; 44.65°N, 124.35–125.12°W) and Columbia River (CR; 46.16°N, 124.22–125.18°W) lines off the coast of Oregon.

northern coast of Oregon in May 2018 was largely unremarkable in terms of composition and relative concentrations of the dominant taxa (fig. 26). Total mean larval concentration was the fifth highest in the 12-year time series. Larval flatfish in 2018 were found in the third highest concentration of the time series, myctophids in the second highest, and "other" taxa in the highest concentration, although this last group accounted for only 4% of the total mean larval concentration.

The post-larval fish community in the northern California Current in May 2018 had the second lowest abundance of the seven-year time series, continuing its decline since 2016 (fig. 27). The abundance of "other" taxa was the lowest in the time series, primarily due to the complete absence of Pacific hake (*Merluccius productus*; hake) in the 2018 samples, which had comprised 83% of the mean abundance of "other" taxa and ~60% of the total mean abundance of all post-larval fish in 2017. Rockfish (*Sebastes*) abundance in 2018 was average for the time series, with the dominant species consisting of shortbelly (*Sebastes jordani*; 64% of total rockfish), darkblotched (*S. crameri*; 20%), chilipepper (*S. goodei*; 5%), blue[25] (*S. mystinus*; 3%), and canary (*S. pinniger*; 2%). In addition, pyrosomes continued to be found in extraordinarily high numbers throughout the sampling area (data not shown).

Columbia River Plume Region: Juvenile Salmon and Ocean Ecosystem Survey (JSOES)

The fish and invertebrate assemblage collected from trawls in the upper 20 m[26] in June in the northern California Current was very distinct between 2015 and 2017 (fig. 28). During that time, it was dominated by taxa

[25]It is possible that some of the rockfish identified as Blue were the recently-described Deacon rockfish, *S. diaconus* (Frable et al. 2015)

[26]This survey has been conducted by the Northwest Fisheries Science Center (NWFSC) in late June every year between 1998 and 2018. Sampling occurred along 11 east–west transect lines off Washington and Oregon (fig. 1), ranging from approximately 45° to 48°N. Trawls were conducted at 6 to 8 stations on each transect from the shallowest bottom depth possible (~30 m) out to ~50 km from shore, often extending beyond the continental shelf (Brodeur et al. 2005, Barcelo et al. 2018). Sampling was conducted during daytime in the upper 20 m of the water column at every station using a pelagic rope trawl with the head rope at about 1 m, that had a 336 m^2 mouth opening with variable mesh sizes (162.6 cm at mouth to 8.9 cm at cod end). To retain catches of small nekton, a 6.1-m long, 0.8-cm mesh knotless liner was sewn into the cod end. The rope trawl was towed for 30 minutes at a speed over ground of approximately 6 km h^{-1}.

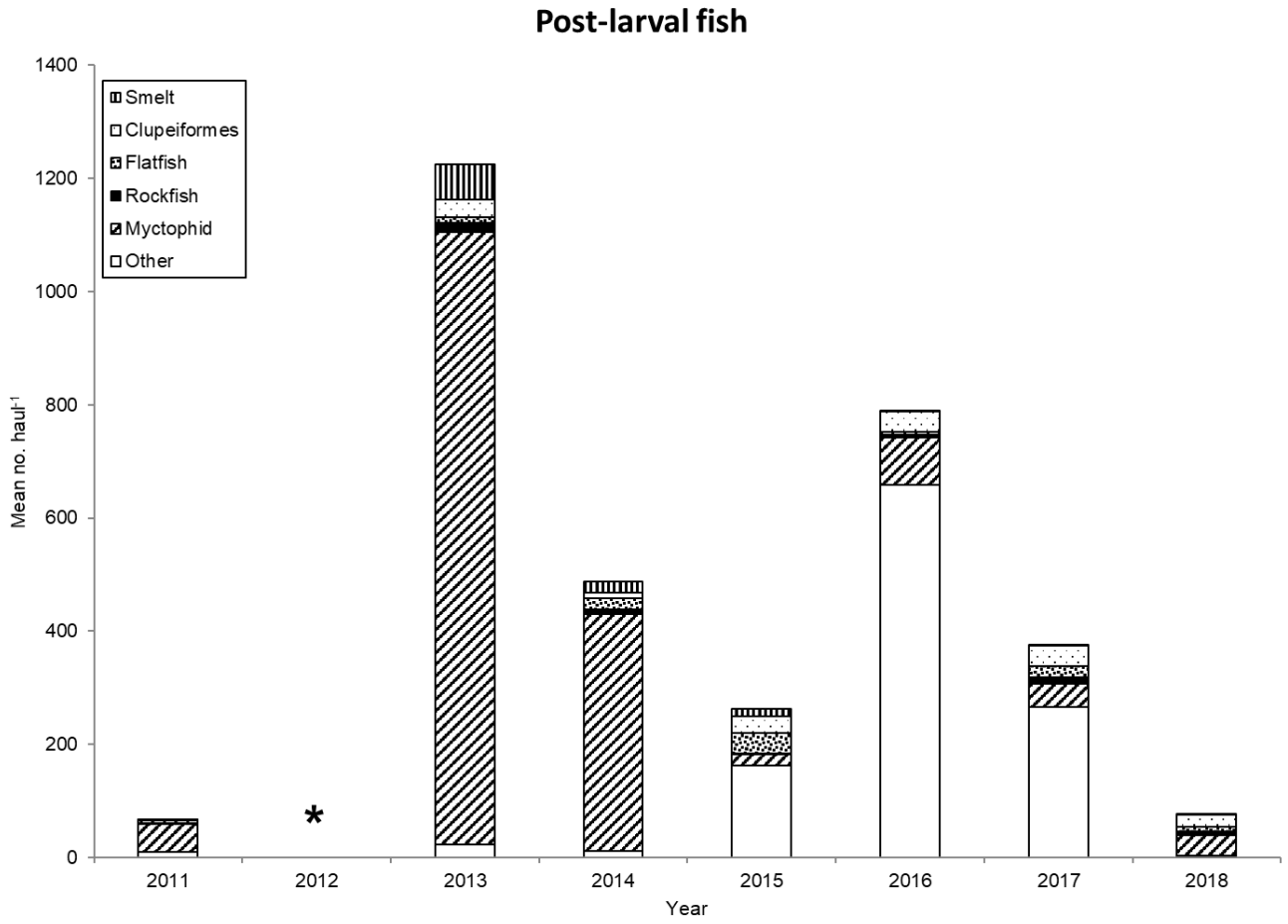

Figure 27. Mean catches (no. haul^{-1}) of the dominant post-larval fish taxa collected during May–July in 2011–18 along nine half-degree latitudinal transects between 42.0° and 46.0°N latitude in the northern California Current region. * = no samples were collected in 2012.

such as pyrosomes, Pacific mackerel (*Scomber pacificus*), and Jack mackerel (*Trachurus symmetricus*) that normally occur in warmer ocean waters to the south of the study area. An NMS ordination clearly showed that the 2015–17 assemblages were outliers, distinct not only from the 1999 La Niña assemblages, but also from the assemblage sampled during the 2005 warm event (Brodeur et al. 2006) in the northern California Current (fig. 28).

The fish and invertebrate community was less anomalous in 2018 than during the preceding three years (fig. 28). However, some taxa (e.g., market squid [*Doryteuthis opalescens*], Pacific Pompano [*Peprilus simillimus*], Jack mackerel) were present that had previously been absent or very low in our catches prior to 2015. Other common taxa in 2018 included gelatinous species, yearling Chinook (*Oncorhynchus tshawytscha*), coho (*O. kisutch*), juvenile chum (*O. keta*) salmon, and Pacific herring (*Clupea pallasii*). Pyrosomes, that were first captured by this survey in 2017 were still present, although in lower abundances than the in the previous year.

Since 2015, the jellyfish community off Washington and Oregon has been quite different than previous years. Usually, the large, cool-water scyphozoan species, sea nettle (*Chrysaora fuscescens*) is numerically dominant. However, during the warm ocean years of 2015–16, the normally more offshore water jellyfishes (*Aequorea* spp.) were much more abundant while densities of *Chrysaora* were low (fig. 29). In 2017, both *Chrysaora* and *Aequorea* were caught in average densities. However in 2018, while *Chrysaora* numbers remained about average, *Aequorea* increased to 3rd most abundant in the 20 years of sampling jellyfish (jellyfish were not quantified prior to 1998).

Catches of yearling salmon off Washington and Oregon in June are thought to be accurate indicators of early ocean survival of yearling Chinook and coho salmon. The abundance of yearling Chinook salmon during June surveys has a significant, positive relationship to returning spring Chinook jack and adult counts at the Bonneville Dam (with 1 and 2 year lags, respectively; see fig. 1 for dam location), as does the abundance of yearling

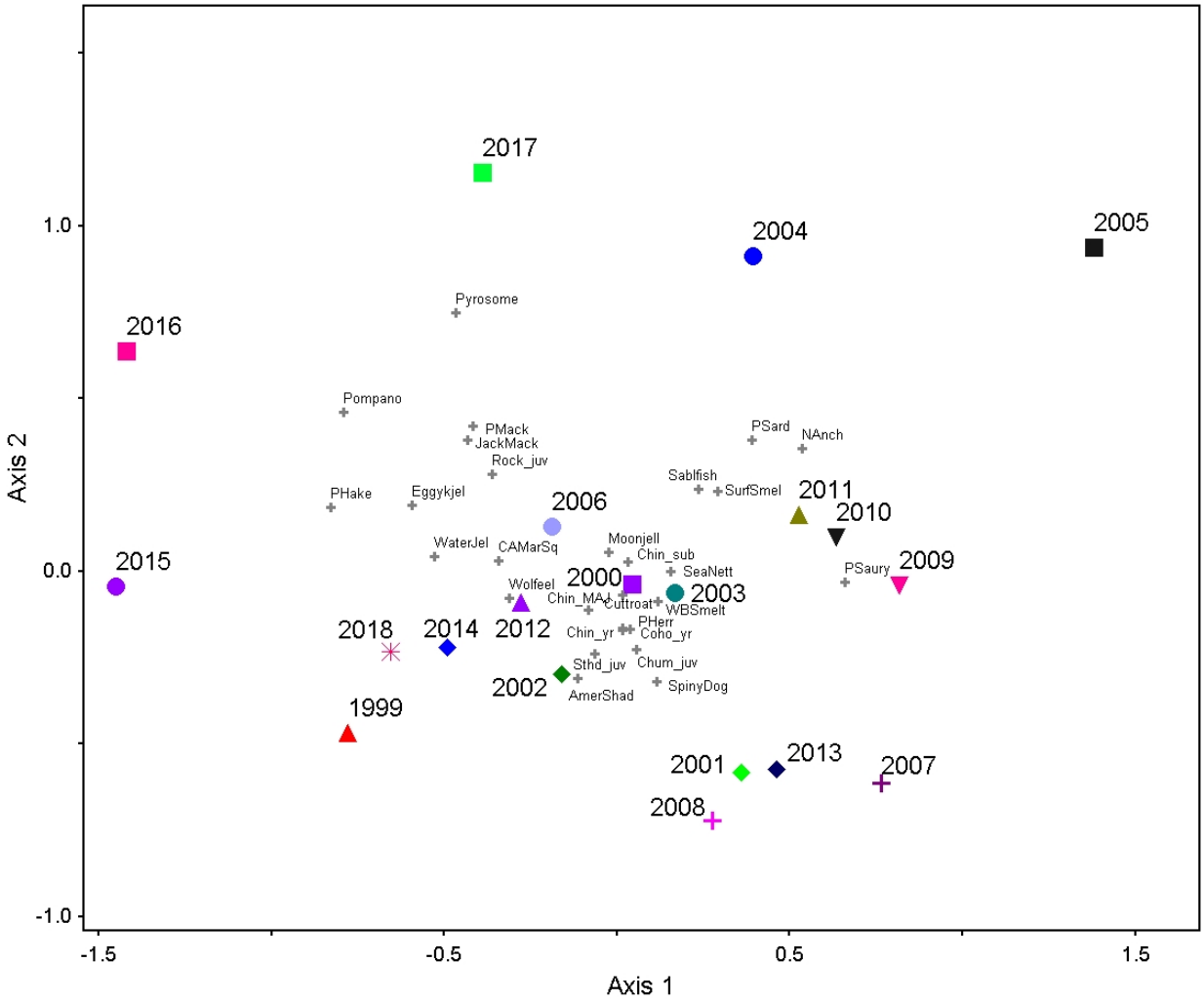

Figure 28. NMS ordination of northern California Current pelagic assemblages. The NMS ordination explained 78.9% of the total variability in the first two dimensions.

coho salmon to subsequent coho smolt to adult survival (Morgan et al. 2018). Catch per unit effort (CPUE, number per km trawled) of both yearling Chinook and coho salmon during the June 2017 survey was the lowest of the 20-year time series from 1998 to 2017 (fig. 30). In June of 2018, yearling Chinook salmon catches were close to average, but yearling coho salmon catches were the 2nd highest in the 21-year time series (fig. 30). Based on correlations observed in previous years, this suggests that adult returns of spring Chinook in 2020 will be close to average and coho salmon returns in 2019 will be higher than average.

Taken as a whole, the nekton community in summer of 2018 off Washington and Oregon indicate that the ecosystem was in a mixed state. On the one hand, the 2014 surface warming and the 2015–16 El Niño still had a noticeable impact on the nekton in this region, as taxa such as water jellyfish, pyrosomes, and Pacific pompano were abundant. On the other hand, higher catches of sea nettles and juvenile salmonids suggest that the ecosystem may be returning to a more "normal" state.

Salmon and salmon forage indicators in northern California Current

Fish larvae in winter (January–March) derived from the Newport Hydrographic[27] line provides an index of juvenile salmon prey when they enter the ocean in spring and summer (Daly et al. 2017). When prey biomass was high, as in 2000 or 2008, smolt to adult returns or salmon adult returns tend to be high in the corresponding return years. When prey biomass was low, such as in 1998 or 2003–04, food conditions were poor and salmon returns were low. For the fourth year in a row,

[27]Ichthyoplankton samples were collected from 5 stations spaced ~9 km apart along the NH line. Sampling was conducted approximately every 2 wk between January and March. Only samples from January–March were used, assuming that larvae collected during these months would have had sufficient time to grow to the average size of prey eaten by juvenile salmon in late spring and early summer.

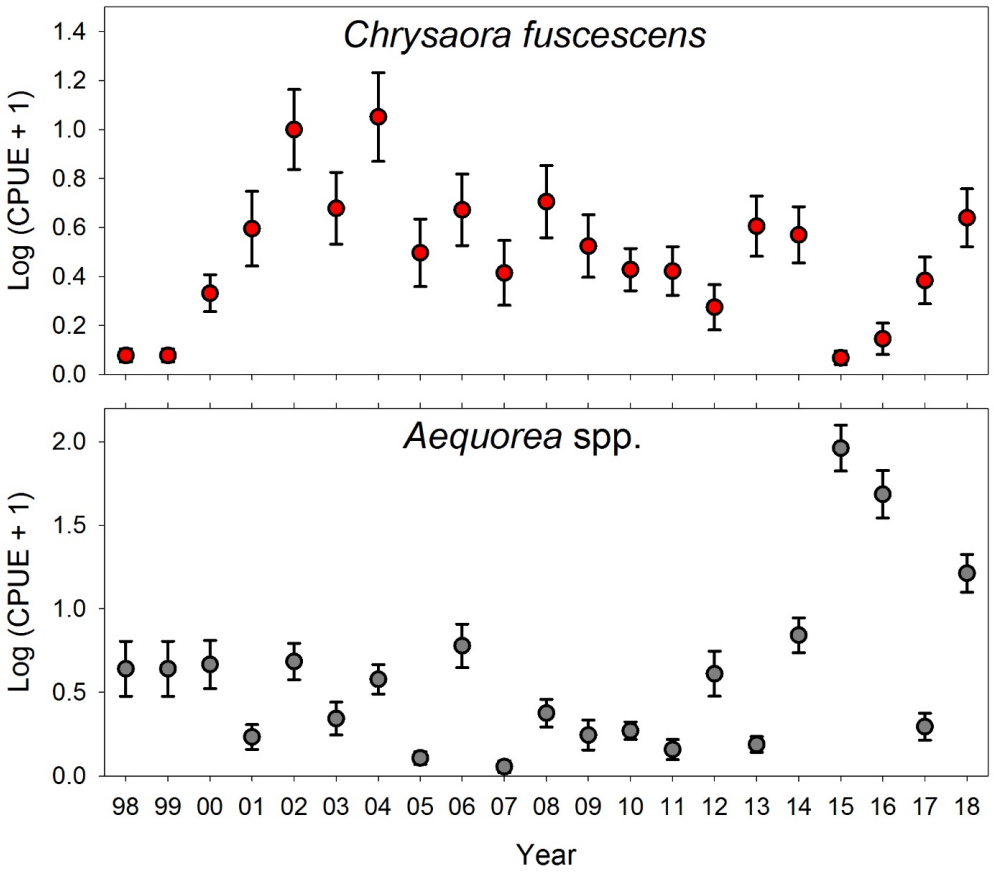

Figure 29. Catches of the dominant jellyfish taxa in pelagic surveys off the coast of Washington and Oregon in June from 1999 to 2018. Data are the means and standard error of the log10(catch per km+1) of *Chrysaora fuscescens* (upper) and *Aequorea* spp. (lower) in the survey area.

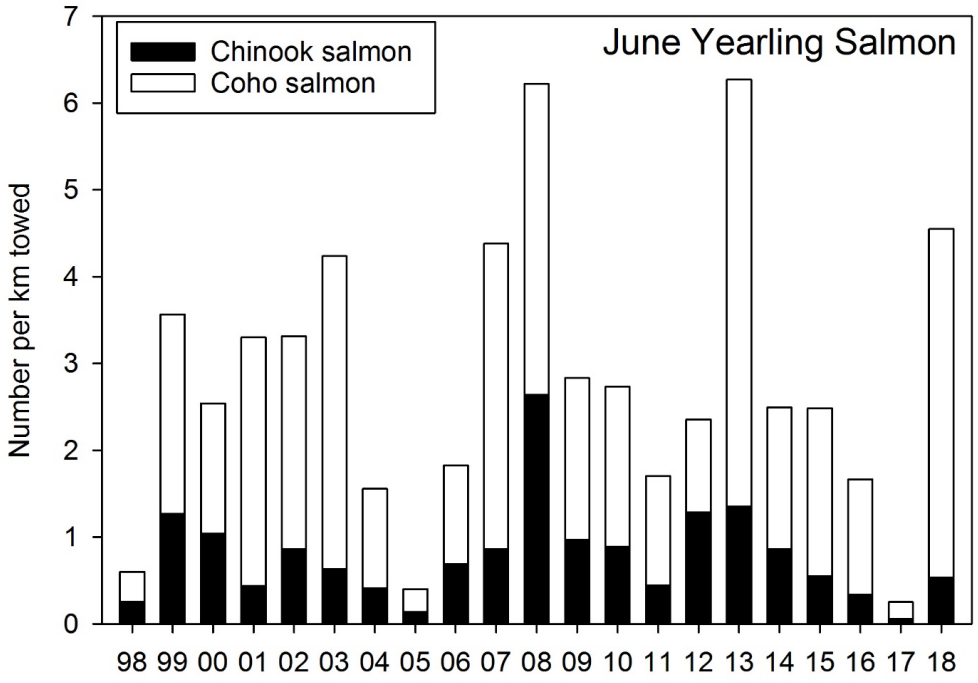

Figure 30. Catches (number per km towed) of juvenile coho (black bars) and Chinook (white bars) salmon off the coast of Oregon and Washington in June from 1998–2018.

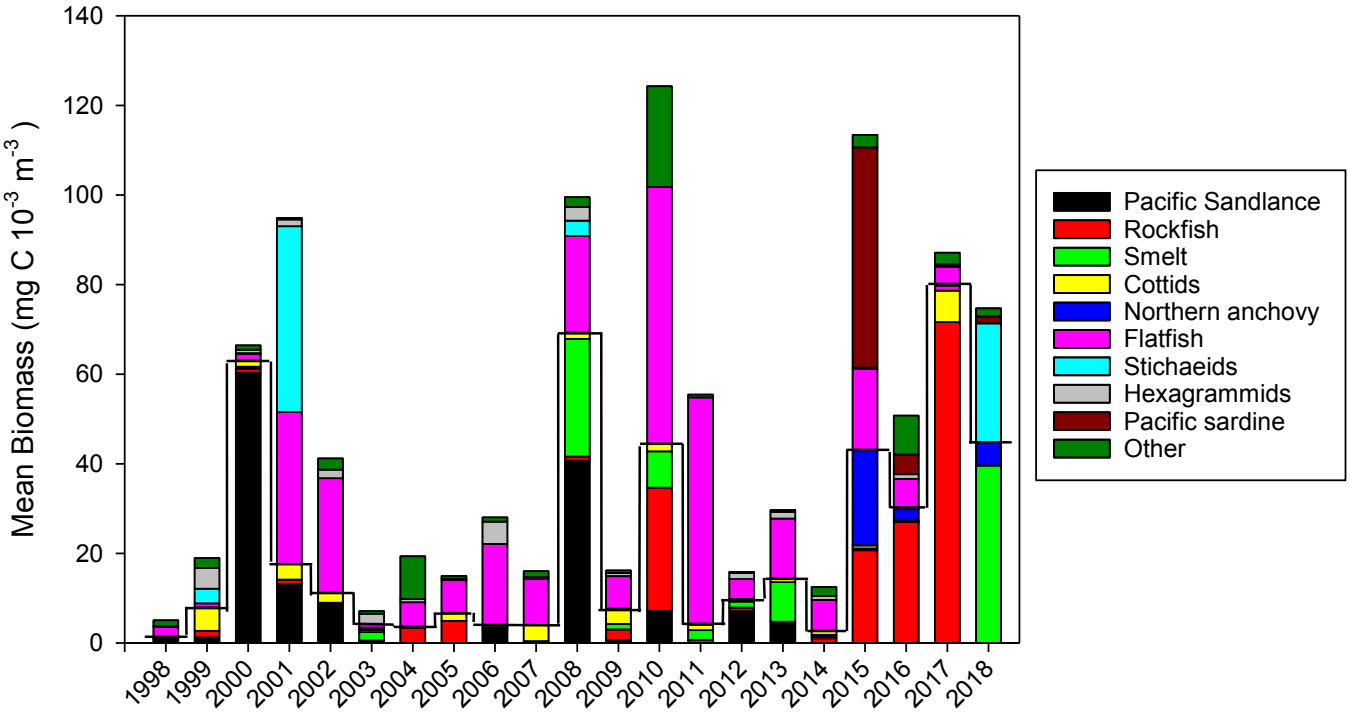

Figure 31. Annual mean biomass (mg C 10^3 m^3) of the five important salmon prey taxa (below solid line) and five other dominant larval fish taxa (above solid line) collected during winter (January–March) in 1998–2018 along the Newport Hydrographic (NH) line off the coast of Oregon (44.65°N,24.18–124.65°W). Figure updated from one presented in Daly et al. (2013).

the biomass of fish larvae in winter was high but generally comprised of offshore taxa indicative of warm ocean conditions (e.g., rockfishes; Auth et al. 2018). The 2018 winter biomass of fish larvae that salmon prey upon was the 4th highest in the 21-year time series and biomasss in 2015–18 were all within the highest 7 biomass years (fig. 31).

Recent work (Daly et al. 2017) demonstrated that in addition to overall prey biomass the taxonomic composition of fish prey (fig. 31) available for salmon to consume can influence salmon survival. Salmon returns tend to be low when the prey assemblage is comprised of offshore taxa that are advected inshore. In 2018, the winter prey assemblage was comprised largely of species associated with relatively warm, offshore water such as rockfishes (fig. 31), which forecasts low returns of spring Chinook salmon in 2020 and coho salmon in 2019.

The PDO is another index that has been used to predict salmon survival. When the PDO in October–December of the prior year is high, salmon survival tends to be low. In fall 2017 the PDO was the 7th most positive (fig. 2A) of the time series

Based on axis 1 values (59.6% variance explained; fig. 32) from the PCO of the prey composition of winter ichthyoplankton, the index of the 2018 prey composition suggests poor food conditions for 2018 out-migrating juvenile salmon. The relationship between the PCO1 axis values (prey composition) with spring Chinook salmon adult returns to Bonneville Dam, Oregon (fig. 1) two years later is: R^2 = 0.44 ; *p-value* = 0.004; (1998–2015; 1999 outlier year excluded). The correlation between overall biomass of ichthyoplankton in winter and returns of spring Chinook salmon to Bonneville Dam, Oregon, estimates around 161,000 adults returning in 2020, whereas the prey composition suggests one of the poorest returns of the time series at ~89,000 (see Daly et al. 2017 for detailed methodology).

From 1998–2014 winter ichthyoplankton biomass was high when the ocean was cool and vice versa, and salmon survival was low in warm years, possibly due to reduced food resources in spring and summer. Since 2014, however, conditions have been warm, but with high ichthyoplankton biomass. Since 2015, the biomass of offshore warm ocean taxa that have been increasingly observed in the diets of juvenile salmon (Daly et al. 2017), may have led to lower return rates of adults. For example, when juvenile salmon consumed nearshore taxa such as Pacific sand lance (*Ammodytes hexapterus*), sculpins (Cottidae), and smelts (Osmeridae), adult returns were high in subsequent years. By contrast, when yearling Chinook salmon or steelhead (*Oncorhynchus mykiss*) consumed higher amounts of offshore rockfish in May or June, adult returns were typically lower (Daly et al. 2017). Similarly, Dale et al. (2017) found that subyearling Chinook salmon

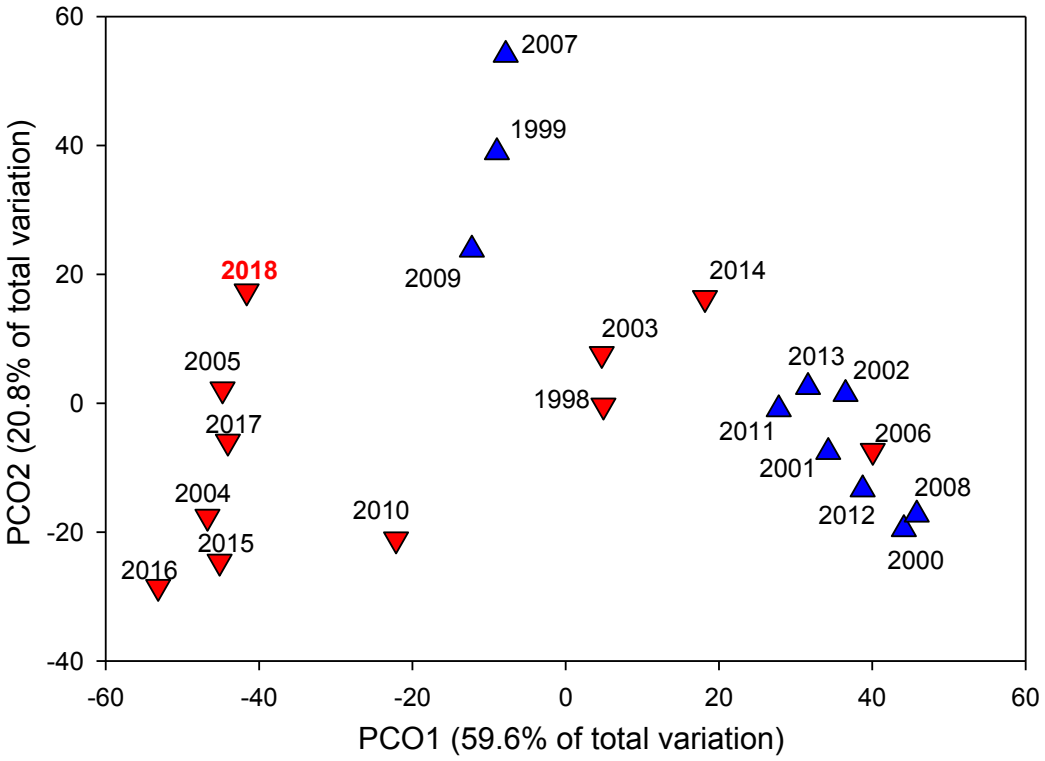

Figure 32. Principal Coordinate Analysis of the prey composition of winter ichthyoplankton that are important prey for out-migrating juvenile salmon (Pacific sand lance, smelts, cottids, northern anchovy, and rockfishes). Red symbols indicate positive winter PDO (warm ocean temperatures) and blue indicate negative winter PDO (cold ocean temperatures). The larvae were collected during winter (January–March) in 1998–2018 along the Newport Hydrographic (NH) line off the coast of Oregon (44.65°N, 124.18–124.65°W). Figure updated from one presented in Daly et al. (2017).

returns were low when feeding upon northern anchovy (*Engraulis mordax*; anchovy) which spawn under warm water conditions off Oregon.

Central California

Catches of juvenile groundfish and epipelagic micronekton from the Rockfish Recruitment and Ecosystem Assessment Survey (RREAS)[28] (Sakuma et al. 2016) in late spring of 2018 indicated declines from the high abundance levels during 2015–17 for pelagic young-of-the-year (YOY) rockfishes and sanddabs (*Citharichthys* spp.) throughout most regions off California (fig. 33). The exception was the fairly high YOY rockfish abundance sampled within the southern California Bight. There was a significant increase in the abundance of adult northern anchovy in the core and south central regions (fig. 32), and their abundance exceeded the previous highs in 2005–06. A small number of adult Pacific sardine (*Sardinops sagax*; sardine) were encountered, more than in roughly the last ten years, but still very low relative to high abundance levels in the late 1990s and early 2000s. YOY anchovy and sardine (not shown) were also at relatively high levels in the survey, particularly in the southern survey region. Market squid and krill (Euphausiids) were at fairly high abundance levels in most regions, particularly the core and Southern California Bight (not shown). Pelagic red crabs (*Pleuroncodes planipes*) were also abundant in the Southern California Bight during the late spring of 2018, a phenomenon sustained since 2015 (not shown).

Shifts in the abundance of various gelatinous organisms reversed in 2018. Catches of *Thetys* salps and other salps were at higher levels in 2018, while catches of pyrosomes dropped considerably from the very high levels seen in 2017 in most regions, particularly in southern and core regions (fig. 34). Pyrosomes continued to be quite abundant in the northern regions, consistent with the high pyrosome catches observed off Oregon and Washington in northern surveys. There was a sharp reversal of the previously low catches of scyphozoan jellyfish (primarily *Aurelia* spp. and *Chrysaora fuscescens*) from previous years, as both of those species were encountered at their greatest relative abundances since the survey commenced in 1990 (fig. 34).

The nMDS analysis based on mean log catch of the fish and cephalopod community from the core RREAS

[28]Epipelagic micronekton samples were collected during May and June by the Southwest Fisheries Science Center Rockfish Recruitment and Ecosystem Assessment Survey and the Northwest Fisheries Science Center Pre-recruit Groundfish Survey, covering a geographic range from the US/Mexico border (32.5°N) to southern Washington (46.5°N). A modified midwater Cobb trawl (10–30 m headrope depth) was used to sample pelagic species along the CCE in the mixed layer where juvenile salmon are typically found. Methods were standardized between regions beginning in 2011 (Sakuma et al. 2016).

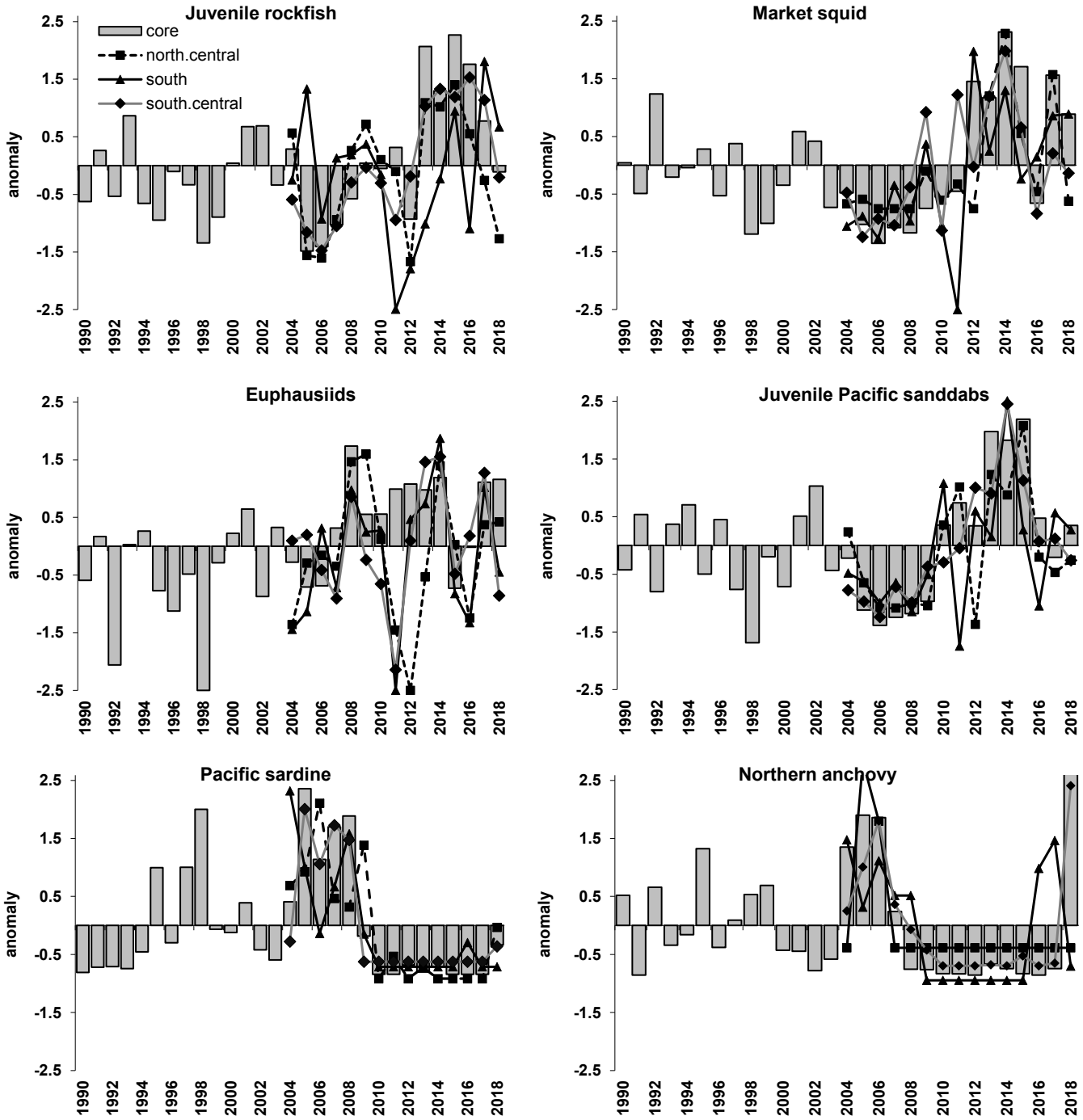

Figure 33. Standardized anomalies (of average (ln(catch+1)) catches) for key forage taxa sampled by the Rockfish Recruitment and Ecosystem Assessment Survey.

region between 1990 and 2018 showed that 2018 clustered close to 2013–15 and was most similar to 2017 (fig. 35 top). The top five most abundant taxa between 1990 and 2017 were, in order, sanddabs, rockfish, young of the year hake, squid and myctophids, and all of these taxa were the top six most abundant in 2018. Adult anchovy, however, were the one exception in 2018 as it was the 3rd most abundant taxa (fig. 35 bottom; red dot represents anchovy while blue dots are other taxa). The influence of anchovy was reflected by a high value of nMDS axis 2 in 2018 (fig. 35 top). The 2018 sampling year was somewhat uncommon as it featured high abundances of both anchovy and sanddabs (there is negative correlation between these species throughout the time-series; sanddab abundance = –0.75⋆anchovy abundance + 2.57, r = 0.45). In 2018 adult sardine

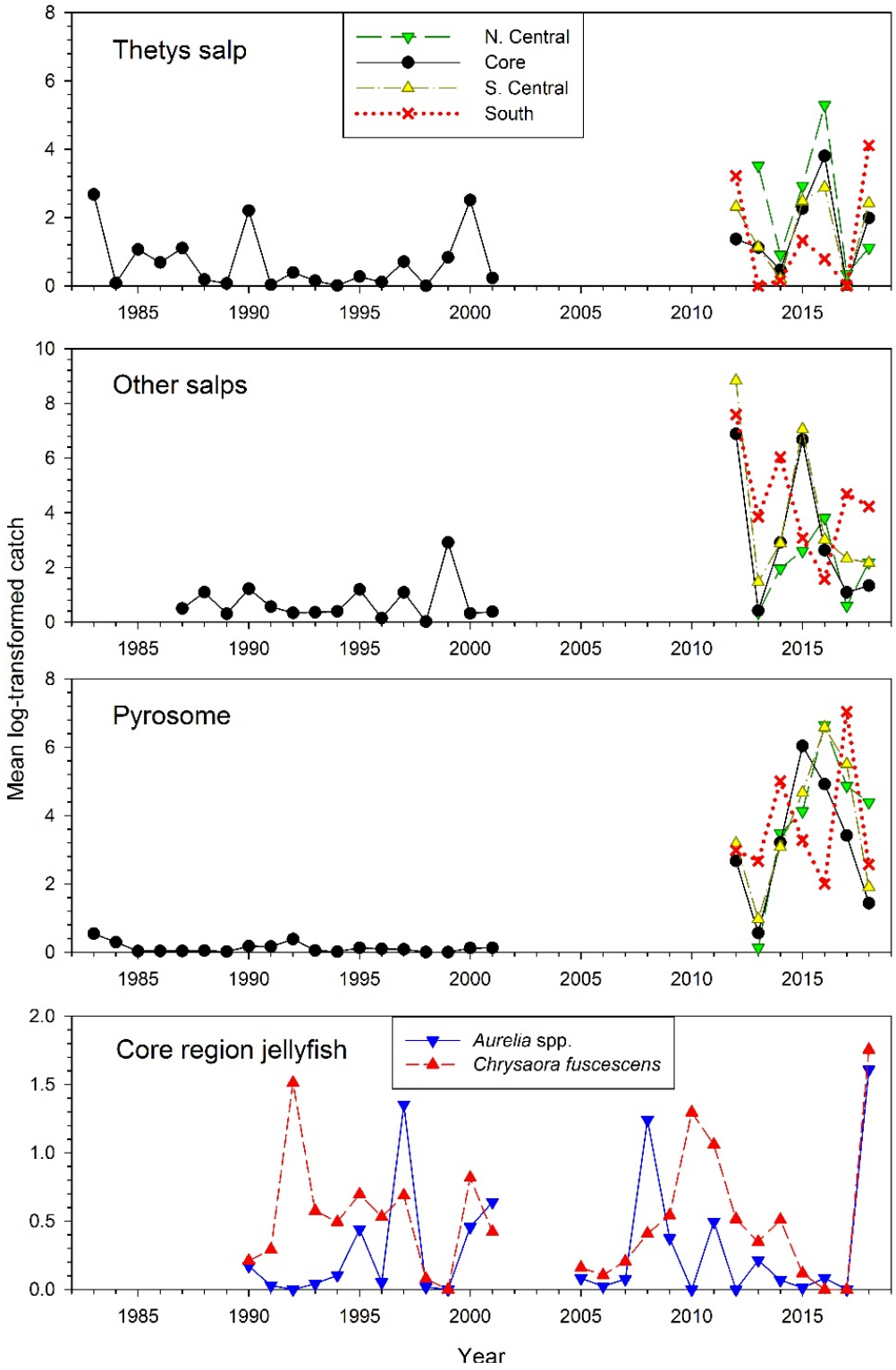

Figure 34. Standardized catches of and pelagic tunicates (*Thetys* salps, other salps, and pyrosomes) and jellyfish (*Aurelia* spp. and *Chrysaora fuscescens*) in the core and expanded survey regions.

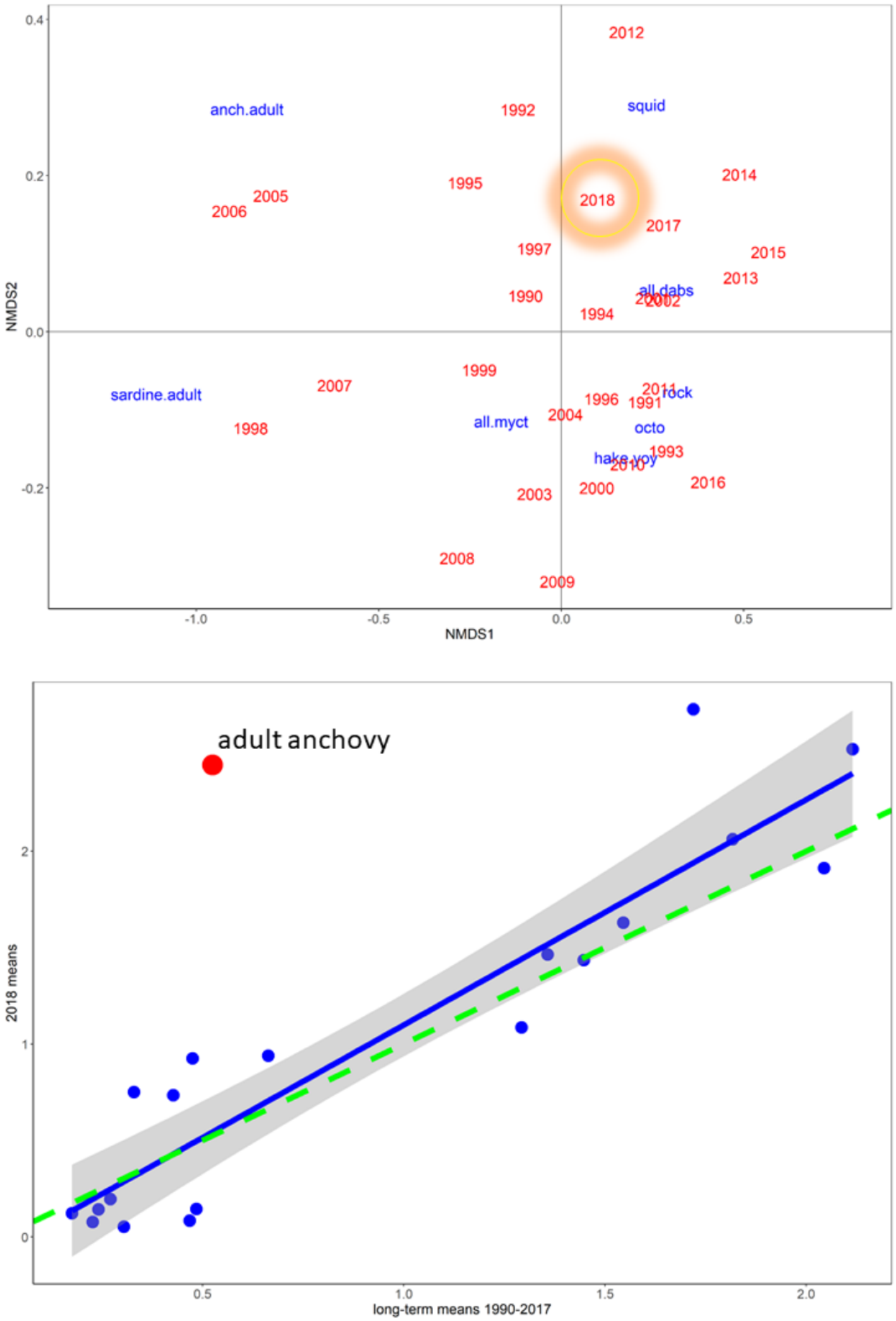

Figure 35. Top) NMDS analysis for eight key taxonomic groups of forage species sampled in the central California core region from 1990–2018. The following species are included: all.dabs = combined speckled and Pacific sanddab; all.myct = myctophids; anch.adult = northern anchovy; hake.yoy = young of the year hake; octo = octopus; rock = juvenile rockfish; squid = market squid. 2018 is circled. Bottom) Mean (average (ln(catch+1)) in 2018 (y axis) vs. sum of mean (average (ln(catch+1)) from 1990–2017 for the 20 most common taxa collected in the core region. Each dot represents a unique taxon. The main outlier, anchovy, is in red. The blue line is the best fit line for all species except anchovy ($R^2 = 0.86$, $p < 0.0001$). The green line is the line of unity (intercept = 0, slope = 1). A species' abundance would be exactly average if fell directly on the green line; values below the green line are lower than normal and vice-versa.

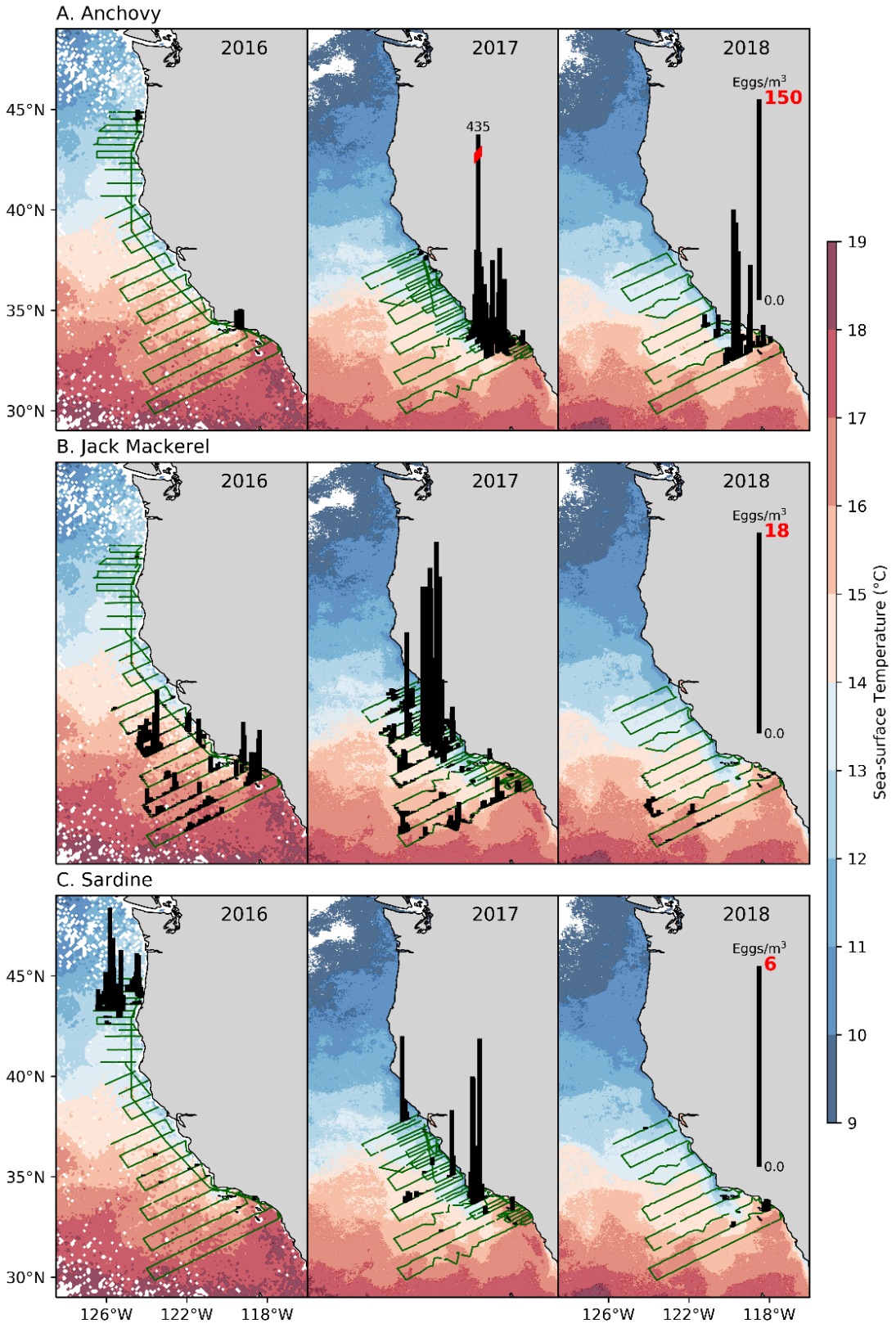

Figure 36. Density of eggs of northern anchovy A), Jack mackerel B), and sardine C) collected with the continuous underway fish-egg sampler (CUFES) during the spring 2016–18 CalCOFI cruise. Data are overlaid on satellite-derived sea surface temperatures (AVHRR 1.4-km resolution; C). Note that scales differ among species.

abundance was very low and 2018 loaded far in multivariate space from years when this species was relatively abundant. Plotting 2018 means for each taxa versus long-term means further emphasized that the assemblage in the core region of the RREAS reflected long-term means for most taxa with the glaring exception of anchovy (fig. 35 bottom).

Southern California

Anchovy eggs collected with a continuous underway fish egg sampler[29] (CUFES) in spring 2018 were somewhat less abundant than in 2017 (fig. 36) but much more abundant than any other year since the mid-1990s (CUFES sampling began in 1996). Most anchovy eggs were collected in the Southern California Bight along CalCOFI line 90, with smaller abundances occurring near Point Conception and the Channel Islands (fig. 36). No anchovy eggs were collected north of Point Conception in 2018. We note that sampling of eggs occurred as part of the spring CalCOFI cruise (5–27 April 2018). Anchovy spawning peaks during March in most years (Moser et al. 2001). Thus, the spawning pattern may not be representative of the full anchovy spawning season.

CUFES sampling also showed that Jack mackerel and sardine egg abundances were extremely low in spring of 2018 (fig. 36); this is consistent with a declining trend since the mid-2000s. Where Jack mackerel eggs did occur in 2018, they were far offshore in the southwest portion of the CalCOFI core sampling area (fig. 36). The only year in the available time series in which Jack mackerel egg abundances were comparably low was during the severe El Niño of 1998. Sardine eggs generally were restricted to the inshore area of the Southern California Bight (fig. 36). Sardine eggs have been rare since 2014 but were the least abundant during 2018 of any year in the available time series.

Whereas fish assemblages were trending towards average conditions in the first half of 2018 throughout most of the CCS, this was not the case in southern California. Rather, the 2018 ichthyoplankton assemblage collected from the spring CalCOFI cruise from lines 80 and 90[30] was more similar to 2014–16 than it was to 2017. In spring 2018 several mesopelagic taxa that are associated with warm water and have biogeographic centers of distribution south of southern California were highly abundant. Specifically, Panama lightfish (*Vinciguerria lucetia*) had the 7th highest abundance on record, Mexican lampfish (*Triphoturus mexicanus*) the 2nd highest (behind only 2015), dogtooth lampfish (*Ceratoscopelus townsendi*) 15th highest, and species in the family Gonostomatidae (bristlemouths, comprised largely of species in the genera *Cyclothone* 3rd highest (fig. 37). By contrast, northern lampfish (*Stenobrachius leucopsarus*) and blue lanternfish (*Tarletonbeania crenularis*), the most common mesopelagic species with centers of distribution north of southern California, had some of the lowest abundances since 1951 in spring 2018 (fig. 37).

Similar to CUFES results (fig. 36), abundances of sardine, Jack mackerel, and Pacific mackerel larvae remained at historically low levels in southern California in spring 2018 (fig. 38). However, while CUFES suggested a decrease in anchovy eggs between 2017–18 (fig. 36), anchovy larvae in CalCOFI samples were much higher in 2018 than 2017 (fig. 38). Indeed, spring anchovy abundance was the 3rd highest since 1951 and the highest since the mid-1960s (fig. 38).

Larval abundances of common groundfishes in southern California also were extreme in 2018 (fig. 39). Sanddabs (mostly Pacific sanddab, *Citharichthys sordidus*, and speckled sanddab, *C. stigmaeus*) have been very low since 2015 and were low again in 2018 (fig. 38). Slender sole (*Lyopsetta exilis*) and English sole (*Parophrys vetulus*) abundances, however, were very high in 2018, displaying the 5th and 2nd highest abundances, respectively, on record (fig. 39). Abundances of rockfishes were close to average in 2018 (25th highest out of 56 years; fig. 39).

From a multivariate (nMDS) perspective, 2018 aligned closely on nMDS1 with 1985–87 and 2014–16 (fig. 40 top). All of these years were characterized by having high abundances of the four southern mesopelagic species shown in Figure 37 (red font in figs. 40 top and 40 bottom). Larval abundances in 2018 were lower on the nMDS2 axis relative to 1985–87 and 2014–16, likely reflecting the influence of anchovy, which loaded negatively on nMDS2. Notably, the 2018 assemblage was quite different from 2017 as the 2017 assemblage was characterized by taxa with centers of distribution within or close to southern California (colored green in fig. 40 top). Plotting mean abundances of taxa in 2018 versus long-term means further emphasized how different from average the assemblage was in 2018 (fig. 40 bottom). Two species with northern biogeographic ranges (northern lampfish and hake) and one centered on southern California (Jack mackerel) were well below long-term means in 2018 (fig. 40 bottom), while the three species with southern ranges (Mexican lampfish, Panama lightfish, and bristlemouths) as well as the cosmopolitan English sole and California smoothtongue (*Leuroglossus stilbius*) were well above long-term means (fig. 40 bottom). Anchovy and sardine were not included in Figure 40

[29]Water is continuously pumped from 3-m depth and particles are collected over sequential sampling intervals (e.g., 5–30 minutes) on a cod end.

[30]Ichthyoplankton is collected with bongo nets equipped with a flowmeter, 0.71-m diameter rings and 505-µm mesh. Nets are lowered to 210 m (or within 20 m of the bottom at shallow stations) and towed at a constant rate at a 45° angle to the surface. This analysis uses only samples from CalCOFI lines 80 and 90.

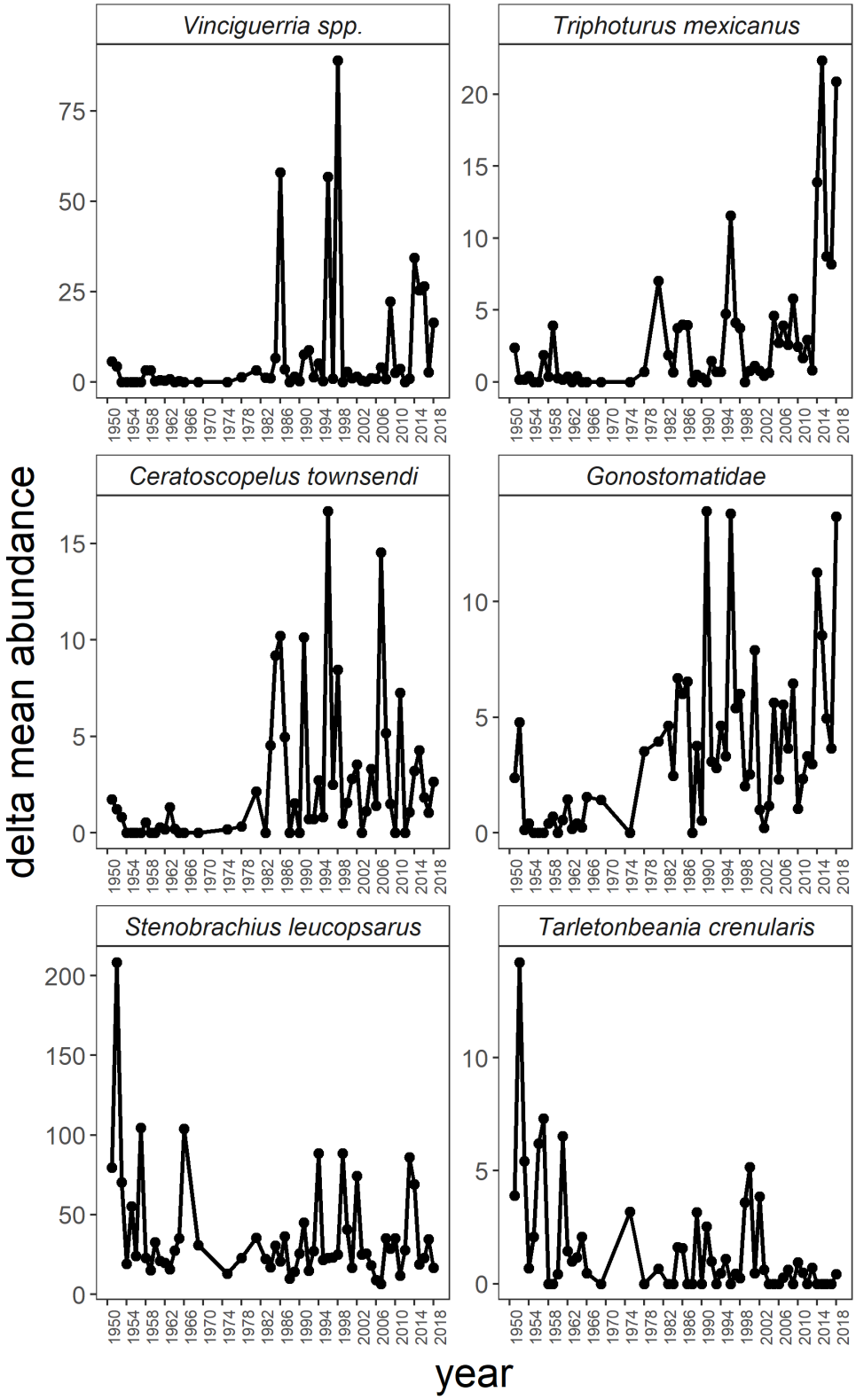

Figure 37. Mean abundances from CalCOFI lines 80 and 90 of larvae from four mesopelagic taxa with southern (*Vinciguerria lucetia*, *Triphoturus mexicanus*, *Ceratoscopelus townsendi*, and Gonostomatidae) and northern (*Stenobrachius leucopsarus* and *Tarletonbeania crenularis*) biogeographic distributions relative to southern California from 1951–2018.

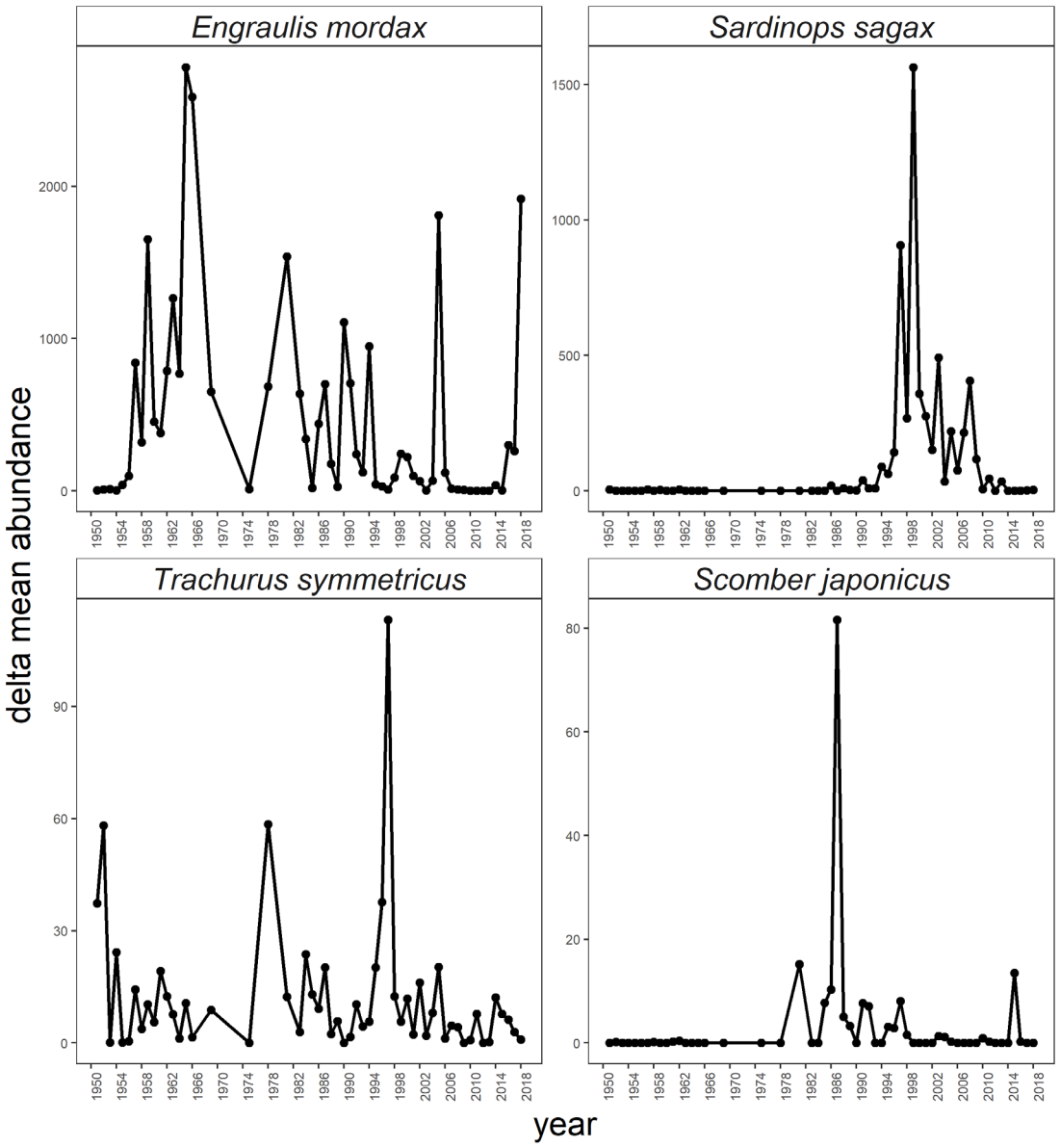

Figure 38. Mean abundances from CalCOFI lines 80 and 90 of larvae of four coastal pelagic species from 1951–2018.

bottom because the scale of their abundances are so much higher than the other taxa, but anchovy were much higher and sardine much lower than long-term means.

Management of the spiny lobster (*Panulirus interruptus*) fisheries in California currently relies exclusively on fisheries-dependent data streams. Thus, leveraging the value of lobster larval (phyllosoma) collections by CalCOFI to understand fishery productivity and assess the influence of ocean conditions is an important goal for the California Department of Fish and Wildlife, who are charged with managing this fishery. A 57-year time series of the offshore abundance of early stage phyllosoma larvae from CalCOFI bongo net samples within the Southern California Bight was generated by Koslow et al. (2012) who concluded that phyllosoma tend to be higher when ocean conditions are warm (e.g., years with high SST, positive PDO

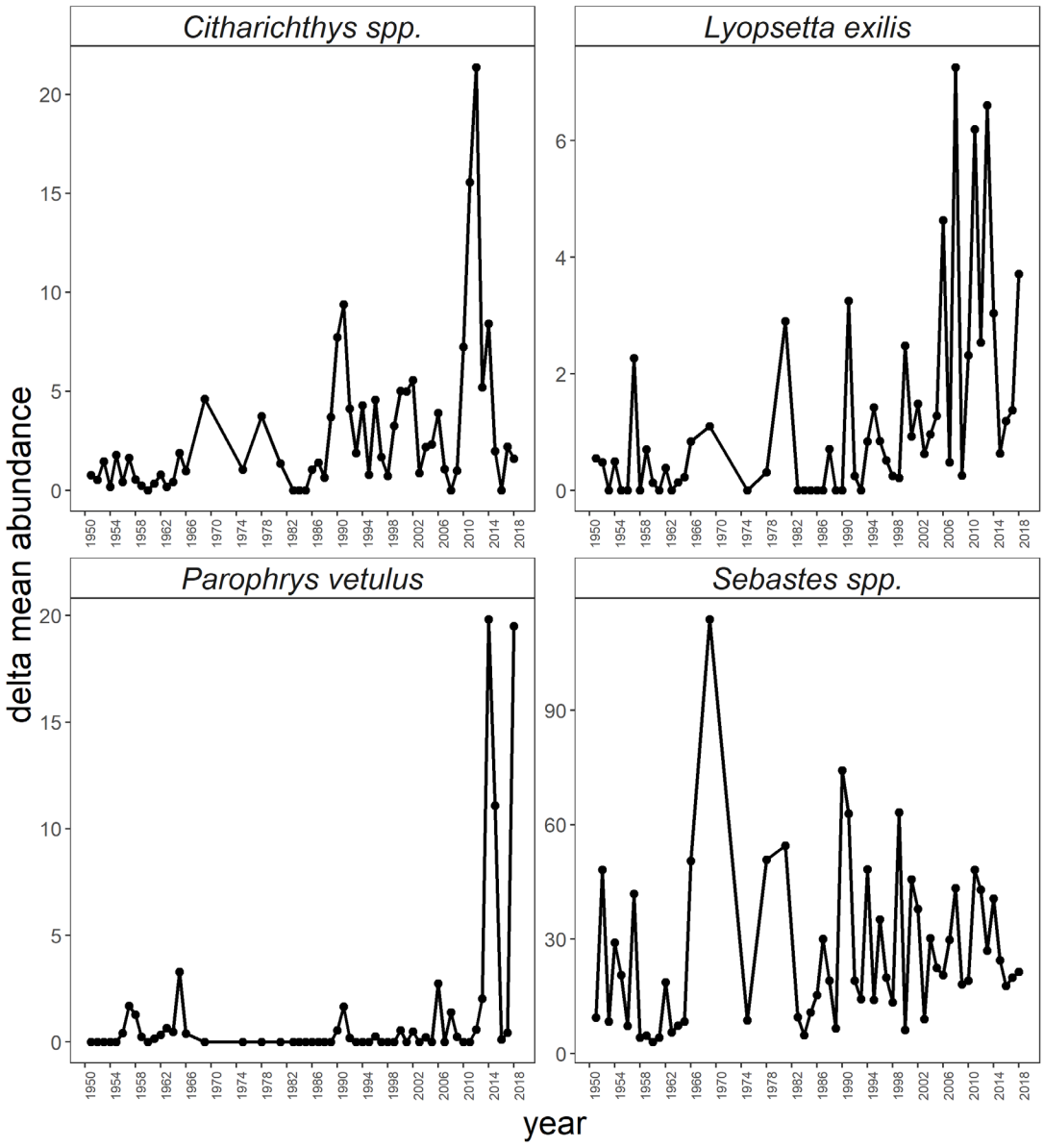

Figure 39. Mean abundances from CalCOFI lines 80 and 90 of larvae of four groundfish species from 1951–2018.

and MEI indices). In addition, phyllosoma abundance was significantly correlated with lobster landings seven years later.

CalCOFI phyllosoma data are now available through 2015, thus allowing us to examine the impact of the warm conditions of 2014–15 on lobster productivity and determine if the relationship between SST and phyllosoma abundance persists after adding years subsequent to 2008 (the last year analyzed by Koslow et al. 2012). Phyllosoma abundance was at a record high in 2014 and 14th highest in 2015 (fig. 41 top). The relationship between SST and phyllosoma abundance with data through 2015 was essentially the same ($r = 0.38$, $p = 0.006$) as reported by Koslow et al. (2012) ($r = 0.39$, $p < 0.001$; fig. 41 bottom). Based on this relationship, we expect that phyllosoma abundances remained elevated from 2016–18, and will test this prediction as data becomes available.

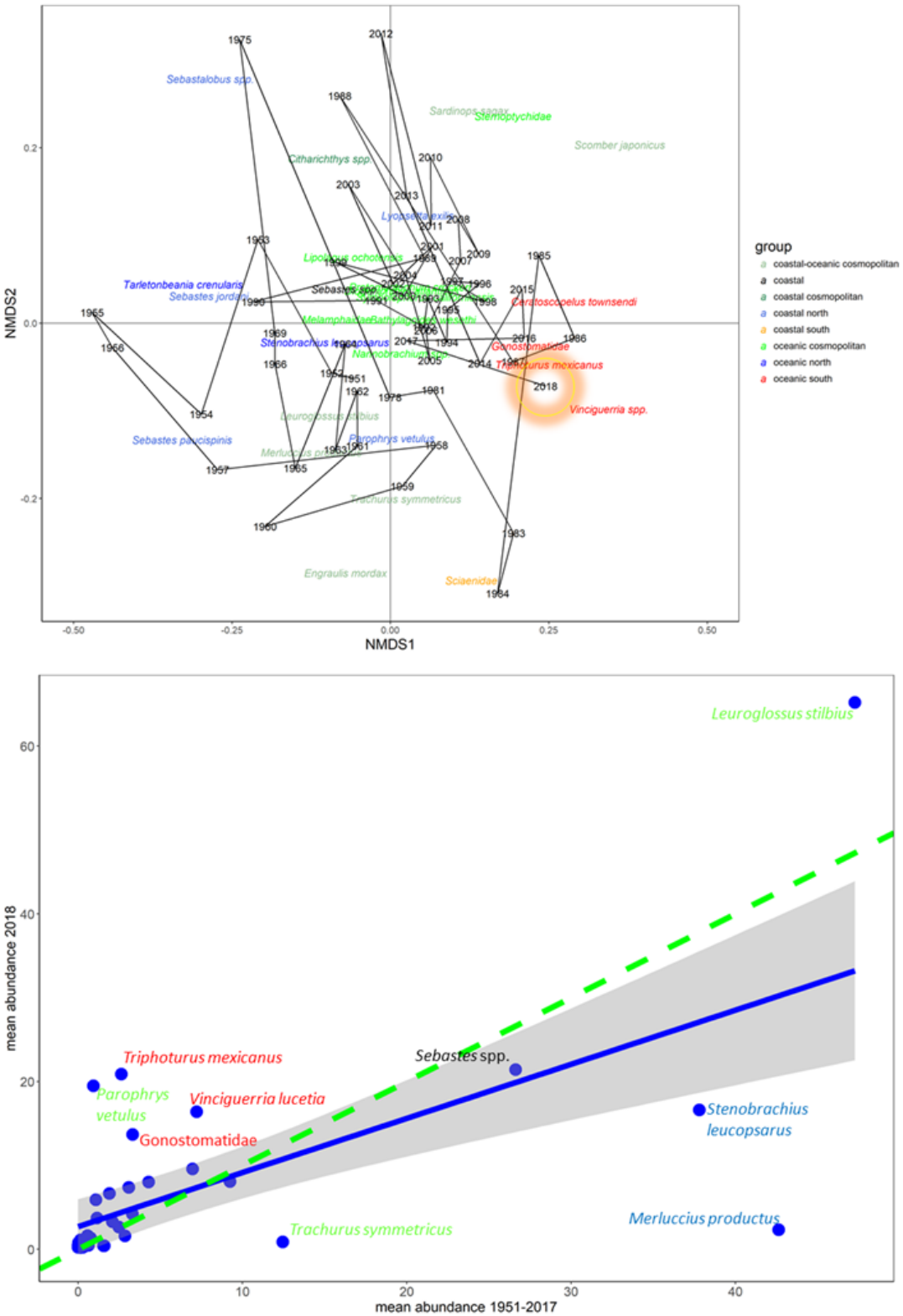

Figure 40. Top) NMDS analysis for taxa sampled from CalCOFI lines 80 and 90 from 1951–2018. Taxa names are colored based on habitat and biogeographic ranges. Bottom) Mean in 2018 (y axis) vs. long-term mean (1951–2018) of common taxa collected from CalCOFI lines 80 and 90. Each dot represents a unique taxon. The blue line is the best fit line for all species except anchovy and sardine ($R^2 = 0.42$, $p < 0.001$). The green line is the line of unity as in Figure 35. Species far above and below the line are demarcated with colors that correspond to habitat and biogeographic range as defined in panel A.

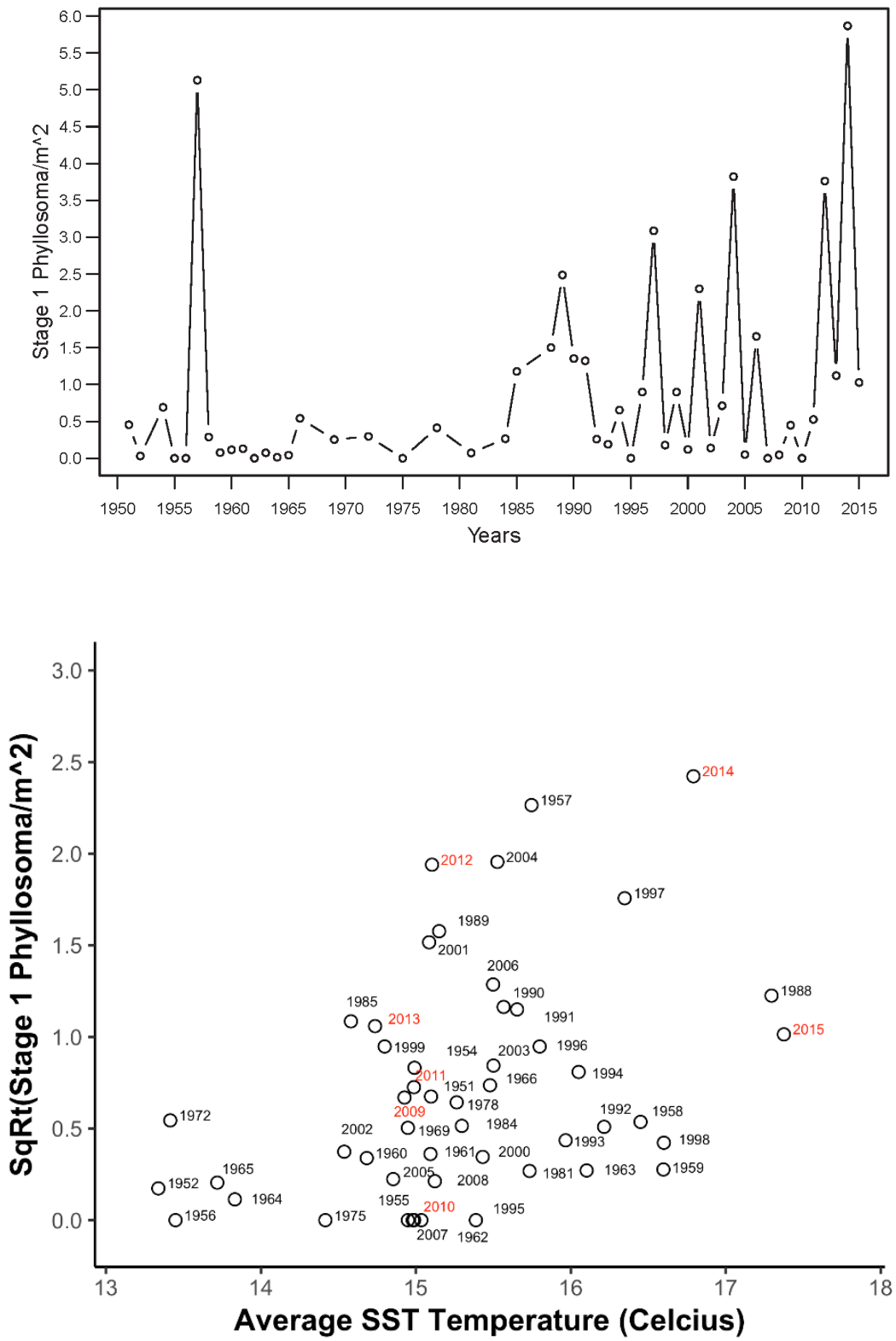

Figure 41. Top) Abundance of stage 1 lobster (*Panulirus interruptus*) phyllosoma larvae from 1951-2015. Bottom) Mean annual sea surface temperature (10 m) plotted against square-root transformed early-stage phyllosoma abundance. All sampling was from core CalCOFI stations over the continental shelf (≤ station 60). Years in black represent years that were previously analyzed in Koslow et al. (2012) while years in red represent the most recent years not previously analyzed.

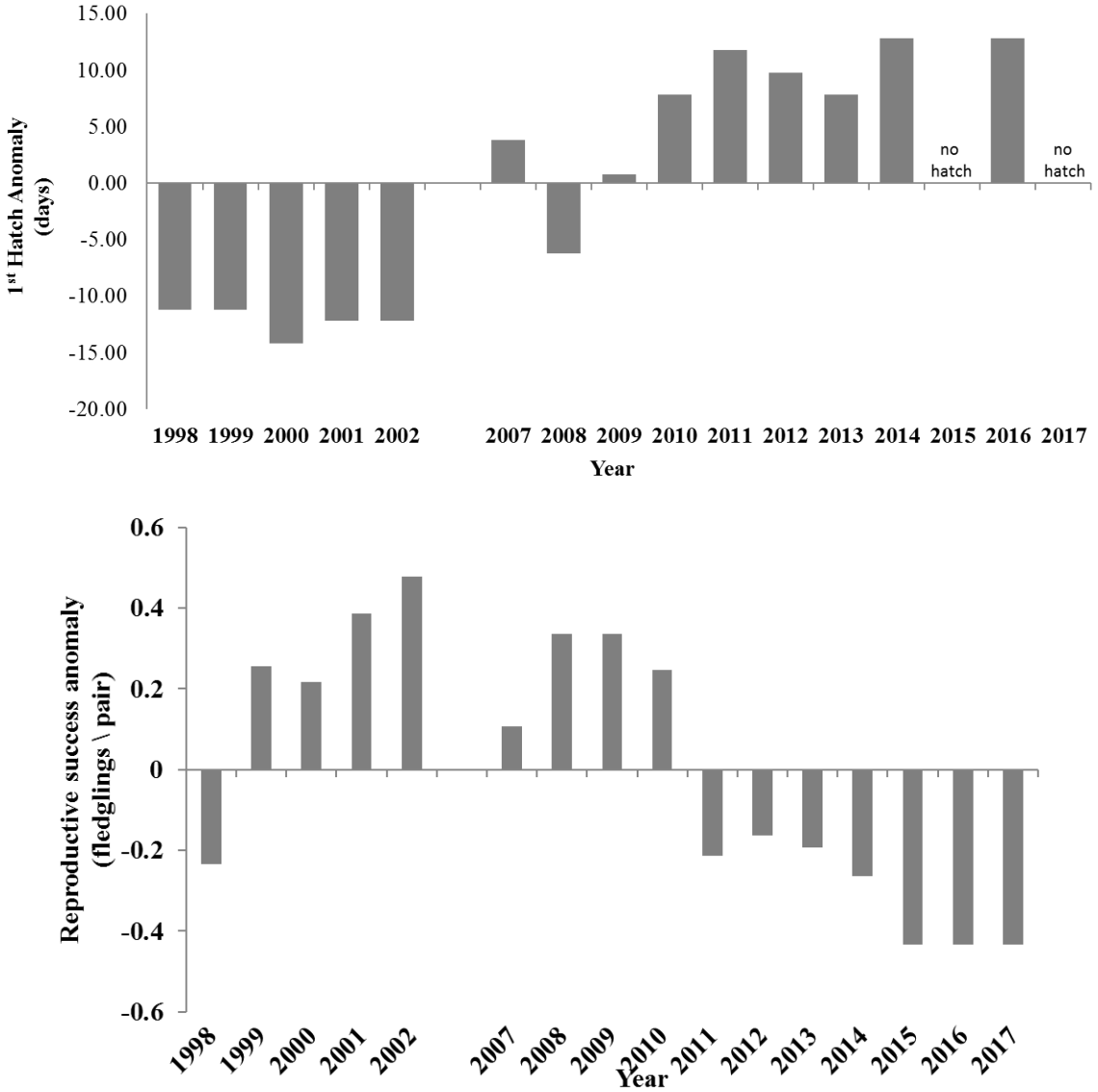

Figure 42. Anomalies of first chick hatch date (upper panel) and reproductive success (lower panel) for common murres nesting at Yaquina Head, Oregon, 1998–2017. 2017 was the third year that the colony failed to produce chicks from all but one small area where <10 chicks fledged each year.

REGIONAL PATTERNS IN BIRDS

Northern California Current: Yaquina Head, Oregon

Common murre (*Uria aalge*; murre) at Yaquina Head, Oregon, experienced complete reproductive failure throughout the entire colony in 2017. This was the first year in 16 years of data collection that no eggs were incubated long enough to hatch a chick at any location in the colony. This also was the third consecutive year that no murre chicks were produced throughout most of the colony, and breeding conditions in 2017 were the worst of the past three years (fig. 42). As in previous years the reproductive failure was caused by both top-down predation and bottom-up food limitation. While the top-down signal is the most evident, the bottom-up signal was notable. For example, the only location where a few murre chicks fledged in 2015 and 2016 was a small rock near sea level that is generally not affected by avian predators. Even at this mostly predator-free site, no eggs survived for chicks to hatch in 2017. Murre reproductive success was 0 fledglings/pair, which is the lowest recorded for the colony since surveys began in 1998 and was even lower than during the 1998 El Niño (Gladics et al. 2015). Preliminary results from 2018 indicate that murre experienced improved reproductive success compared to the past three years of colony failure (data not shown).

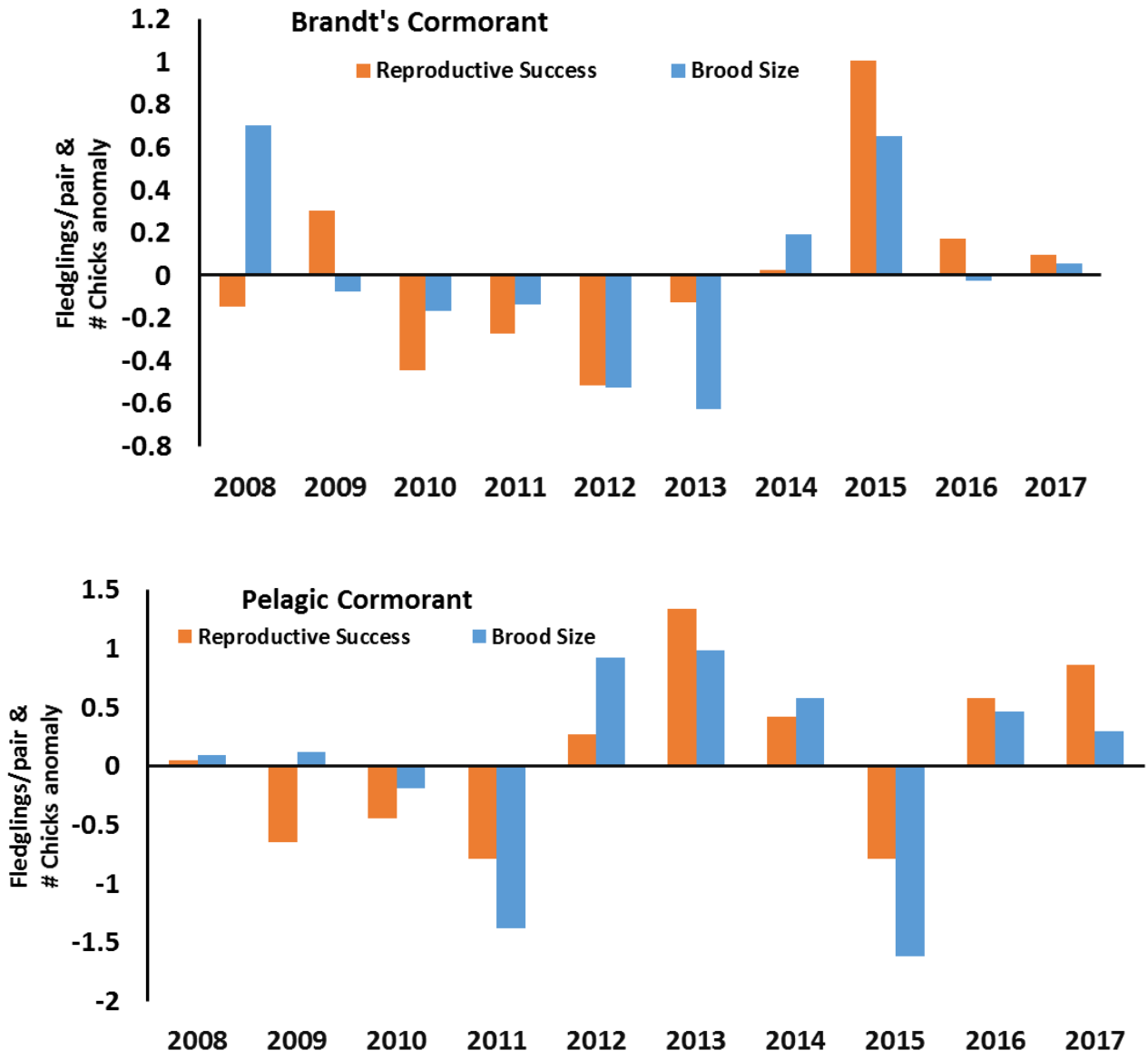

Figure 43. Anomalies of reproductive success and brood size for cormorants nesting at Yaquina Head, Oregon, 2008–17. Cormorants had average to above average reproductive success and brood size.

Since 2011 much of the reproductive loss for murre at Yaquina Head has been due to egg and chick predation (Horton 2014). Murre egg and adult losses in 2017 were less than in 2016, but still similar (2.38 eggs destroyed per hour of observation, n = 203 hours) to the post 2011–16 mean of high disturbance years. Lower egg depredation rates compared to 2016 is partly because fewer eggs were present to be consumed. In 2017, predation pressure was so intense, and murre were not committed to breeding (due to predation pressure and lack of sufficient prey resources), that average incubation time was less than 3 days before the egg was lost—well under the approximately 30 or more days needed to hatch a chick. As in most previous years, disturbances were primarily (80%) caused by bald eagles (*Haliaeetus leucocephalus*).

In contrast to murre, Brandt's (*Phalacrocorax penicillatus*) and pelagic (*P. pelagicus*) cormorants both successfully reared young in 2017. Brandt's cormorants' reproductive success (0.79 fledglings/nest) was similar to 2014 and 2016, but less than 2015 (1.70 fledglings/nest) and overall slightly above the long-term mean (fig. 43). Median hatch date (July 6) was slightly earlier than average for Brandt's cormorant (fig. 44), while average brood size (1.73 chicks) was close to the long-term mean (fig. 43).

Pelagic cormorants had their second highest reproductive success since 2008 (1.65 fledglings/nest), only surpassed by 2013 (2.13 fledglings/nest; fig. 43).

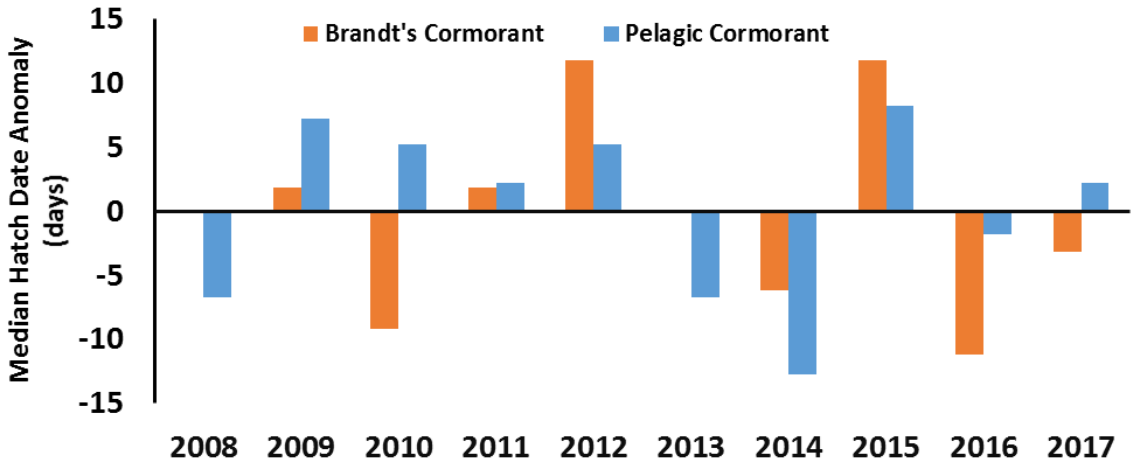

Figure 44. Anomalies of median hatch dates for Brandt's and pelagic cormorants at Yaquina Head, Oregon 2008–17. Brandt's hatch date was over a week earlier, while pelagic cormorant hatch date was near the long-term mean.

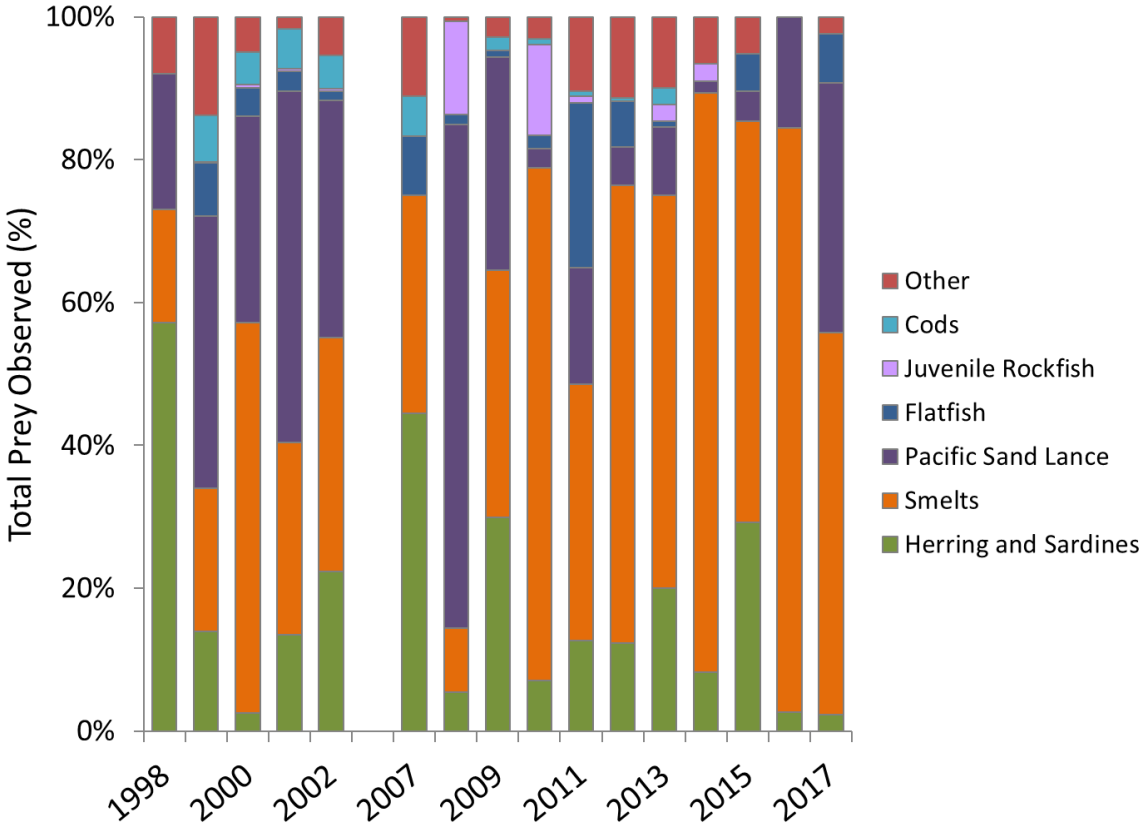

Figure 45. Prey fed to common murre chicks (% occurrence) at Yaquina Head, Oregon, 1998–2017.

There were 46 nests visible from observation platforms, second only to 2014 (34 nests) and a more than 400% increase from 2015 and 50% increase from 2016 (data not shown). Pelagic cormorant reproductive success has been highly variable during our time series (fig. 43). Median hatch date, which can track potential systemic changes to phenology, was July 18, which was a bit later than the long-term average (fig. 44).

During the duration of the time-series the four main forage fish species fed to murre chicks were smelt (Osmeridae), herring, sardine, and Pacific sand lance (fig. 45). The failure of most of the colony prior to chick rearing made it challenging to quantify diet composition in 2015–17. Although there were no instances when fish were actually fed to chicks in 2017, we were able to directly observe which fish were in the

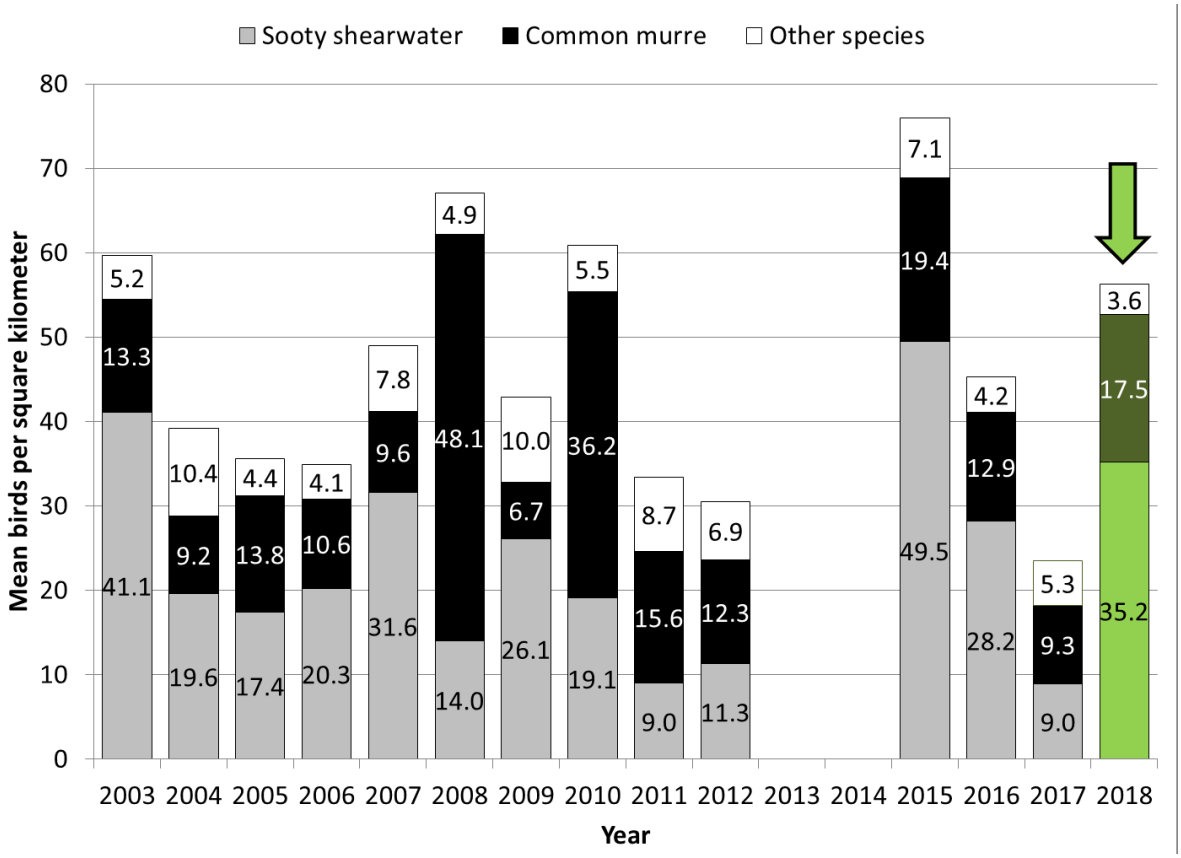

Figure 46. Mean seabird density observed on the continental shelf between Cape Flattery, WA (48.23°N) and Newport, OR (44.67°N) during annual JSOES surveys during late June. In 2018 sooty shearwater and common murre are depicted by light and dark green, respectively.

beaks of birds flying into the colony. Diets in 2017 were again dominated by smelt (53%), similar to 2015, but less so than 2014 (81%) and 2016 (82%), continuing a trend of smelt-dominated diets for six of the past eight years (since 2010; fig. 45). Murre diets in 2017 had an unexpectedly high percentage of sand lance (35%), which has been scarce in the diets since 2010 and is generally associated with cold water temperatures (Gladics et al. 2014, Gladics et al. 2015). Clupeids (primarily Pacific herring) are generally associated with warmer water off Oregon and positive PDO indices (Gladics et al. 2015; Daly et al. 2017), although their occurrence in recent warm and positive PDO years has been lower than during previous warm water events.

Northern California Current: Cape Flattery, Washington to Newport, Oregon

Information on seabird density patterns for the northern domain of the California Current during June is provided from the JSOES (this survey also provided data from Figures 28–30). Bird densities in 2018 were more typical compared to the extremely low densities in 2017 (fig. 46). Mean total bird densities for the 2018 survey were the 5th highest reported in the 14-year JSOES data set (56.2 birds per km^2 compared to a median value of 44.1 birds per km^2). The majority of birds observed during the survey (93.8% of all individuals counted) were sooty shearwaters (*Ardenna grisea*, 68.2%) and murre (25.6%). Sooty shearwater abundance was the 3rd highest on record for this survey (35.2 birds per km^2, compared to the time-series median of 19.9 birds per km^2; fig. 46). Sooty shearwater were highly aggregated as 93.3% of all individuals observed during the survey were on the two transects closest to the mouth of the Columbia River (between the Columbia River at 46.16°N and Cape Meares, OR, at 45.48°N). Given that sooty shearwaters do not breed in the northern hemisphere, this aggregation pattern probably indicates that birds were aggregating on prey items such as forage fishes, squid, or krill abundant near the Columbia River mouth.

Similar to the pattern seen in sooty shearwaters, murre abundance in 2018 was the 4th highest on record (17.5 birds per km^2, compared to the time-series median of 13.1 birds per km^2). Murre were also aggregated near the Columbia River mouth, with 72.9% of all individuals observed on the two transects closest to the Columbia River (Columbia River and Cape Meares, Oregon; fig. 1). While aggregations of murre are to be expected near Cape Meares regardless of prey abundance due to

the large murre breeding colonies located in this area (~200,000 birds), the Columbia River transect is ~80 km north of Cape Meares, and ~30 km from the nearest murre colony that is near Tillamook Head, Oregon (fig. 1). It is reasonable to infer the large numbers of murre seen near the Columbia River mouth—like the shearwaters in the same area—were attracted to abundant prey items.

The 2018 JSOES surface trawls during this same survey showed that market squid were present in fairly high abundance (fig. 28), although it is not known whether birds were consuming squid. Pacific herring and surf smelt (*Hypomesus pretiosus*) were also present in surface trawls (fig. 28), and these species are known to occur in both shearwater and murre diets. There is mounting evidence that the region near the Columbia River mouth is an important foraging habitat in the northern California Current for both sooty shearwater and common murre, and that there is a direct connection between river plume dynamics and seabird prey abundance in the marine environment (Adams et al. 2012; Zamon et al. 2014; Phillips et al. 2017; Phillips et al. 2018). Data from 2018 seabird distributions support the hypothesis that the Columbia River plume plays an important role in trophic interactions for seabirds in this domain of the California Current.

Northern California Current: Castle Rock National Wildlife Refuge

Murre are the most abundant surface nesting seabird at Castle Rock, California[31], and their reproductive success, nesting phenology, and chick diet have been studied since 2007. The percent of nesting pairs that successfully fledged young in 2017 was based on 77 breeding pairs monitored every other day for the duration of nesting. As at Yaquina Head, Oregon, murre experienced complete reproductive failure at this island (0 fledglings per pair) in 2017 for the first time since monitoring began 11 years ago (fig. 47A). Many murre (83%) abandoned nests prior to hatching, presumably due to inability to maintain incubatory obligations while meeting their own energetic needs from prey available in waters within flight distance of Castle Rock. For the few nests producing chicks, 100% of the chicks died prior to fledging, with starvation being the primary cause of death. While the bottom-up food limitation was the primary cause of mortality, the food limitation caused murre to frequently leave chicks alone at the colony in search of prey, and these unprotected chicks were sometimes consumed opportunistically by western gulls (*Larus occidentalis*) that also nest at the island. Reproductive failure of murre at Castle Rock is consequential for the overall population of murre nesting in the California Current as this island is one of the most populous colonies south of Alaska (Carter et al. 2001).

In 2017, the average nest initiation date for common murre was 23 May, which was 13 days later than the long-term average at this colony (fig. 47B). This delay in nesting is indicative of a delay in upwelling or other environmental conditions that limit the abundance of prey (Schroeder et al. 2009). Although the timing of nesting by murre is not a direct response to the onset of upwelling in the spring, the increased availability of food associated with upwelling improves the body condition of egg-laying females and thereby influences the timing of nesting (Reed et al. 2006).

Typically, diet surveys would be conducted 6 days per week during the chick-rearing period to determine composition of prey fed to common murre chicks. In 2017, however, very few prey were actually seen at Castle Rock despite extensive survey efforts. We assume that the lack of observations was due to the scarcity of prey and early starvation of chicks. Only four individual fish were observed: two anchovy, one Pacific sand lance, and one flatfish (fig. 47C). These observations provide further evidence that, as detected from fish surveys off Oregon (figs. 26–28, 31–32), the prey community in much of the northern California Current continued to be comprised of atypical species that are associated with relatively warm water (similar to 2016), and that the 2016–17 forage community differed greatly from those found between 2007–15 (fig. 47C). Although it is not possible to draw conclusions about the composition of prey based on 4 observations, we can state with confidence that prey was scarce around Castle Rock in 2017.

Brandt's cormorant is the second-most abundant surface-nesting seabird at Castle Rock, and their reproductive success has been studied since 2011. In 2017, we observed 31 breeding pairs at Castle Rock. These pairs typically initiated nesting but, of the 31, only 58% (n=18) produced eggs in 2017. In addition to this reduced breeding effort, all nests that were initiated failed prior to hatching due to nest abandonment and no chicks were observed in 2017 (fig. 47D). Notably, this finding contrasts with Yaquina Head, Oregon, where Brandt's cormorant reproductive success was slightly above the long-term average (fig. 43). Similar to murre, this level of failure has never been documented at Castle Rock, and provides further evidence that prey was so scarce that adult cormorants were unable to meet their own energetic needs by foraging within flight distance of Castle Rock and had to abandon nests to avoid starvation.

[31]Castle Rock National Wildlife Refuge, an island off Crescent City, California has frequently been the most populous single-island seabird breeding colony in California (Carter et al. 2001). A remotely-controlled video monitoring system was installed at this island in 2006. For purposes of assessing the state of the California Current, the reproductive performance of common murre and Brandt's cormorants is provided. For common murre, nesting phenology and chick diet between 2007 and 2016 is also provided.

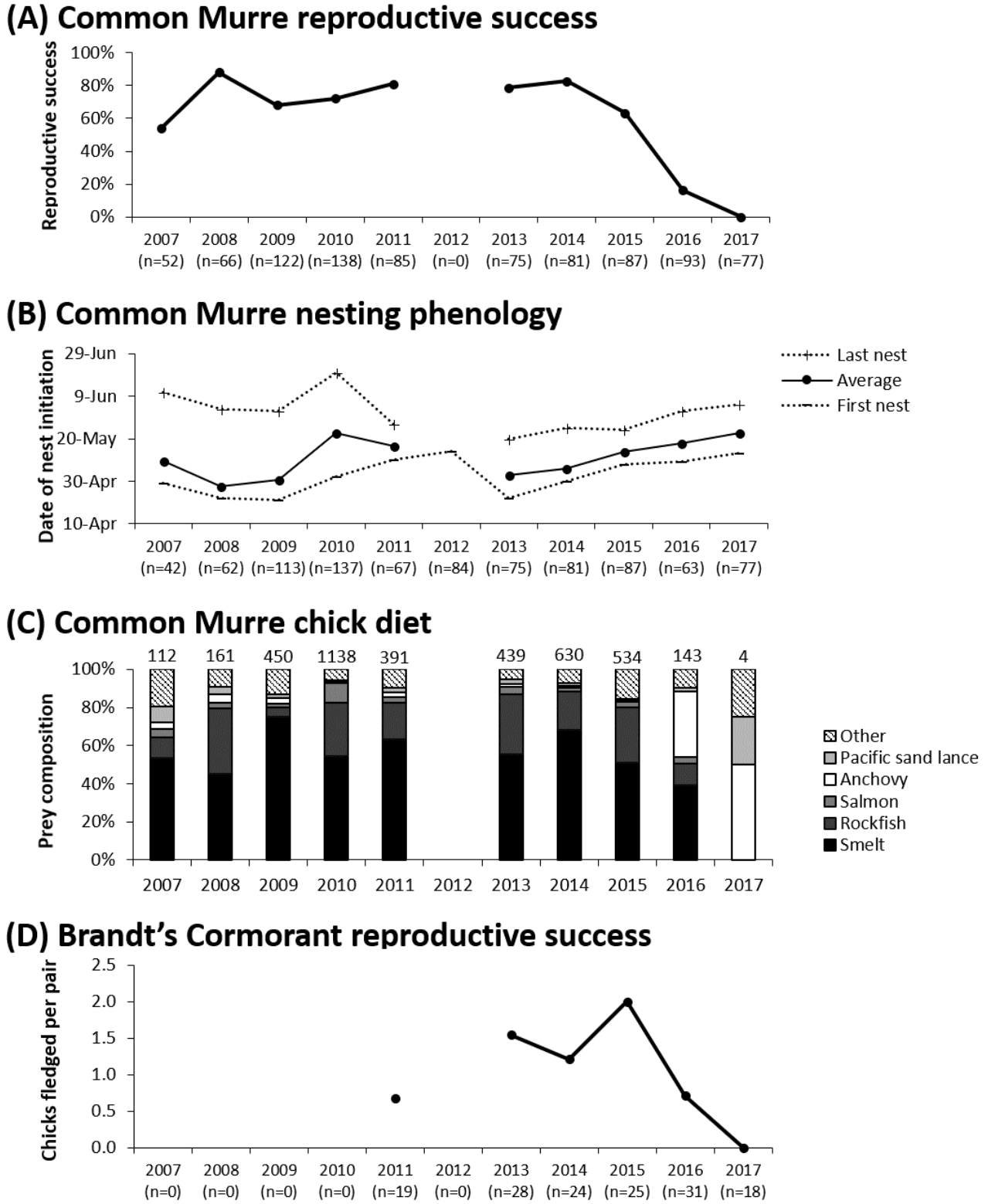

Figure 47. Reproductive data for seabirds nesting at Castle Rock National Wildlife Refuge, Del Norte County, CA between 2007 and 2017; (A) Percent of common murre nesting pairs that successfully fledged young. The sample size (n) represents the total number of nesting pairs observed per year, and this figure does not include the success of replacement clutches. (B) First, average, and last dates for nests initiated by common murre. The date of nest initiation was defined as the day that an egg was laid at a nest site. The sample size (n) represents the total number of nests observed each year where nest initiation dates were accurate to ±3.5 days. (C) Composition of prey delivered to chicks by common murre. Numbers above each bar indicate the total number of prey identified each year. (D) Chicks fledged per nesting pair of Brandt's cormorant. The sample size (n) represents the total number of nesting pairs observed per year, and this figure does not include the success of replacement clutches. For each section, data from 2012 is lacking due to premature failure of the video monitoring system.

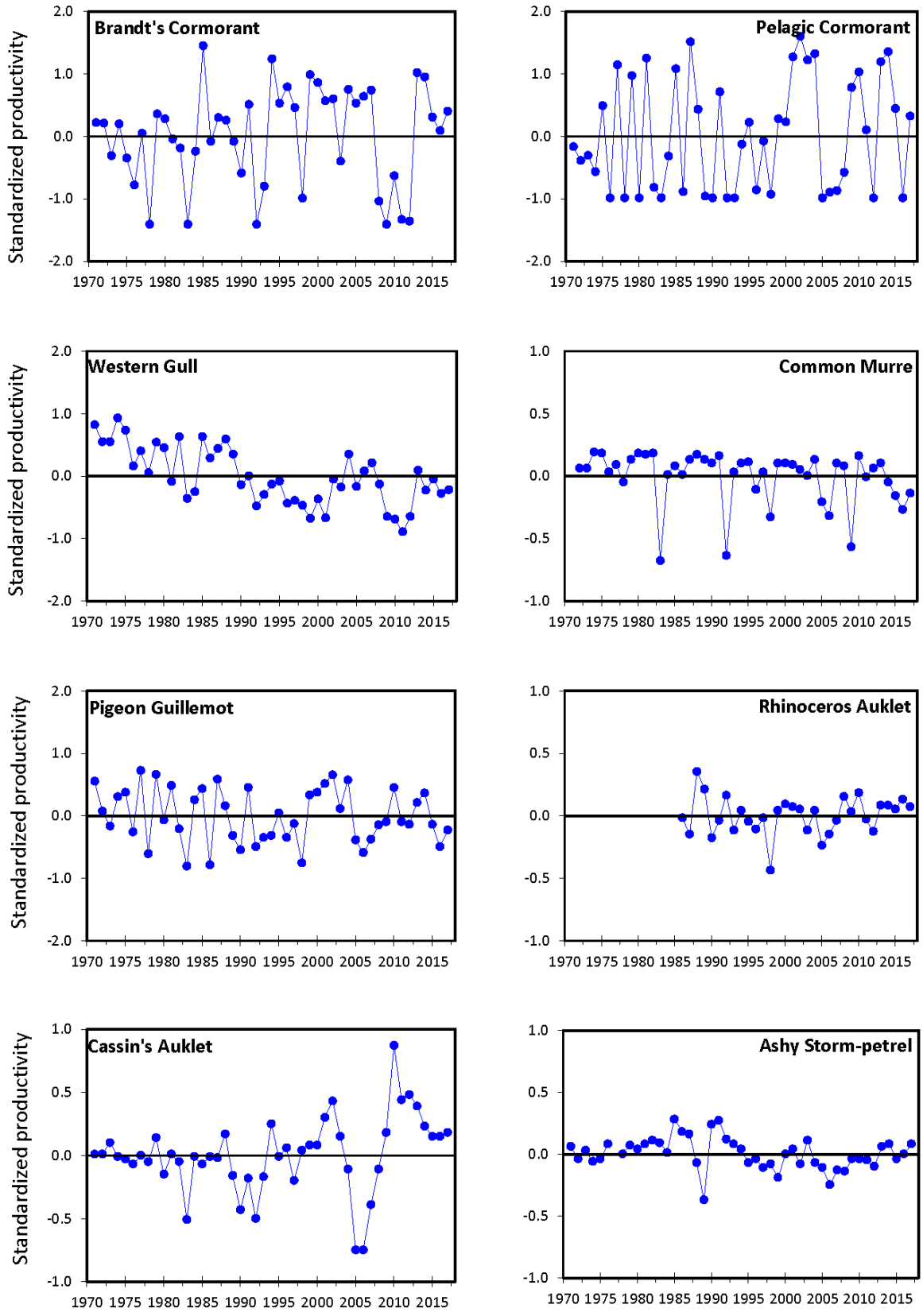

Figure 48. Standardized productivity anomalies through 2017 (annual productivity minus the 1971–2017 mean) for 8 species of seabirds on Southeast Farallon Island.

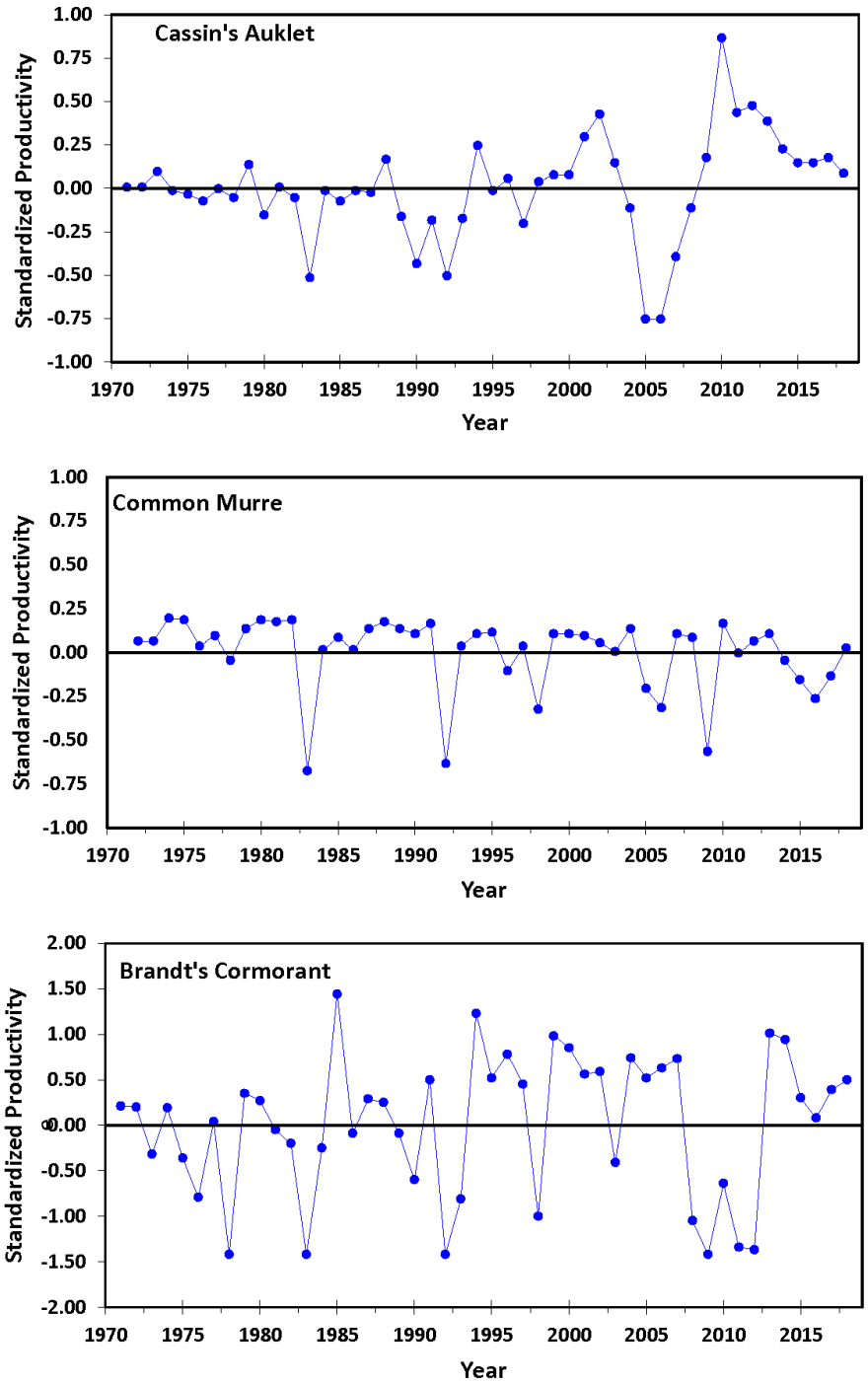

Figure 49. Standardized productivity anomalies through 2018 (annual productivity minus the 1971–2018 mean) for 3 species of seabirds on Southeast Farallon Island.

Central California: Southeast Farallon Island

Reproductive success was average or below average for most birds at Southeast Farallon Island in 2016, which is typical during El Niño conditions (Wells et al. 2017). Productivity increased for all birds but rhinoceros auklet in 2017. In 2017 Brandt's cormorant, pelagic cormorant, Cassin's auklet (*Ptychoramphus aleuticus*), rhinoceros auklet (*Cerorhinca monocerata*), and ashy storm petrel (*Oceanodroma homochroa*) production was above average, while western gull, murre, and pigeon guillemot (*Cepphus columba*) were just below average (fig. 48). Productivity values were available for 3 species in 2018, and Brandt's cormorant was well above average, Cassin's auklet just above average, and murre average (fig. 49).

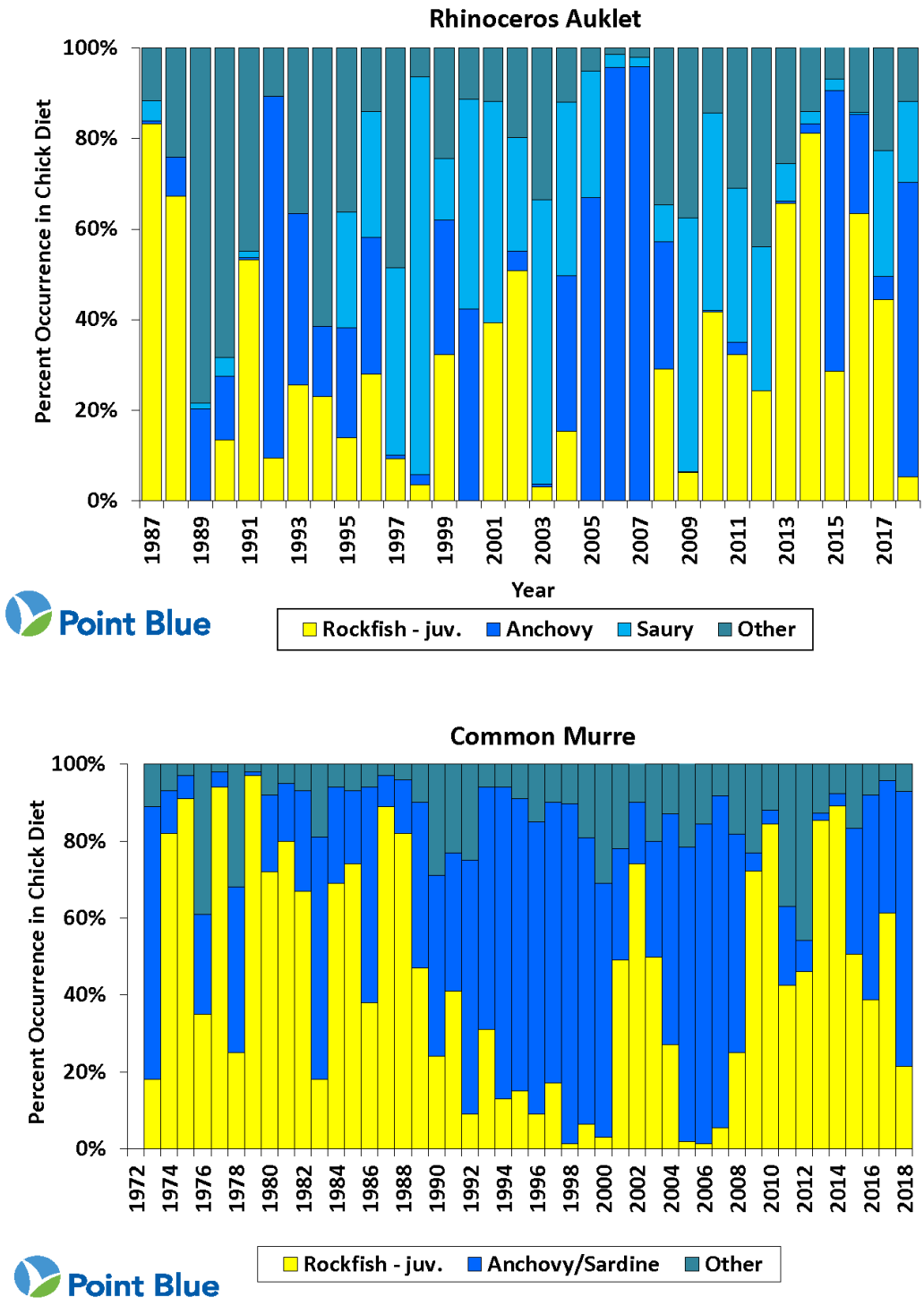

Figure 50. Diets of rhinoceros auklet and common murre returning to feed chicks on Southeast Farallon Island.

The recent increase in anchovy abundance off central California (fig. 33) was reflected in the fish that birds fed their chicks. Whereas juvenile rockfish was the most common component of rhinoceros auklet and common murre chick diets in 2017, over 50% of diet for both species was comprised of anchovy in 2018 (fig. 50).

Central and Southern California: RREAS and CalCOFI

Seabird distribution and abundance anomalies are presented from the RREAS core region (fig. 51). The RREAS typically encounters higher concentrations of resident breeding species within the Gulf of the

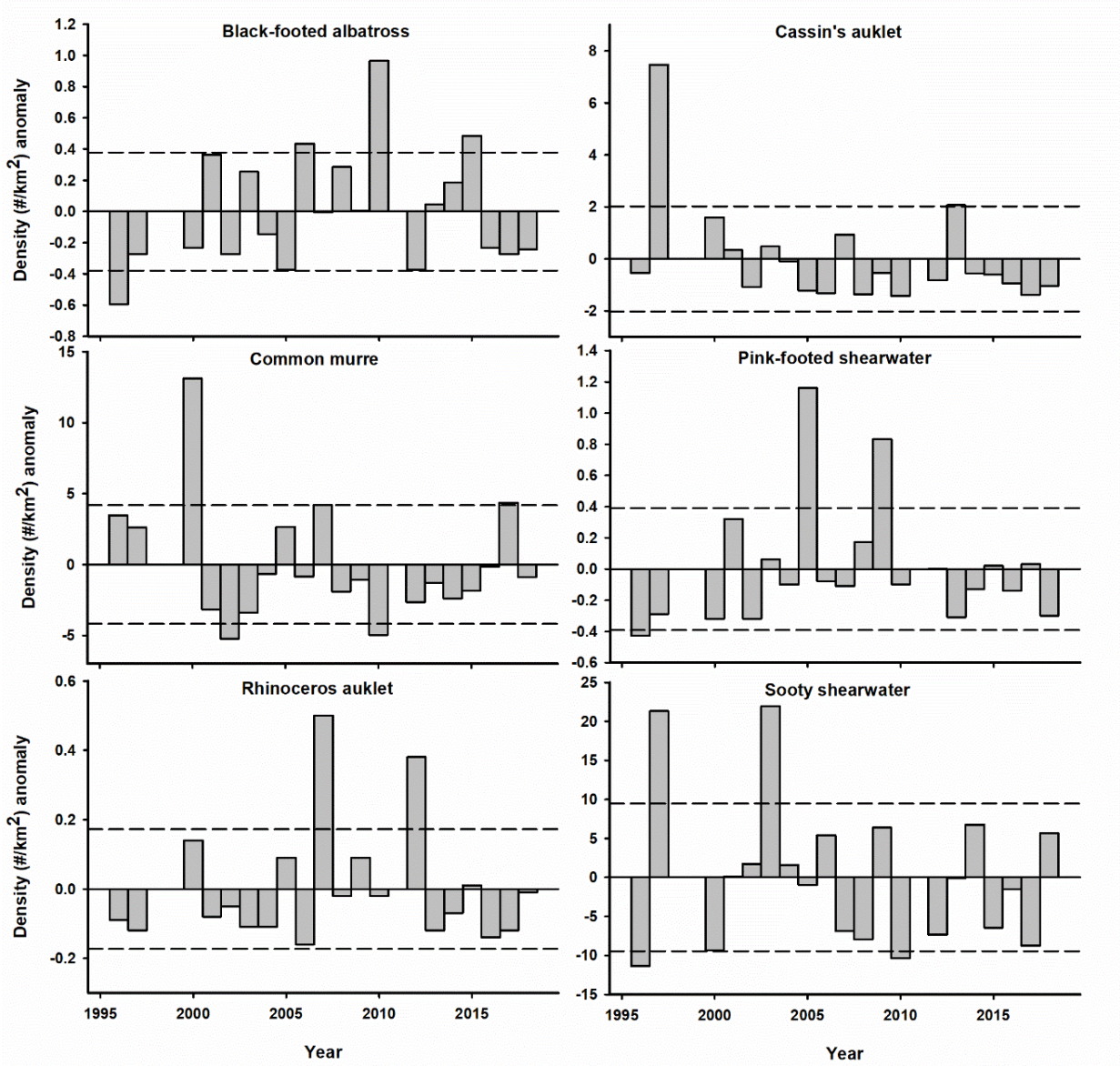

Figure 51. Density anomalies (#/km²) for seabirds on the core area (central California) of the Rockfish Recruitment and Ecosystem Assessment Survey (RREAS) survey 1996–2018. Surveys were not conducted in 1998, 1999, and 2011. The dashed lines indicate ± 1 standard deviation.

Farallones. Resident breeders such as murre, Cassin's auklet, and rhinoceros auklet displayed negative density anomalies during the recent large marine heat wave (2014–16; fig. 51). However, the murre density anomaly in 2017 was strongly positive for the first time since 2005 and 2007, and may be related to increased concentrations of non-breeding individuals. By contrast, migrant black-footed albatross (*Phoebastria nigripes*) densities were anomalously low since 2015 and pink-footed shearwaters (*Puffinus creatopus*) continued to display negative anomalies subsequent to 2009. Interestingly, compared to the CalCOFI region (below), the sooty shearwater density anomaly was positive off central California during spring 2018 and may indicate that shearwater aggregations were concentrated in response to good foraging conditions (e.g., increase adult anchovy; figs. 33, 35) in this region (fig. 51).

Anomalies of seabird density in spring within the CalCOFI region can be indicative of variation in species' habitat affinities such as warm- (black-footed albatross, Cook's petrel [*Pterodroma cookii*], and elegant tern [*Thalasseus elegans*]) and cold-water (pink-footed shearwater, Sabine's gull [*Xema sabini*], and sooty shearwater) conditions (Hyrenbach and Veit 2003; Santora and Sydeman 2015). Spring seabird density anomalies may also be correlated with other factors such as prey availability (Sydeman et al. 2015) and population trends or range shifts in breeding or wintering distributions (Velarde et al. 2015). Within the CalCOFI region, anomalies of cold-water species

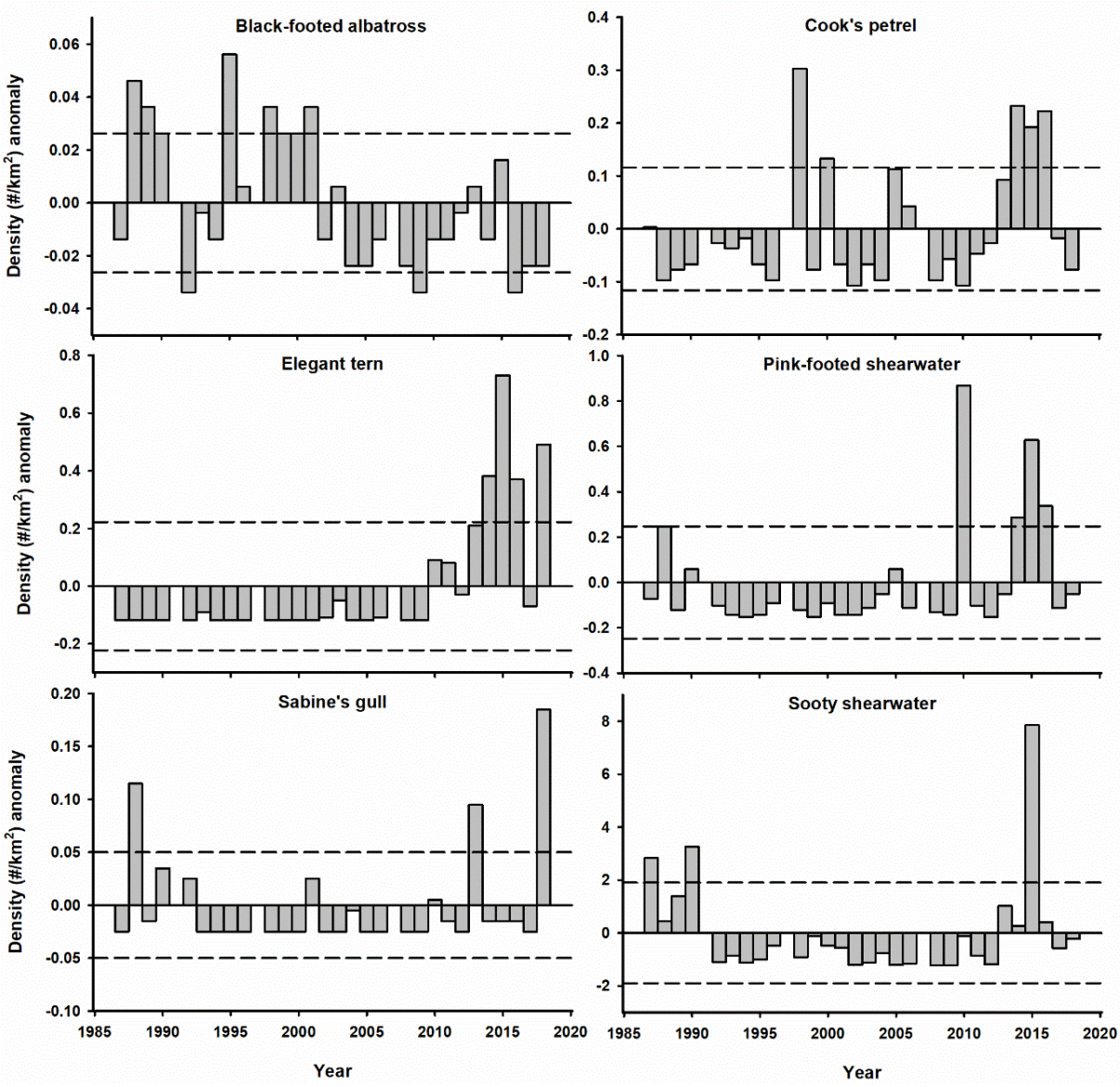

Figure 52. Density anomalies (#/km²) for seabirds from the spring CalCOFI surveys, 1987–2018. No survey was conducted in 1991, 1997, or 2007. The dashed lines indicate ± 1 standard deviation.

were generally neutral compared to the consecutive strong positive anomalies observed during the recent large marine heat wave (2014–16). For example, the trans-hemisphere migrants, sooty shearwater and pink-footed shearwater, displayed strong positive anomalies during the large marine heat wave and slight negative anomalies during spring 2017 and 2018 (fig. 52). The strong positive anomalies for shearwaters during the heat wave likely represent increased concentrations of these numerically dominant species within productive coastal waters of the Southern California Bight due to the lack of suitable foraging habitat within the northern CCS and Gulf of Alaska (Veit et al. 1996; Thompson et al. 2012). However, Sabine's gull, another cold-water species, displayed the strongest positive density anomaly on record in 2018, which may indicate this species' migration was impacted by the return to relatively cool ocean conditions during spring. Species with warm-water affinity, such as Cook's petrel, showed negative density anomalies during spring 2018 compared to their sustained strong positive anomalies during 2014–16 (fig. 52). Black-footed albatross density anomalies also continued to display a long-term decline which may be related to the overall decline of their populations in Hawaii and elsewhere in the North Pacific (fig. 52). By contrast, the second highest spring density anomaly of elegant tern was observed during 2018 (fig. 52), and the recent increasing trend suggests this pattern reflects the continuing northward range expansion of this species within the CCS (Velarde et al. 2015).

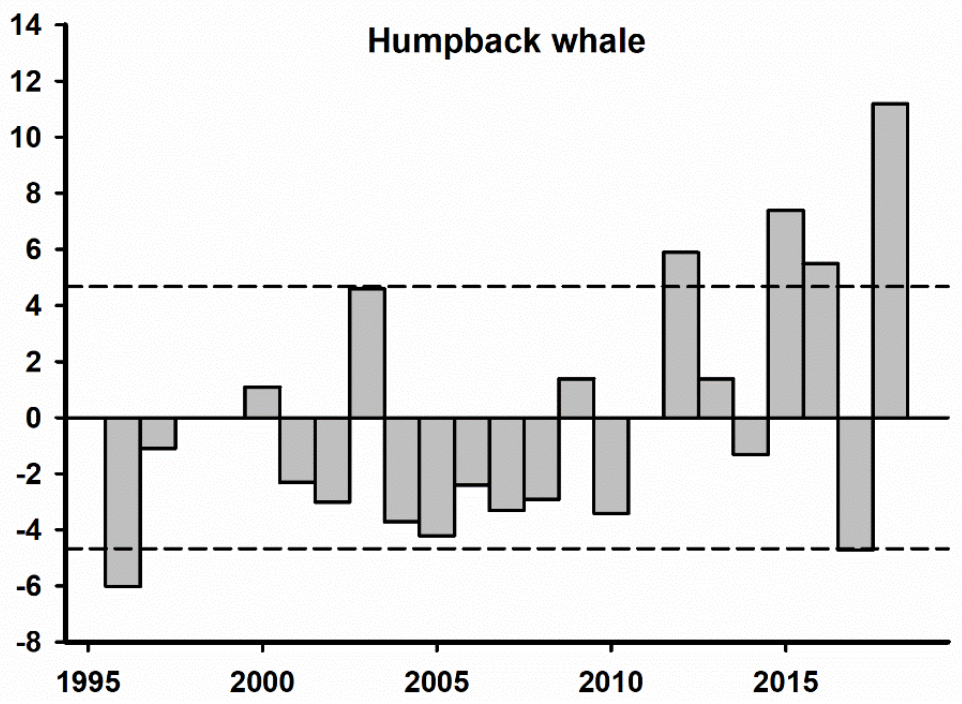

Figure 53. Encounter rate anomaly (#/100 km) for humpback whales from the core area of the RREAS survey 1996–2018. No survey was conducted in 1998, 1999, and 2011. The dashed lines indicate ± 1 standard deviation.

MARINE MAMMALS

Central CA: Humpback Whales

Whale surveys on the RREAS within central California documented that the humpback whale (*Megaptera novaeangliae*) encounter rate anomaly continued to increase over the past decade. In fact, encounter rates in spring 2018 were the highest ever observed (fig. 53). This may indicate either that humpback whale populations are increasing or that foraging conditions (e.g., availability of krill and anchovy aggregations) are favorable for concentrating whales during spring. Furthermore, compared to the recent marine heat wave (e.g., 2014–16), where humpback whales were concentrated closer to shore (Santora et al. unpublished data), during 2018, humpback whales were both frequently sighted along the outer shelf and within submarine canyons, coinciding with high concentrations of euphausiids, and inshore where increased adult anchovy were observed during the RREAS.

Southern CA: Sea Lions

California sea lions (*Zalophus californianus*) are permanent residents of the CCS, breeding in the California Channel Islands and feeding throughout the CCS in coastal and offshore habitats. They are also sensitive to changes in the CCS on different temporal and spatial scales and so provide a good indicator species for the status of the CCS at the upper trophic level (Melin et al. 2012). Four indices are used to measure trends in the population: 1) live pup census, 2) pup condition at 4 months of age, 3) pup growth rates during the period of maternal nutritional dependence, and 4) nursing female diet during the maternal care period on San Miguel Island, California.[32] The live pup census is a measure of successful births and is an indicator of prey availability to and nutritional status of nursing females from October to the following June.[33] Pup condition and growth rates during the period of nutritional dependence measure the transfer of energy from the mother to the pup through lactation between June and the following February, which is dependent on prey available to nursing females during that time. The frequency of occurrence of prey in the diet of nursing females provides a relative measure of the available for-

[32]San Miguel Island, California (fig. 1, right panel) is one of the largest colonies of California sea lions, representing about 45% of the US breeding population. As such, it is a useful colony to measure trends and population responses to changes in the marine environment.

[33]We used the number of pups alive at the time of the live pup census conducted in late July and the average weights of pups at 4 months and 7 months of age between 1997 and 2017 as indices of the population response to annual conditions in the CCS. The number of live pups in late July represents the number of pups that survived from birth to about 6 weeks of age. Live pups were counted after all pups were born (between 20–30 July) each year. A mean of the number of live pups was calculated from the total number of live pups counted by each observer. A long-term average live pup count based on counts between 1997 and 2017 was used to create annual anomaly percentages from the long-term average.

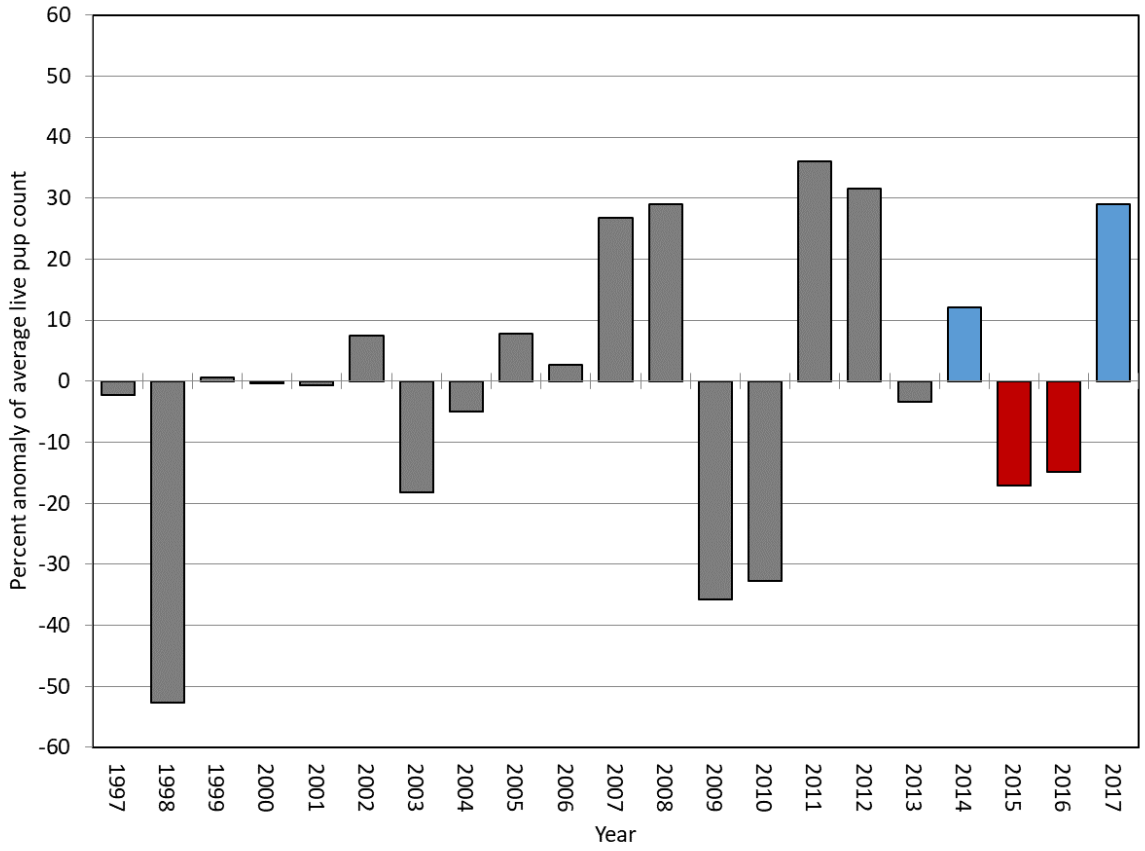

Figure 54. The percent anomaly of live California sea lion pup counts at San Miguel Island, California, based on a long-term average of live pup counts between 1997–2017 in late July when surviving pups were about 6 weeks old. Red (negative) bars represent shifts in index in relation to 2014–15 heat wave and 2015–16 El Niño; blue (positive) bars represent positive anomalies as conditions transitioned back to more typical conditions.

age community during the period of pup nutritional dependence.[34]

The 2014–15 marine heat wave and 2015–16 El Niño conditions affected the number of births (fig. 54), pup condition (fig. 55) and pup growth (fig. 56) of three cohorts of California sea lions in 2014, 2015, and 2016. The effects varied for each cohort based on the timing of the events relative to pupping and rearing seasons. The onset of the marine heat wave in November 2014 followed a normal pupping season with the number of live pups similar to the long-term average (fig. 57). However, as the event intensified in the following winter and spring foraging conditions rapidly deteriorated for nursing females resulting in poor pup condition and lower growth rates for the 2014 cohort (figs. 55, 56). The 2015 cohort was born as the CCS transitioned from the marine heat wave to El Niño conditions in summer 2015. This lead to a lower number of births in 2015 (fig. 54) and as El Niño conditions intensified, the 2015 pup cohort was in poor condition (fig. 55) and had the lowest growth rates (fig. 56) for pups in the time series. As El Niño conditions subsided in spring 2016, the number of births remained low (fig. 54) but pup condition (fig. 55) and growth rates (fig. 56) returned to normal. By 2017, when the south and central CCS returned to cooler oceanic patterns, all the indices returned to normal or exceeded the long-term averages (figs. 54–56).

Relative to the entire 1997–2017 time series, the annual number of live California sea lion pups[35] has been quite variable since 2007 (fig. 54) owing to several regional events that altered the availability of prey to pregnant and nursing females, the strongest of which were the 2009 upwelling relaxation event and 2010 El Niño conditions. However, the marine heat wave in 2014–15 resulted in a significant decline (26%) in the

[34]Each year, between 200 and 500 pups were weighed when about 4 months old. Pups were sexed, weighed, tagged, branded, and released. Up to 60 pups were captured in February and weighed and measured at 7 months of age. Of the 60 pups captured in February, up to 30 pups were branded and provided a longitudinal dataset for estimating a daily growth rate between 4 months and 7 months old.

[35]We used a linear mixed-effects model fit by REML in R to predict average weights on 1 October and 1 February in each year because the weighing dates were not the same among years. The model contained random effects with a sex and days interaction (days = the number of days between weighing and 1 October and 1 February) which allowed the growth rate to vary by sex and year, and a full interaction fixed effects of sex and days. The average weights between 1997 and 2017 were compared to the long-term average for the average pup weights between 1975 and 2017.

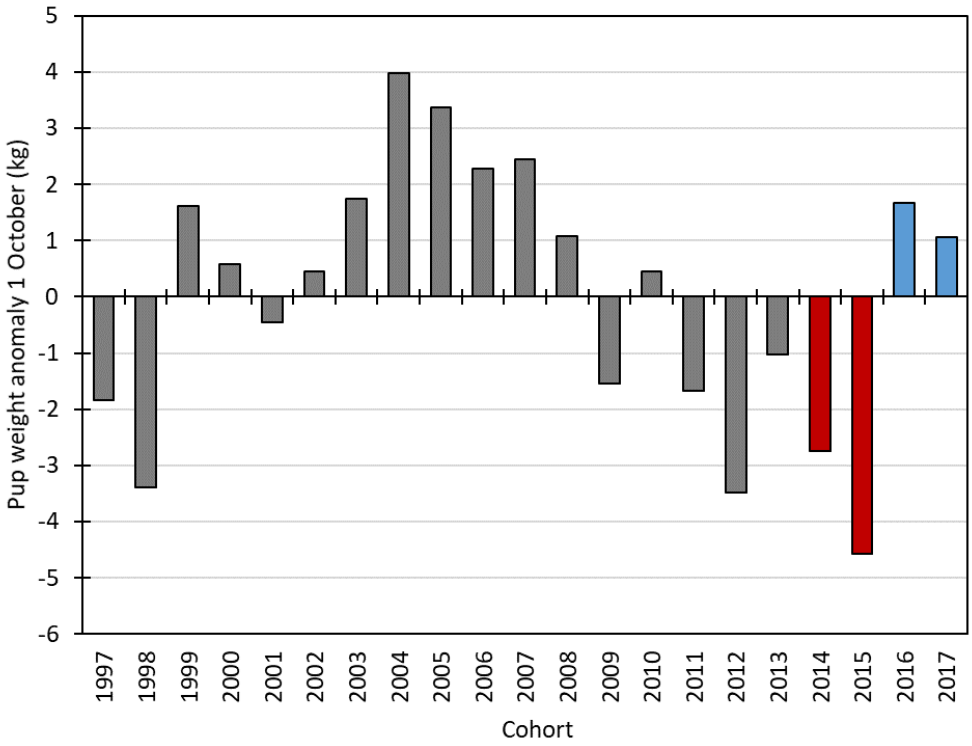

Figure 55. Average pup weight anomaly (kg) from predicted average weights of 4-month-old female California sea lion pups at San Miguel Island, California, from the long-term average between 1997 and 2017. Red (negative) bars represent shifts in index in relation to 2014–15 heat wave and 2015–16 El Niño; blue (positive) bars represent positive anomalies as conditions transitioned back to more typical conditions.

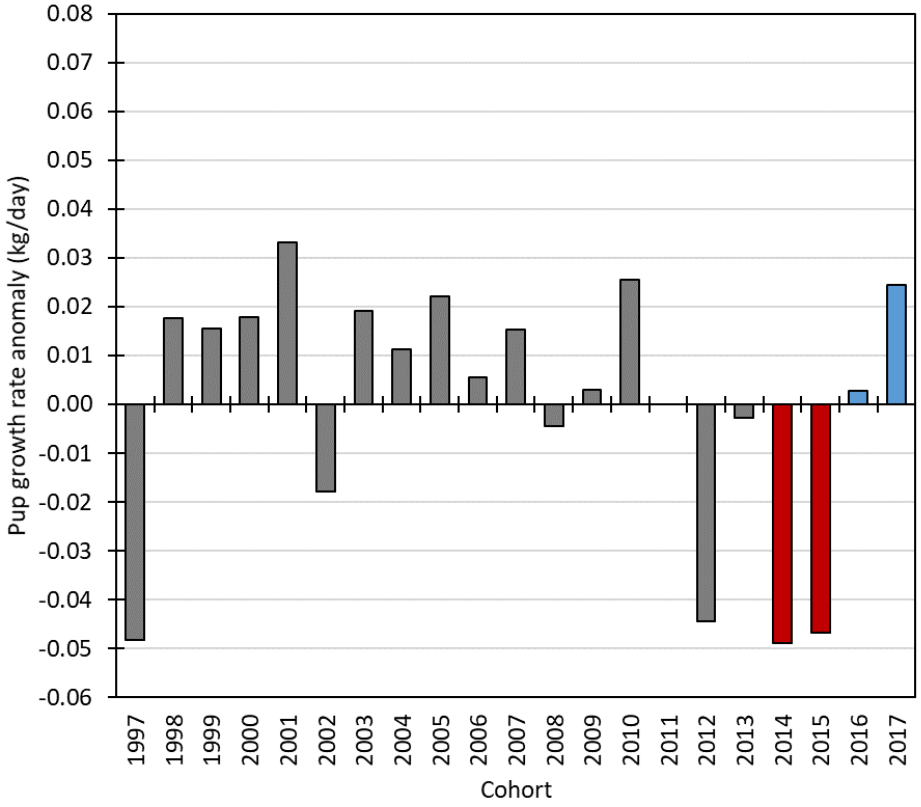

Figure 56. Average daily growth rate anomaly (kg/day) of California sea lion pups from 4 and 7 months old at San Miguel Island, California, from the long-term average between 1997 and 2017. Red (negative) bars represent shifts in index in relation to 2014–15 heat wave and 2015–16 El Niño; blue (positive) bars represent positive anomalies as conditions transitioned back to more typical conditions.

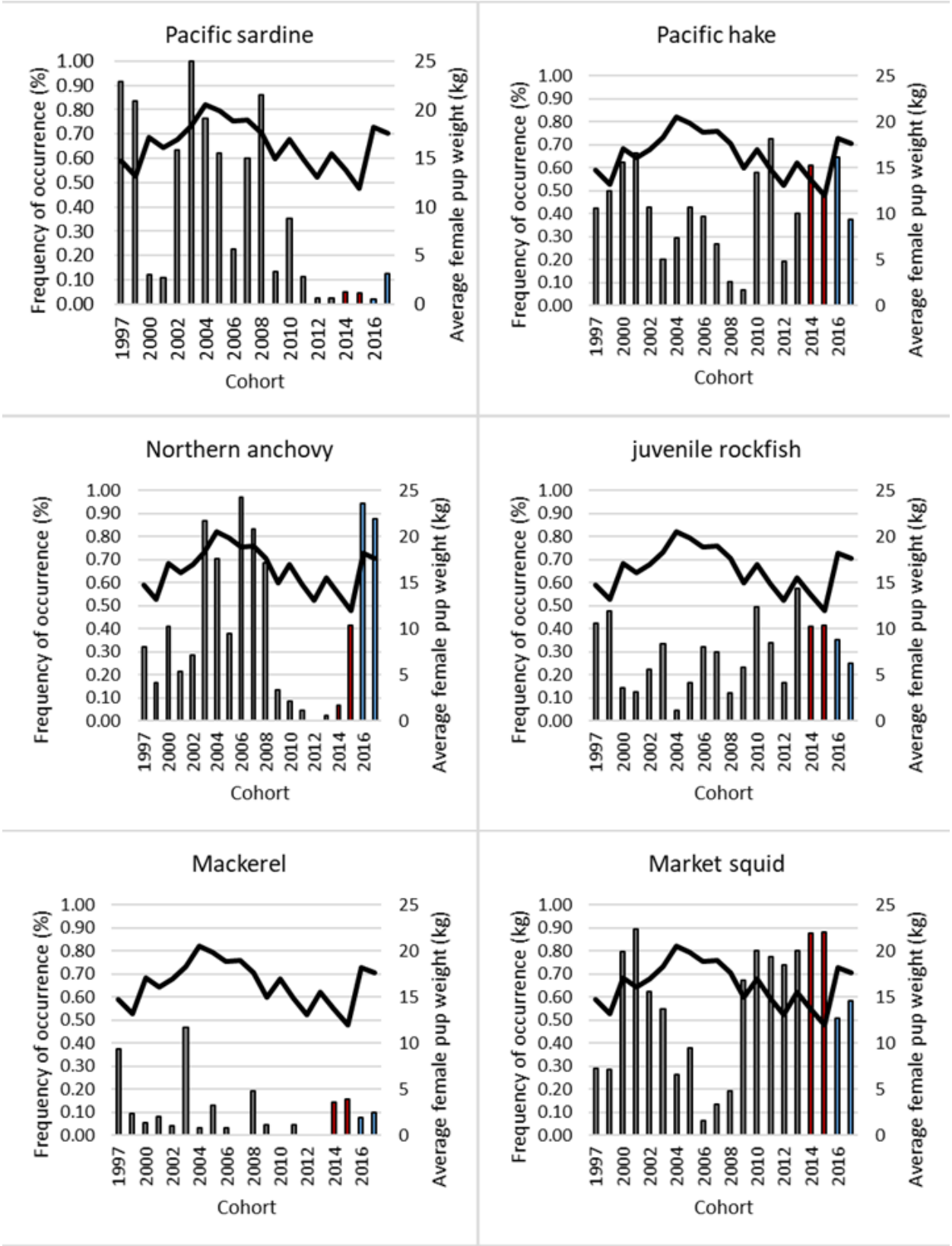

Figure 57. Frequency of occurrence of prey taxa (bars) identified from nursing female fecal samples collected at San Miguel Island during the first 4 months of lactation and average California sea lion pup weight at 4-months-old (line), 1997–2017. Red (negative) and blue (positive) bars represent shifts in index in relation to 2014–15 heat wave and 2015–16 El Niño.

number of live California sea lion pups between 2014 and 2015. The live pup census in 2016 showed some improvement with the number of pups increasing 3% from 2015 to 2016, however it was still 15% below the time series average (fig. 54). In 2017, the number of live pups increased 52% from 2016 and exceeded the long-term average by 29%. The return of births to the long-term average in 2017 indicates that the lower number of births in 2015 and 2016 were not simply the result of fewer reproductive females in the population, but that due to the poor foraging conditions during the gestation period, fewer reproductive females were able to energetically support pregnancies.

Between 1999 and 2008, pup condition at 4 months of age was above or near the long-term average. Since 2009, California sea lion pup condition has remained below the time series average with the 2015 cohort representing the poorest condition on record (fig. 55). Pup condition improved and returned to above normal in 2016 and 2017. The trend in pup growth rate was relatively stable over the time series with most years showing average or above average pup growth between October and February until 2012 (fig. 56), when growth rates declined significantly and marked the onset of the 2013–17 Unusual Mortality Event. Pup growth rates reached record lows for the 2014 and 2015 cohorts before returning to normal in 2016 and improving substantially in 2017, with the third highest growth rate since 1997.

The summer diet of nursing females between 1997 and 2017 showed a marked shift beginning in 2009 with a significant decline in the frequency of occurrence of sardine and anchovy from over 50% from 2003–08 to less than 5% from 2012–14 for both species (fig. 57). Sardine and anchovy were replaced in the diet by higher frequencies of hake and juvenile rockfish, but the dominant species was market squid, consistently occurring at frequencies greater than 60% from 2009–15. This diet persisted during the 2014–15 marine heat wave and the following 2015–16 El Niño conditions. The diet began to shift in 2015 when anchovy began to increase, rising to 94% occurrence in 2016 and remaining high in 2017. In addition, other taxa remained above 20% in 2016 and 2017, increasing the diversity of taxa in the diet. However, the occurrence of sardine in the diet remained at record lows.

The California sea lion population response to the unusually warm marine conditions in 2014–16 affected a greater number of pup cohorts than past El Niño events due to the persistence of the conditions over three reproductive cycles. In addition, these cohorts continued the trend of poor condition and growth that began in 2009, resulting in six of the last eight pup cohorts having below average condition and growth rates. Poor condition at 4 months of age has been linked to lower survival rates of pups (DeLong et al. 2017) that contributed to a slowing of the population growth rate in recent years (Laake et al. 2018). The declining trend in pup condition at 4 months of age was associated with a shift in the species composition of the nursing female diet over the same period, most notably the almost complete disappearance of sardine and anchovy from the diet (fig. 57). Indeed, McClatchie et al. (2016a) documented a strong, positive correlation between the availability of anchovy and sardine and sea lion pup weight from 2004–14. An improvement in pup condition in 2016 and 2017 coincided with an increase in anchovy and greater taxa diversity in the nursing female diet. The quantity of high quality food consumed by nursing females affects the transfer of energy from the female to the pup during the period that the pup is nutritionally dependent on its mother, and therefore affects pup condition and growth rates. Based on the nursing female diet, the shifts in the prey community clearly began before the marine heat wave and El Niño and reflect a sustained period of abnormally warm marine conditions that altered the sea lion prey community. The resurgence of anchovy populations along the central and southern California coast (figs. 33, 36, 38) was reflected in the diet of nursing females and coincided with an improvement in pup condition and greater growth rates of the 2017 cohort. However, the fattest pups in the time series occurred in the mid-2000s when sardine and anchovy dominated the diet, suggesting that a more diverse diet with inclusion of sardine into sea lion diet results in optimal reproductive efforts of California sea lion females. The rebounding of all three population indices in 2017 and the commensurate shift in the composition of the nursing female diet supports the use of these indices as a measure of forage community shifts in the CCS that affect upper trophic level predators.

DISCUSSION

The biggest takeaway from CCS-wide analyses from mid-2017 to mid-2018 is that many of the indices, from SST and chlorophyll *a* to fish assemblages, were close to average long-term values. However, the CCS is characterized by strong interannual variability, and deviations from the long-term mean are more common than exceptional (Goericke et al. 2004). Indeed, several variables were highly anomalous in 2017–18, and we highlight these in the ensuing paragraphs.

Very low NPGO

Basin scale climate indices (PDO and ONI) were very close to neutral. The NPGO, however, was very low in 2017–18. In fact, through February 2018, three of the lowest monthly NPGO values since January 1950

were recorded (December 2017—3rd lowest; November 2017—8th lowest; and February 2018—9th lowest).

The NPGO is related to the strength of the North Pacific Current (NPC) which flows eastward and meets the west coast of North America at approximately 40°N (Di Lorenzo et al. 2008). At the West Coast, the NPC divides and becomes the northward-flowing Alaska Current and the southward-flowing California Current (CC). Low NPGO values are associated with weaker current flows and warmer, nutrient poor conditions (Di Lorenzo et al. 2008; Di Lorenzo et al. 2009).

The NPGO is based directly on conditions in the CCS, and past studies show that it correlates with ecosystem fluctuations in the CCS (Sydeman and Thompson 2010). For example, Cloern et al. (2010) found that the NPGO index correlated significantly with populations of demersal fishes, crabs, and shrimps in San Francisco Bay, California, and the sign of this correlation varied by species. More recently, Sydeman et al. (2013) provided evidence that oceanographic conditions reflected by the NPGO affect multiple trophic levels in central California. Specifically, there is a positive relationship between *Thysanoessa spinifera* krill abundance and the NPGO (Sydeman et al. 2013). *T. spinifera* is an important prey item for young fishes, and juvenile rockfish abundance is strongly, positively correlated with the abundance of this krill species. Juvenile rockfishes, in turn, are consumed by salmon and seabirds, and there was a very strong ($R^2 = 0.87$), positive relationship between rockfish abundance and that of salmon and seabirds over 8 years in the early 21st century (Sydeman et al. 2013). Our finding that krill and rockfish abundances in 2018 off central California (fig. 33) were low, when winter NPGO values were very low, relative to 2016–17 supports the trophic relationships identified by Sydeman et al. (2013). The low NPGO in winter 2017–18 also indicates that salmon abundances are likely to be low in central California.

Higher Trophic Level Species in the North in 2017

We can now conclusively state that 2017 was a terrible year for many upper trophic level species in the northern California Current. Common murre experienced total reproductive failure in both Yaquina Head, Oregon, and Castle Rock, California, in 2017, and at-sea bird sightings were at the lowest level since records began in 2003 (Wells et al. 2017).

Poor forage conditions for murre likely contributed to their sorry state in the north in 2017. At both Yaquina Head and Castle Rock, there were very few observations of adults carrying fish into the colonies and no observations of adults feeding chicks. Predators also affected murre chick survival as bald eagles and western gulls were observed consuming numerous eggs and/or chicks at Yaquina Head and Castle Rock, respectively.

The number of salmon returning to spawn in their natal rivers is affected greatly by the abundance of yearlings leaving the river two years prior and the prey field in the ocean encountered by yearlings (Peterson et al. 2014). In 2017 almost all indices related to coho and Chinook salmon return predicted very low returns in 2019. Specifically, the abundance of yearlings, which correlates positively with subsequent returns (Morgan et al. 2018) was very low for both species. In addition, salmon survival tends to be higher when northern, lipid-rich copepods are abundant, and these copepods were very low in 2017. Finally, ichthyoplankton assemblage structure and biomass can affect yearling salmon survival, as higher survival is correlated with overall ichthyoplankton biomass and the presence of species such as sandlance, sculpins, and smelts associated with colder ocean conditions and inshore biogeographic ranges, as opposed to lower survival associated with taxa such as sardine, anchovy, and rockfishes representing warmer ocean conditions and offshore ranges (Daly et al. 2017). In 2017, although the overall ichthyoplankton biomass was relatively high (fig. 29), the assemblage was dominated by taxa with offshore distributions and associated with warm ocean conditions. Hence, by most accounts, we would expect low salmon returns in 2019.

Prospects for salmon returns in 2020 are still equivocal but perhaps less bleak than for 2019. First, the abundance of coho salmon in coastal samples was among the highest on record in 2018. The abundance of yearling Chinook salmon also increased greatly relative to 2017 and was close to average in 2018. Second, the biomass of northern copepods increased greatly in 2018 and was close to average while southern copepods were only slightly above normal. Third, ichthyoplankton biomass was high, although the assemblage was still characterized by warm water taxa that correlate negatively with salmon returns (Daly et al. 2017).

Return to Normal in California . . . Except That Anchovy Abundance Was Way Up

Conditions in 2018 in the CC largely appeared to be following the trend from 2016–17, returning to average conditions following the impacts of the North Pacific warming and El Niño of 2014–15. Off Trinidad Head, Monterey Bay, central, southern, and northern Baja California, SST and chlorophyll *a* were close to average from late 2017 to mid-2018.

Salinity in southern California during spring 2018, however, was the one physical feature that stood out from previous years. In fact, the salinity anomaly in the mixed layer in southern California was the 2nd highest since 1994. Typically, high salinity water in spring in

southern California is a signature of cool, upwelled, nutrient rich water near the coast (McClatchie 2014). In 2018, however, upwelling was close to normal in southern California, chlorophyll *a* at 10 m was almost exactly the same as the long-term mean, temperature in the mixed layer was only slightly below normal, and salinity at 10 m was actually higher offshore than inshore. These features are all inconsistent with high upwelling, and examination of sea surface salinity from new satellite imagery showed that saline waters were offshore from the CalCOFI grid and impinged on the sample frame by mid-2018. Movement of saline water from offshore and the south (i.e., North Pacific Central water) into southern California is not uncommon during El Niños (McClatchie 2014), but North Pacific Central water is normally warm as well as saline (Brinton 1962; Moser et al. 1987; McClatchie 2014). Further analysis is necessary to better understand the characteristics of the waters offshore from the CalCOFI grid in 2018 and its impact on physical and biological features of the CCS.

While most physical conditions, with the exception of salinity, trended towards average levels in California, a major biological feature was notable in 2018: anchovy abundances were extremely high in many locations. Indeed, RREAS trawls documented record high anchovy abundance off central California and bongo tows off southern California documented the highest abundance of larval anchovy since the mid-1960s.

The mechanisms that allowed anchovy to increase do not align cleanly with our current understanding of drivers of anchovy populations. The traditional view of sardine and anchovy dynamics is that sardine thrive under warm conditions while anchovy do better when it is cold (Lluch-Belda et al. 1989; Chavez et al. 2003). This concept was largely informed by CalCOFI data showing low sardine and high anchovy abundances from the 1950s to the mid-1970s (cold conditions), an increase in sardine and decrease in anchovy from the 1980s to the early 2000s and then a decrease in sardine (but not an increase in anchovy) between 2000 and 2011 (Zwolinski and Demer 2012). However, McClatchie (2012) pointed out that a time frame of 70 years is too short to understand how fish respond to temperature regimes that last 20–40 years. In addition, paleontological records of anchovy and sardine scale depositions show that over hundreds of years there is no correlation between the PDO and sardine abundance (McClatchie 2012) and that anchovy and sardine populations dynamics seem to be positively correlated (Baumgartner et al. 1992; McClatchie et al. 2017). In light of our current finding that anchovy increased under mostly warm conditions, and that sardine did not, suggests that the paradigm of sardine thriving under warm conditions and anchovy increasing when it is cool is overly simplistic.

An alternative mechanism governing sardine and anchovy dynamics is that, due to differences in size of gill rakers, sardine do well when small-bodied zooplankton prey is plentiful, and anchovy thrive with copious amounts of larger-bodied prey (Rykaczewski and Checkley Jr. 2008). In addition, Rykaczewski and Checkley Jr. (2008) found that larger prey items tend to flourish under high levels of coastal upwelling, while smaller prey are plentiful when wind-stress curl initiates upwelling. Indeed, despite El Niño conditions that typically mute upwelling (McClatchie 2014), upwelling was actually greater than normal in winter 2015–16 in southern California and greater than normal leading into winter 2015–16, and then close to normal within winter 2015–16 in central California. In addition, despite overall warm conditions in 2014–15, upwelling was close to normal in Central California. The mix of normal-high upwelling close to shore with warm water offshore in 2015–16 produced an unusual mix of semitropical species offshore (e.g., pelagic red crabs, *Pleuroncodes planipes*, subtropical mesopelagic fishes) coupled with high abundance of species that favor cooler conditions (e.g., rockfishes) inshore (McClatchie et al. 2016b, Sakuma et al. 2016). It is therefore possible that large-bodied anchovy prey were abundant inshore in California, and that high anchovy abundance in 2018 was the product of a strong recruitment class in winters of 2015 and 2016. Further analysis of prey size and abundance in recent years is needed to evaluate whether the type of prey that is thought to favor anchovy survival was plentiful in recent years.

It is also possible that an unknown mechanism spurred anchovy population growth leading up to 2018. In their recent review of sardine and anchovy dynamics Checkley Jr. et al. (2017) state that our understanding of what controls anchovy and sardine dynamics is based on correlative analyses using data collected mostly from the past ~70 years. They go on to say that our current level of understanding of factors controlling sardine and anchovy "might be sufficient if future climate change were to be similar to past climate variability and if we had a sufficient duration of high quality historical observations to represent all modes of natural variability. Neither is likely true." Given that unprecedented physical and biological conditions defined much of the last five years, it is conceivable that recent anchovy dynamics were driven by forces novel to researchers.

Regardless of the variables that ultimately govern anchovy dynamics, high anchovy abundances have important economic and ecological implications. Anchovy are important forage for many higher tropic level species (Szoboszlai et al. 2015) and are a potentially valuable resource for commercial fisheries, particularly in recent years as the sardine fishery has been closed since

2015 (McClatchie et al. 2018). Harvest guidelines will necessarily be drawn based from a full anchovy stock assessment (McClatchie et al. 2018), which will consider the historically low levels of anchovy populations in central and southern California through 2015 (MacCall et al. 2016; Davison et al. 2017). However, if the indices reported here are any indication, it is likely that recent assessments will find that anchovy abundances have risen considerably in 2017–18, which could bring relief to commercial fishing in California.

In addition to benefiting fishing, resurgence of anchovy was likely tied to improved sea lion reproduction on San Miguel Island in California. In the early 20th century sea lions were hunted and population reduced to very low levels (Cass 1985). Sea lions became protected under the U.S. Marine Mammals Protection Act in 1972 and surveys since 1975 show that the population has increased approximately 7-fold and is likely near carrying capacity (Laake et al. 2018). Given the high population sizes, sea lion populations are affected when high quality forage is scarce and mothers become malnourished, resulting in low birth rates, lactation, and pup survival (Melin et al. 2010; Melin et al. 2012). The increased production and survival of sea lion pups in 2017 coincided with a spike in anchovy abundance; anchovy remains were observed in nearly all scat samples and fit with the pattern that sea lion pups do well in years when anchovies and/or sardine are abundant (McClatchie et al. 2016a). Anchovy appear to have been abundant in California through 2018, suggesting that sea lion pups will again exhibit high rates of survival in 2018.

Increased anchovy abundance also has the potential to augment bird survival. 2018 surveys from the Southeast Farallon Island indicated that both rhinoceros auklet and common murre chick diets consisted of high proportions of anchovy. Although measurement of rhinocerous auklet productivity was not yet available, common murre productivity at Southeast Farrallon Island increased greatly in 2018 and was the highest since 2013.

. . . and Semitropical Fish Were Prominent in Southern California

Another novel finding in 2018 was that the southern California larval fish assemblage in spring had high abundances of mesopelagic taxa with southern biogeographic distributions even though the ocean was not warm at this time. These species have been viewed as indicators of warm conditions in southern California that were largely caused by El Niño events (Hsieh et al. 2005, Hsieh et al. 2009). Indeed, analyses of early CalCOFI data demonstrated that this suite of species was associated with the Central North Pacific water mass, and this community was detected in CalCOFI samples when this water mass impinged upon southern California (Moser et al. 1987). Prior to 1977, it was rare to find these species in the core CalCOFI area outside of summer but following the cool to warm regime shift around 1976 (Hare and Mantua 2000), these species have become increasingly common in CalCOFI samples (Hsieh et al. 2009). Despite the increased overall presence of the southern mesopelagics over the past 40 years, spring 2018 is the first time that these species were so well represented when water temperatures were below average.

A potential explanation for the abundance of the southern mesopelagics is that because of the predominantly warm conditions over the last five years in southern California, fishes in this assemblage are still relatively close to the CalCOFI sampling area even when physical conditions in southern California are cool. Satellite images of SST show that although it was cool in southern California in May 2018, anomalously warm water was just offshore. In addition, highly saline water, which is characteristic of southern mesopelagic fish habitat (McClatchie 2014), was detected in the offshore CalCOFI region in spring 2018, and the mesopelagic fishes may have been transported into the region along with this water. Further analysis will be needed to more definitively determine why the abundance of warm-water associated southern mesopelagics was so high in 2018 even though the water was relatively cool.

. . . and It Was Historically Warm in Southern California and Northern Baja California in Summer 2018

While surface water temperatures began at seasonally adjusted normal values in 2018, they rapidly rose to extremely high levels off southern California and northern Baja California in July and August 2018. Over the last 70 years elevated water temperatures in southern California were almost always associated with El Niño events. 2018, however, was Niño-neutral, and it appears that the record warmth was generated by mechanisms similar to the 2014 surface warming event. The warm water in 2014 originated in the Gulf of Alaska in response to regional high sea level pressure leading to low winds and lower than normal loss of heat from the upper ocean (Bond et al. 2015). Leading up to August 1, air pressure was anomalously high over the southwestern United States which caused abnormally high air temperatures and anomalously low wind in southern California (https://www.esrl.noaa.gov/psd/map/clim/). In addition, high sea level pressure was centered in the Gulf of Alaska rather than over central-northern California from mid-June to August (https://www.esrl.noaa.gov/psd/map/clim/), resulting in lower than normal southerly winds and reduced upwelling in southern California in summer 2018. As such, high air temperature, coupled with relatively still conditions

drove sea surface temperatures to record highs in many parts of southern California by August, 2018. Subsequent work will reveal the biological impacts of extreme water temperatures in the southern parts of the CCS.

SUMMARY

Following the large marine heat wave from 2014–16, much of the CCS trended towards more typical conditions in 2018. In the north many invertebrates and fish that are associated with cool conditions were found at the highest level since 2013. However, signatures of the recent warming remained in the north as taxa such as pyrosomes and lipid-poor copepods were still plentiful. In the central region, conditions also were more aligned with long-term averages although anchovy were at all-time highs. In southern California most oceanographic parameters were close to normal through spring 2018. By summer, however, water temperature at the surface hit record high and the spring ichthyoplankton assemblage was characterized by many semitropical taxa along with high abundances of anchovy. Off Baja California, SST was slightly above normal at the beginning of 2018 and chlorophyll *a* and primary production were average. In sum, the CCS appeared to be trending as a whole back to pre-2014 conditions through spring 2018. In summer 2018, however, strong regional warming off southern California and northern Baja California decoupled these regions from the rest of the system. Ongoing research will continue to evaluate the full extent of this latest extreme warming event.

ACKNOWLEDGEMENTS

We wish to thank everyone who contributed to collecting myriad data presented in this report. The manuscript was improved greatly by comments from Noelle Bowlin, Greg Williams, and an anonymous reviewer.

LITERATURE CITED

Adams, J., C. MacLeod, R. M. Suryan, K. D. Hyrenbach, and J. T. Harvey. 2012. Summer-time use of west coast US National Marine Sanctuaries by migrating sooty shearwaters (*Puffinus griseus*). Biological Conservation 156:105–116.

Alexander, M. A., C. Deser, and M. S. Timlin. 1999. The reemergence of SST anomalies in the North Pacific Ocean. Journal of Climate 12.

Auth, T. D., E. A. Daly, R. D. Brodeur, and J. L. Fisher. 2018. Phenological and distributional shifts in ichthyoplankton associated with recent warming in the northeast Pacific Ocean. Global Change Biology 24:259–272.

Bakun, A. 1973. Coastal upwelling indices, west coast of North America, 1946–71. US Department of Commerce NOAA Technical Report NMFS-SSRF 671:1–103.

Barcelo, C., L. Ciannelli, and R. D. Brodeur. 2018. Pelagic marine refugia and climatically sensitive areas in an eastern boundary current upwelling system. Global Change Biology 24:668–680.

Baumgartner, T. R., A. Soutar, and V. Ferreira-Bartrina. 1992. Reconstruction of the history of Pacific sardine and northern anchovy populations over the past two millennia from sediments of the Santa Barbara Basin, California. California Cooperative Oceanic Fisheries Investigations Reports 33:24–40.

Black, B. A., I. D. Schroeder, W. J. Sydeman, S. J. Bograd, and P. W. Lawson. 2010. Wintertime ocean conditions synchronize rockfish growth and seabird reproduction in the central California Current ecosystem. Canadian Journal of Fisheries and Aquatic Sciences 67:1149–1158.

Black, B. A., P. van der Sleen, E. Di Lorenzo, D. Griffin, W. J. Sydeman, J. B. Dunham, R. R. Rykaczewski, M. Garcia-Reyes, M. Safeeq, I. Arismendi, and S. J. Bograd. 2018. Rising synchrony controls western North American ecosystems. Global Change Biology 24:2305–2314.

Bograd, S. J., and R. J. Lynn. 2003. Long-term variability in the Southern California Current System. Deep-Sea Research II 50:2355–2370.

Bograd, S. J., I. D. Schroeder, N. Sarkar, X. M. Qiu, W. J. Sydeman, and F. B. Schwing. 2009. Phenology of coastal upwelling in the California Current. Geophysical Research Letters 36.

Bond, N. A., M. F. Cronin, H. Freeland, and N. Mantua. 2015. Causes and impacts of the 2014 warm anomaly in the NE Pacific. Geophysical Research Letters 42:3414–3420.

Brinton, E. 1962. The distribution of Pacific euphausids. Bulletin of Scripps Institute of Oceanography 8:251–270.

Brodeur, R. D., J. P. Fisher, R. L. Emmett, C. A. Morgan, and E. Casillas. 2005. Species composition and community structure of pelagic nekton off Oregon and Washington under variable oceanographic conditions. Marine Ecology Progress Series 298:41–57.

Brodeur, R. D., I. Perry, J. Boldt, L. Flostrand, M. Galbraith, J. King, J. Murphy, K. M. Sakuma, and A. R. Thompson. 2018. An unusual gelatinous plankton event in the NE Pacific: The Great Pyrosome Bloom of 2017. PICES Press 26:22–27.

Brodeur, R. D., S. Ralston, R. L. Emmett, M. Trudel, T. D. Auth, and A. J. Phillips. 2006. Anomalous pelagic nekton abundance, distribution, and apparent recruitment in the northern California Current in 2004 and 2005. Geophysical Research Letters 33:L22S08.

Carter, H. R., U. W. Wilson, R. W. Lowe, M. S. Rodway, D. A. Manuwal, and J. L. Yee. 2001. Population trends of the Common Murre (*Uria aalge californica*). Pages 33–132 *in* D. A. Manuwal, H. R. Carter, T. S. Zimmerman, and D. L. Orthmeyer, editors. Biology and conservation of the common murre in California, Oregon, Washington, and British Columbia, Volume 1: Natural history and population trends United States Geological Survey, Information and Technology Report USGS/BRD/ITR-2000-0012, Fish & Wildlife Service, Northern Prairie Wildlife Research Center, Dixon, CA.

Cass, V. 1985. Exploitation of California sea lions, *Zalophus californianus*, prior to 1972. Marine Fisheries Review 47:36–38.

Chavez, F. C., J. Ryan, S. E. Lluch-Cota, and M. C. Niquen. 2003. From anchovies to sardines and back: Multidecadal change in the Pacific Ocean. Science 299:217–221.

Checkley Jr., D. M., R. G. Asch, and R. R. Rykaczewski. 2017. Climate, anchovy, and sardine. Annual Review of Marine Science 9:469–493.

Cloern, J. E., K. A. Hieb, T. Jacobson, B. Sanso, E. Di Lorenzo, M. T. Stacey, J. L. Largier, W. Meiring, W. T. Peterson, T. M. Powell, M. Winder, and A. D. Jassby. 2010. Biological communities in San Francisco Bay track large-scale climate forcing over the North Pacific. Geophysical Research Letters 37:L21602.

Dale, K. E., E. A. Daly, and R. D. Brodeur. 2017. Interannual variability in the feeding and condition of subyearling Chinook salmon off Oregon and Washington in relation to fluctuating ocean conditions. Fisheries Oceanography 26:1–26.

Daly, E. A., R. D. Brodeur, and T. D. Auth. 2017. Anomalous ocean conditions in 2015: impacts on spring Chinook salmon and their prey field. Marine Ecology Progress Series 566:169–182.

Davison, P., W. J. Sydeman, and J. A. Thayer. 2017. Are there temporal or spatial gaps in recent estimates of anchovy off California? California Cooperative Oceanic Fisheries Investigations Reports 58:1–13.

DeLong, R. L., S. R. Melin, J. L. Laake, P. Morris, A. J. Orr, and J. D. Harris. 2017. Age- and sex-specific survival of California sea lions (*Zalophus californianus*) at San Miguel Island, California. Marine Mammal Science 33:1097–1125.

Di Lorenzo, E., J. Fiechter, N. Schneider, A. Bracco, A. J. Miller, P. J. S. Franks, S. J. Bograd, A. M. Moore, A. C. Thomas, W. Crawford, A. Pena, and A. J. Hermann. 2009. Nutrient and salinity decadal variations in the central and eastern North Pacific. Geophysical Research Letters 36:L14601.

Di Lorenzo, E., and N. Mantua. 2016. Multi-year persistence of the 2014/15 North Pacific marine heatwave. Nature Climate Change 6:1042–1048.

Di Lorenzo, E., N. Schneider, K. M. Cobb, P. J. S. Franks, K. Chhak, A. J. Miller, J. C. McWilliams, S. J. Bograd, H. Arango, E. Curchister, T. M. Powell, and P. Riviere. 2008. North Pacific Gyre Oscillation links ocean climate and ecosystem change. Geophysical Research Letters 35:L08607.

Frable, B. W., D. W. Wagman, T. N. Frierson, and B. L. Sidlauskas. 2015. A new species of *Sebastes* (Scorpaeniformes: Sebastidae) from the northeastern Pacific, with a redescription of the blue rockfish, *S. mystinus* (Jordan and Gilbert, 1881). Fisheries Bulletin 113:355–377.

Frischknecht, M., M. Münnich, and N. Gruber. 2015. Remote versus local influence of ENSO on the California Current System. Journal Geophysical Research Oceans 120:1353–1374.

Frischknecht, M., M. Münnich, and N. Gruber. 2017. Local atmospheric forcing driving an unexpected California Current System response during the 2015–2016 El Niño. Geophysical Research Letters 41:304–311.

Gladics, A. J., R. M. Suryan, R. D. Brodeur, L. M. Segui, and L. Z. Filliger. 2014. Constancy and change in marine predator diets across a shift in oceanographic conditions in the Northern California Current. Marine Biology 161:837–851.

Gladics, A. J., R. M. Suryan, J. K. Parrish, C. A. Horton, E. A. Daly, and W. T. Peterson. 2015. Environmental drivers and reproductive consequences of variation in the diet of a marine predator. Journal of Marine Systems 146:72–81.

Goericke, R., E. Venrick, J. A. Koslow, W. J. Sydeman, F. B. Schwing, S. J. Bograd, B. Peterson, R. L. Emmett, J. R. L. Lara, G. G. Castro, J. G. Valdez, K. D. Hyrenbach, R. W. Bradley, M. J. Weise, J. T. Harvey, C. Collins, and N. C. H. Lo. 2007. The State of the California Current, 2007–2007: Regional and local processes dominate. California Cooperative Oceanic Fisheries Investigations Reports 48:33–66.

Goericke, R., E. Venrick, A. Mantyla, S. J. Bograd, F. B. Schwing, A. Huyer, R. L. Smith, P. A. Wheeler, R. Hooff, W. T. Peterson, G. Gaxiola-Castro, J. Gomez-Valdez, B. E. Lavaniegos, K. D. Hyrenbach, and W. J. Sydeman. 2004. The State of the California Current, 2003–04: A rare "normal" year. California Cooperative Oceanic Fisheries Investigations Reports 45:27–59.

Hare, S. R., and N. Mantua. 2000. Empirical evidence for North Pacific regime shifts in 1977 and 1989. Progress in Oceanography 47:103–145.

Horton, C. A. 2014. Top-down influences of Bald Eagles on Common Murre populations in Oregon. MS thesis. Oregon State University.

Hsieh, C., C. Reiss, W. Watson, M. J. Allen, J. R. Hunter, R. N. Lea, R. H. Rosenblatt, P. E. Smith, and G. Sugihara. 2005. A comparison of long-term trends and variability in populations of larvae of exploited and unexploited fishes in the Southern California region: A community approach. Progress in Oceanography 67:160–185.

Hsieh, C. H., H. J. Kim, W. Watson, E. Di Lorenzo, and G. Sugihara. 2009. Climate-driven changes in abundance and distribution of larvae of oceanic fishes in the southern California region. Global Change Biology 15:2137–2152.

Hyrenbach, D. K., and R. R. Veit. 2003. Ocean warming and seabird communities of the Southern California Current System (1987–98): response at multiple temporal scales. Deep Sea Research II 50:2537–2565.

Jackson, J. M., G. C. Johnson, H. V. Dosser, and T. Ross. 2018. Warming from recent marine heatwave lingers in deep British Columbia fjord. Geophysical Research Letters 45:2018GL078971.

Jacox, M. G., M. A. Alexander, N. J. Mantua, J. D. Scott, G. Hervieux, R. S. Webb, and F. E. Werner. 2018a. Forcing of multiyear extreme ocean temperatures that impact California Current living marine resources in 2016. Bulletin of the American Meteorological Society 99:S27–S33.

Jacox, M. G., C. A. Edwards, E. L. Hazen, and S. J. Bograd. 2018b. Coastal upwelling revisited: Ekman, Bakun, and improved upwelling indices for the U.S. west coast. Geophysical Research Letters in press.

Jacox, M. G., J. Fiechter, A. M. Moore, and C. A. Edwards. 2015. ENSO and the California Current coastal upwelling response. Journal Geophysical Research Oceans 120:1691–1702.

Jacox, M. G., E. L. Hagen, K. D. Zaba, D. L. Rudnick, C. A. Edwards, A. M. Moore, and S. J. Bograd. 2016. Impacts of the 2015–16 El Niño on the California Current System: Early assessments and comparison to past events. Geophysical Research Letters 43:7072–7080.

Jacox, M. G., A. M. Moore, C. A. Edwards, and J. Fiechter. 2014. Spatially resolved upwelling in the California Current System and its connections to climate variability. Geophysical Research Letters 41:3189–3196.

Jeronimo, G., and J. Gomes-Valdes. 2010. Mixed layer depth variability in the tropical boundary of the California Current, 1997–2007. Journal Geophysical Research Oceans 115:C05014.

Kahru, M., M. G. Jacox, and M. D. Ohman. 2018. CCE1: Decrease in the frequency of oceanic fronts and surface chlorophyll concentration in the California Current System during the 2014–16 northeast Pacific warm anomalies. in press.

Koslow, J. A., L. Rogers-Bennett, and D. J. Neilson. 2012. A time series of California spiny lobster (*Panulirus interruptus*) phyllosoma from 1951 to 2008 links abundance to warm oceanographic conditions in southern California. California Cooperative Oceanic Fisheries Investigations Reports 53:132–139.

Laake, J. L., M. S. Lowry, R. L. DeLong, S. R. Melin, and J. V. Carretta. 2018. Population growth and status of California sea lions. The Journal of Wildlife Management 82:583–595.

Lavaniegos, B., and M. Ohman. 2007. Coherence of long-term fluctuation of zooplankton in tow sectores of the California Current System. Progress in Oceanography 75:42–69.

Leising, A. W., I. D. Schroeder, S. J. Bograd, J. Abell, R. Duranzo, G. Gaxiola-Castro, E. P. Bjorkstedt, J. C. Field, K. M. Sakuma, R. R. Robertson, R. Goericke, W. T. Peterson, R. D. Brodeur, C. Barcelo, T. D. Auth, E. A. Daly, R. M. Suryan, A. J. Gladics, J. M. Porquez, S. McClatchie, E. D. Weber, W. Watson, J. A. Santora, W. J. Sydeman, S. R. Melin, F. C. Chavez, R. T. Golightly, S. R. Schneider, J. Fisher, C. A. Morgan, R. Bradley, and P. Warybok. 2015. State of the California Current 2014–15: Impacts of the warm-water "Blob." California Cooperative Oceanic Fisheries Investigations Reports 56:31–68.

Lluch-Belda, D., R. J. M. Crawford, T. Kawasaki, A. D. Maccall, R. H. Parrish, R. A. Schwartzlose, and P. E. Smith. 1989. Worldwide fluctuations of sardine and anchovy stocks—the regime problem. South African Journal of Marine Science 8:195–205.

MacCall, A. D., W. J. Sydeman, P. Davison, and J. A. Thayer. 2016. Recent collapse of northern anchovy biomass off California. Fisheries Research 175:87–94.

Mantua, N., S. R. Hare, Y. Zhang, J. M. Wallace, and R. C. Francis. 1997. A Pacific decadal climate oscillation with impacts on salmon. Bulletin of the American Meteorological Society 78:1069–1079.

McClatchie, S. 2012. Sardine biomass is poorly correlated with the Pacific Decadal Oscillation off California. Geophysical Research Letters 39.

McClatchie, S. 2014. Regional fisheries oceanography of the California Current System and the CalCOFI program. Springer.

McClatchie, S., J. C. Field, A. R. Thompson, T. Gerrodette, M. Lowry, P. C. Fiedler, W. Watson, K. M. Nieto, and R. D. Vetter. 2016a. Food limitation of sea lion pups and the decline of forage off central and southern California. Royal Society Open Science 3:150628.

McClatchie, S., R. Goericke, A. Leising, T. D. Auth, E. Bjorkstedt, R. R. Robertson, R. D. Brodeur, X. Du, E. A. Daly, C. A. Morgan, F. P. Chavez, A. J. Debich, J. Hildebrand, J. C. Field, K. M. Sakuma, M. G. Jacox, M. Kahru, R. Kudela, C. Anderson, B. E. Lavaniegos, J. Gomes-Valdes, S. P. A. Jimenez-Rosenberg, R. McCabe, S. R. Melin, M. D. Ohman, L. M. Sala, B. Peterson, J. L. Fisher, I. D. Schroeder, S. J. Bograd, E. L. Hazen, S. R. Schneider, R. T. Golightly, R. M. Suryan, A. J. Gladics, S. Loredo, J. M. Porquez, A. R. Thompson, E. D. Weber, W. Watson, V. Trainer, P. Warzybok, R. Bradley, and J. Jahncke. 2016b. State of the California Current 2015–16: Comparisons with the 1997–98 El Niño. California Cooperative Oceanic Fisheries Investigations Reports 57:5–61.

McClatchie, S., I. L. Hendy, A. R. Thompson, and W. Watson. 2017. Collapse and recovery of forage fish populations prior to commercial exploitation. Geophysical Research Letters 44:1877–1885.

McClatchie, S., R. D. Vetter, and I. L. Hendy. 2018. Forage fish, small pelagic fisheries and recovering predators: managing expectations. Animal Conservation 1367: 9430.

McClatchie, S., J. Gao, E. J. Drenkard, A. R. Thompson, W. Watson, L. Ciannelli, S. J. Bograd, and J. T. Thorson. 2018. Interannual and secular variability of larvae of mesopelagic and forage fishes in the southern California Current System. Journal Geophysical Research Oceans 123:6277–6295.

Melin, S. R., A. J. Orr, J. D. Harris, J. L. Laake, and R. L. DeLong. 2012. California sea lions: An indicator for integrated ecosystem assessment of the California Current System. California Cooperative Oceanic Fisheries Investigations Reports 53:140–152.

Melin, S. R., A. J. Orr, J. D. Harris, J. L. Laake, R. L. DeLong, F. M. Gulland, and S. Soudt. 2010. Unprecedented mortality of California sea lion pups associated with anomalous oceanographic conditions along the central California coast in 2009. California Cooperative Oceanic Fisheries Investigations Reports 51:182–194.

Morgan, C. A., A. M. Baptista, B. R. Beckman, R. D. Brodeur, B. I. Burke, E. A. Daly, D. D. Huff, K. C. Jacobson, A. J. Miller, E. M. Phillips, D. M. Van Doornik, and J. E. Zamon. 2018. Ocean Survival of Salmonids RME, 1/1/2017–12/31/2017. https://www.cbfish.org/Document.mvc/Viewer/P159726.

Moser, H. G., R. L. Charter, P. E. Smith, D. A. Ambrose, W. Watson, S. R. Charter, and E. M. Sandknop. 2001. Distributional atlas of fish larvae and eggs in the Southern California Bight region: 1951–98. CalCOFI Atlas No. 34.

Moser, H. G., P. E. Smith, and L. E. Eber. 1987. Larval fish assemblages in the California Current region, 1954–60, a period of dynamic environmental change. California Cooperative Oceanic Fisheries Investigations Reports 28:97–127.

Newman, M., M. A. Alexander, T. R. Ault, K. M. Cobb, C. Deser, E. Di Lorenzo, N. J. Mantua, A. J. Miller, S. Minobe, H. Nakamura, and N. Schneider. 2016. The Pacific decadal oscillation, revisited. Journal of Climate 29:4399–4427.

Peabody, C. E., A.R. Thompson, D.F. Sax, R.E. Morse, and C.J. Perretti. 2018. Decadal regime shifts in southern California's ichthyoplankton assemblage. Marine Ecology Progress Series 607: 71-83

Peterson, W. T., J. L. Fisher, J. O. Peterson, C. A. Morgan, B. I. Burke, and K. L. Fresh. 2014. Applied fisheries oceanography: ecosystem indicators of ocean conditions inform fisheries management in the California Current ecosystem. Oceanography 27:80–89.

Peterson, W.T., J. L. Fisher, P.T. Strub, X. Du, C. Risien, J. Peterson, and C.T. Shaw. 2017. The pelagic ecosystem in the Northern California Current off Oregon during the 2014–2016 warm anomalies within the context of the past 20 years. Journal of Geophysical Research: Oceans 122:7267–7290.

Phillips, E. M., J. K. Horne, J. Adams, and J. E. Zamon. 2018. Selective occupancy of a persistent yet variable coastal river plume by two seabird species. Marine Ecology Progress Series 594:245–261.

Phillips, E. M., J. K. Horne, and J. E. Zamon. 2017. Predator-prey interactions influenced by a dynamic river plume. Canadian Journal of Fisheries and Aquatic Sciences 74:1375–1390.

Reed, T. E., S. Waneless, M. P. Harris, M. Frederiksen, L. E. B. Kruuk, and E. J. A. Cunningham. 2006. Responding to environmental change: plastic responses vary little in a synchronous breeder. Proceedings of the Royal Society of London B 273:2713–2719.

Rudnick, D. L., K. D. Zaba , R. E. Todd, and R. E. Davis. 2017. A climatology of the California Current System from a network of underwater gliders. Progress in Oceanography 154:64–106.

Rykaczewski, R. R., and D. M. Checkley Jr. 2008. Influence of ocean winds on the pelagic ecosystem in upwelling regions. Proceedings of the National Academy of Science 105:1965–1970.

Sakuma, K. M., J. C. Field, B. B. Marinovic, C. N. Carrion, N. J. Mantua, and S. Ralston. 2016. Anomalous epipelagic micronekton assemblage patterns in the neritic waters of the California Current in spring 2015 during a period of extreme ocean conditions. California Cooperative Oceanic Fisheries Investigations Reports 57:163–183.

Santora, J. A., and W. J. Sydeman. 2015. Persistence of hotspots and variability of seabird species richness and abundance in the southern California Current. Ecosphere 6:214.

Schroeder, I. D., B. A. Black, W. J. Sydeman, S. J. Bograd, E. L. Hazen, J. A. Santora, and B. K. Wells. 2013. The North Pacific High and wintertime pre-conditioning of California Current productivity. Geophysical Research Letters 40:541–546.

Schroeder, I. D., W. J. Sydeman, N. Sarkar, S. A. Thompson, S. J. Bograd, and F. B. Schwing. 2009. Winter pre-conditioning of seabird phenology in the California Current. Marine Ecology Progress Series 393:211–233.

Schwing, F. B., M. O'Farrell, J. M. Steger, and K. Baltz. 1996. Coastal Upwelling indices west coast of North America. NOAA Technical Report NMFS SWFSC NMFS SWFSC 231.

Sydeman, W. J., J. A. Santora, S. A. Thompson, B. B. Marinovic, and E. Di Lorenzo. 2013. Increasing variance in North Pacific climate relates to unprecedented ecosystem variability off California. Global Change Biology 19:1662–1675.

Sydeman, W. J., and S. A. Thompson. 2010. The California Current Integrated Ecosystem Assessment (IEA), Module II: trends and variability in climate-ecosystem state. Pacific Grove, California.

Sydeman, W. J., S. A. Thompson, J. A. Santora, J. A. Koslow, R. Goericke, and M. D. Ohman. 2015. Climate-ecosystem change off southern California: Time-dependent seabird predator-prey numerical responses. Deep Sea Research II 112:158–170.

Szoboszlai, A. I., J. A. Thayer, S. A. Wood, W. J. Sydeman, and L. E. Koehn. 2015. Forage species in predator diets: Synthesis of data from the California Current. Ecological Informatics 29:45–56.

Thompson, S. A., W. J. Sydeman, J. A. Santora, K. H. Morgan, W. Crawford, and M. T. Burrows. 2012. Phenology of pelagic seabird abundance relative to marine climate change in the Alaska Gyre. Marine Ecology Progress Series 454:159–170.

Veit, R. R., P. Pyle, and J. A. McGowan. 1996. Ocean warming and long-term change in pelagic bird abundance within the California current system. Marine Ecology Progress Series 139:11–18.

Velarde, E., E. Ezcurra, M. H. Horn, and R. T. Patton. 2015. Warm oceanographic anomalies and fishing pressure drive seabird nesting north. Science Advances 1:e1400210.

Wells, B. K., I. D. Schroeder, S. J. Bograd, E. L. Hazen, M. G. Jacox, A. Leising, N. Mantua, J. A. Santora, J. L. Fisher, W. T. Peterson, E. Bjorkstedt, R. R. Robertson, F. P. Chavez, R. Goericke, R. Kudela, C. Anderson, B. E. Lavaniegos, J. Gomez-Valdes, R. D. Brodeur, E. A. Daly, C. A. Morgan, T. D. Auth, J. C. Field, K. M. Sakuma, S. McClatchie, A. R. Thompson, E. D. Weber, W. Watson, R. M. Suryan, J. K. Parrish, J. Dolliver, S. Loredo, J. M. Porquez, J. E. Zamon, S. R. Schneider, R. T. Golightly, P. Warzybok, R. Bradley, J. Jahncke, W. J. Sydeman, S. R. Melin, J. A. Hildebrand, A. J. Debich, and B. Thayre. 2017. State of the California Current 2016–17: Still anything but "normal" in the north. CalCOFI Reports 58:1–55.

Xie, P., T. Boyer, E. Bayler, Y. Xue, D. Byrne, J. Reagan, R. Locarnini, F. Sun, R. Joye, and A. Kumar. 2014. An in situ- satellite blended analysis of global sea surface salinity. Journal Geophysical Research Oceans 119:6140–6160.

Zamon, J. E., E. M. Phillips, and T. J. Guy. 2014. Marine bird aggregations associated with the tidally-driven plume and plume fronts of the Columbia River. Deep-Sea Research Part Ii-Topical Studies in Oceanography 107:85–95.

Zwolinski, J. P., and D. A. Demer. 2012. A cold oceanographic regime with high exploitation rates in the Northeast Pacific forecasts a collapse of the sardine stock. Proceedings of the National Academy of Science 109:4175–4180.